JPRS 77320

4 February 1981

Translation

BIONICS

FBIS FOREIGN BROADCAST INFORMATION SERVICE

NOTE

JPRS publications contain information primarily from foreign newspapers, periodicals and books, but also from news agency transmissions and broadcasts. Materials from foreign-language sources are translated; those from English-language sources are transcribed or reprinted, with the original phrasing and other characteristics retained.

Headlines, editorial reports, and material enclosed in brackets [] are supplied by JPRS. Processing indicators such as [Text] or [Excerpt] in the first line of each item, or following the last line of a brief, indicate how the original information was processed. Where no processing indicator is given, the information was summarized or extracted.

Unfamiliar names rendered phonetically or transliterated are enclosed in parentheses. Words or names preceded by a question mark and enclosed in parentheses were not clear in the original but have been supplied as appropriate in context. Other unattributed parenthetical notes within the body of an item originate with the source. Times within items are as given by source.

The contents of this publication in no way represent the policies, views or attitudes of the U.S. Government.

PROCUREMENT OF PUBLICATIONS

JPRS publications may be ordered from the National Technical Information Service (NTIS), Springfield, Virginia 22161. In ordering, it is recommended that the JPRS number, title, date and author, if applicable, of publication be cited.

Current JPRS publications are announced in Government Reports Announcements issued semimonthly by the NTIS, and are listed in the Monthly Catalog of U.S. Government Publications issued by the Superintendent of Documents, U.S. Government Printing Office, Washington, D.C. 20402.

Indexes to this report (by keyword, author, personal names, title and series) are available through Bell & Howell, Old Mansfield Road, Wooster, Ohio, 44691.

Correspondence pertaining to matters other than procurement may be addressed to Joint Publications Research Service, 1000 North Glebe Road, Arlington, Virginia 22201.

JPRS 77320

4 February 1981

BIONICS

Kiev BIONIKA; RESPUBLIKANSKIY MEZHVEDOMSTVENYY SBORNIK, OSNOVAN V 1969 g. (BIONICS; REPUBLIC INTERAGENCY COLLECTION, FOUNDED IN 1969) in Russian No 12, 1978 signed to press 11 Jul 78 pp 3-117

[Translation of articles in the collection issued by the Institute of Hydromechanics, Ukrainian SSR Academy of Sciences, G.V. Logvinovich, editor in chief, Izdatel'stvo "Naukova dumka," 850 copies, 117 pages, UDK 577]

CONTENTS

[I - USSR - C]

PUBLICATION DATA

English title	:	BIONICS: REPUBLIC INTERAGENCY COLLECTION. FOUNDED IN 1969
Russian title	:	BIONIKA: RESPUBLIKANSKIY MEZHVEDOMSTVENNYY SBORNIK. OSNOVAN V 1969 g.
Author (s)	:	
Editor (s)	:	G. V. Logvinovich
Publishing House	:	Izdatel'stvo "Naukova dumka"
Place of Publication	:	Kiev
Date of Publication	:	1978
Signed to press	:	11 Jul 78
Copies	:	850

Annotation

The collection is devoted to hydrodynamic problems of bionics. Individual problems of general hydromechanics and bioenergetics are considered with respect to the swimming of aquatic animals. Different methods of reducing drag are investigated. The morphological structure of the skins of marine animals is described. The possibilities of using the information in the national economy are investigated. The book is intended for scientific workers, teachers of VUZ's and graduate students involved in problems of bionics.

UDC 591.173+599.537

THEORETICAL INVESTIGATION OF THE HYDRODYNAMICS OF AQUATIC ANIMALS SWIMMING IN SCOMBRIDAE FASHION

Kiev DOKLADY in Russian No 12, 1978 pp 3-12

[Article by L. F. Koslov and S. A. Olaynik, Institute of Hydromechanics of the Ukrainian SSR Academy of Sciences]

[Text] Hydrodynamic problems of biomechanics evoke great interest with regard to study of the mechanisms of swimming of aquatic animals. The specific results of these types of investigations carried out by foreign scientists were summarized at the International Symposium on Swimming and Flight in Nature, held on 8-12 July 1974 at the California Institute of Technology 2 (Pasadena, California) [13]. The results of investigating hydrodynamic problems of biomechanics by Soviet scientists were presented at the Fourth All-Union Congress on Theoretical and Applied Mechanics, which was held in Kiev on 21-28 May 1976 [1].

This article is devoted to the approximate mathematical investigation of the Scombridae method of swimming by aquatic animals. The scientific results of this investigation have already been published [2]. The novelty of the given publication is that formulas were found in the final analysis to determine thrust, the suction force and the hydrodynamic efficiency with respect to elongated freshwater and marine fishes swimming in Scombridae fashion on the basis of general laws of mechanics (variation of the amount of motion and energy). The mentioned method of swimming is very widely distributed in nature (for example, mullet, mackeral, bonito, trout and other marine and freshwater fishes). Academician of the Ukrainian SSR Academy of Sciences G. V. Logvinovich earlier [3-5] proposed a hydrodynamic theory of swimming of fishes by the so-called eel method, according to which the amplitude of the propulsive wave propagated along the body of the fish is a constant value now dependent on the point of location of the wave on the fish's body. It is not accepted as some mathematical model of the Scombridae fashion of swimming that the amplitude of the propulsive wave has a linear dependence on the point of its location on the fish's body.

This more complex method of swimming is investigated theoretically in this paper. Moreover, according to derived formulas which link the hydrodynamic and kinematic characteristics of swimming of aquatic animals for different marine and freshwater fishes whose kinematics has been investigated experimentally, the coefficients of hydrodynamic drag and efficiency were calculated on the assumption of the Scombridae fashion of swimming of these aquatic animals. Necessary data on the kinematics of swimming of fishes were taken from papers of V. Ye. Pyatetskiy and

V. P. Kayan [5-11]. The order of magnitude of the values which we found was very similar to those calculated using boundary layer theory. The latter circumstance confirms to some degree the scientific reliability of the developed approach to study of the hydrodynamics of aquatic animals swimming in Gumbridge fashion.

We shall subsequently regard the body of a swimming fish as a thin deformable body. To study its hydrodynamics, let us make use of the method of plane sections, which is some approximation when describing the spatial flows of liquid and is more justified than a more elongated body. Let us hope that study of the spatial problem brings us closer to an understanding of the mechanism of swimming of various types of aquatic animals.

Following the theory of G. V. Logvinovich [3], let us consider the motion of a thin deformable body of an aquatic animal in the movable coordinate system x, y, z (Figure 1), moving at constant speed along the axis in an unlimited and infinitely quiescent fluid. The longitudinal curvilinear axis of the considered deformable body o hardly deviates from Ox. Deviation of the curvilinear axis of the body in the xOz plane from the Ox axis is denoted by $\eta(x, t)$, the abscissas of the ends of the deformable body are denoted by x_1 and x_2, the length of the body is denoted by $l_p = x_2 - x_1$ and time is denoted by t.

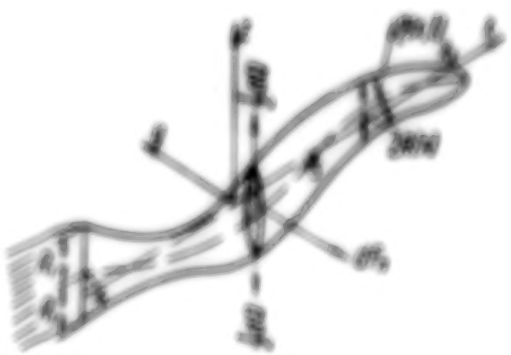

Figure 1. Diagram of Motion of Flexible Body of Fish Through "Permeable Layer" of Fluid

Let us assume that the cross-section of the fish's body is formed of a circle or ellipse with major semiaxis $B = B(x)$ and along the length of the body $dB/dx = 0$. The specific virtual mass will then depend only on the abscissa x and will be equal to $\mu_{22}' = \pi\rho B^2(x)$, where ρ is the density of the fluid, for the adopted cross-section. According to the "permeable layer" concept [3], we assume that the body causes transverse flow very similar to plane flow in an ideal fluid. We also assume that the well-known Zhukovskiy condition on the finiteness of speed is fulfilled on the trailing edge at $x = x_2$. Fulfillment of this condition is equivalent to flow along the tangent of the vortex shroud from the plane of the caudal fin of an aquatic animal or a pulse flow $\pi\rho_2^2 V v_2$. The normal velocity of the layer to the curvilinear axis o is

$$v_n = \frac{\partial \eta}{\partial t} - V\frac{\partial \eta}{\partial x}. \qquad (1)$$

The second condition on the impermeability of the 'permeable layer' with respect to the fluid was used when writing expression (1).

The specific normal force acting on a thin body and occurring when it is passing through the 'permeable layer' is:

$$dF_n = -\frac{\rho}{g}[w(t)]\,ds \tag{2}$$

Since the specific impulse of the fluid is equal to $w_0^2(x)v_{0n}(x,t)$ in this case, the circular pressure acting on element ds is as follows:

$$dQ = -2\pi R(x)\rho\frac{d}{g}\,ds \tag{3}$$

Projection of it onto the x axis yields the longitudinal suction force applied to the body

$$dP = \frac{dQ}{ds}\frac{dR}{dx}\,ds = \left\{-\pi\rho R(x)v_0^2\frac{dR}{dx}\right\}. \tag{4}$$

The excess pressure on the surface of a round cylinder at a point determined by coordinates R and Θ, where Θ is the polar angle in a cylindrical coordinate system, let us calculate from the well-known expression

$$P - P_0 = \frac{\rho v_0^2}{2}(1 - 4\sin^2\Theta) + \rho\frac{\cos\Theta}{R}\frac{d}{dt}(R^2v_{0n}). \tag{5}$$

Substituting expression (5) into equation (2), after simple calculations, we find the force normal to the longitudinal axis:

$$\frac{dF_n}{dx} = -\int_0^{2\pi}(P - P_0)\cos\Theta R\,d(R\Theta) = -\frac{d}{dt}(\rho\pi R^2v_{0n}). \tag{6}$$

Let us determine circular pressure from the expression

$$\frac{dQ}{dx} = \int_0^{2\pi}(P - P_0)\,d(R\Theta) = -2\pi R\rho\frac{d}{g}. \tag{7}$$

Let us consider a thin body tapered from the front. In this case the slope of the generatrix of the body to the Ox axis is a negative value and since dR/ds = dR/dx, the force directed along the Ox axis acts on each unit of length:

$$\frac{dP}{dx} = -2\pi R\frac{\rho v_0^2}{2}\frac{dR}{dx} = -\frac{\rho}{2}\frac{dR^2(x)}{dx}. \tag{8}$$

let us use a lagrangian equation of second kind to determine the specific forces acting on the contour in case of an elliptical shape of the cross-section. In this case let us use the following expression to calculate the kinetic energy in the layer

$$T = m' (R) \frac{v_0^2}{2} \tag{9}$$

Let us use the major semiaxis of the transverse elliptical section $b(x)$ and velocity v_0 as the generalized coordinates and velocities when determining the equation formula by the lagrangian formula. As a result we find the same expressions as for a round section for the specific forces applied to an elliptical section:

$$-\frac{dT}{db} = -\frac{dm'}{db}\frac{v_0^2}{2} = -\pi\rho b\frac{v_0^2}{2} = \frac{dG}{dx} \tag{10}$$

$$\frac{d}{dt}\frac{dT}{dv_0} = \frac{d}{dt}(m'v_0) = \frac{d}{dt}(\rho\pi b^2 v_0) = \frac{dF_0}{dx} \tag{11}$$

We note that the use of lagrangian equations of second kind in the considered case is justified for the following reasons. The velocity potential of transverse flow for a thin body is similar to the corresponding potential of a cylinder. Therefore, the kinetic energy of a transverse section in an elementary layer is determined by the boundary values of the velocity potential and its first derivative along the normal to the contour of the section and varies instantaneously upon variation of the velocity of the center of the layer. Therefore, one may assume that the relationships between the particles inside the elementary layer are holonomic and that the mentioned lagrangian equations of second kind can be applied to this layer.

Projections of the elementary forces applied to the body on the Ox and Oy axes, respectively, are calculated from the following expressions:

$$dF_x = -dF_0\frac{dy}{dx} - dF \tag{12}$$

$$dF_y = dF_0 + dF\frac{dy}{dx} \tag{13}$$

It is obvious that the total instantaneous forces acting on the entire flexible body can be determined by using the integrals

$$F_x = \int_{x_1}^{x_2} dF_x \tag{14}$$

$$F_y = \int_{x_1}^{x_2} dF_y \tag{15}$$

In this case the following boundary conditions must be fulfilled: $b(x_1) = 0$ and $b(x_2) = b_2$ where b_2 is the semispan of the caudal fin.

In case of periodic variation of swimming motions, one can avoid direct calculation of the projections of force F_x and F_y by direct integration of equations (13) and (14). Only the characteristics of the hydrodynamic wake, which can be determined if the trajectory of motion of the caudal fin is known, need be used for this purpose.

A liquid receives the impulse $m^*(\alpha_1)w_1$, directed along the normal velocity component of the caudal fin, per unit length of wake. Projection of the pulse flowing from the caudal fin onto the Ox axis per unit time, taken with reverse sign, determines the instantaneous force acting on the flexible body. Therefore, the pulling force caused by the flow of pulses coming into the hydrodynamic wake is determined by the expression

$$f = m^*(\alpha_1) V \left(\frac{\partial h}{\partial t} - V\frac{\partial h}{\partial x}\right)\frac{\partial h}{\partial x} \qquad (16)$$

at $x = x_1$. The mean value of the pulling force caused by the pulses remaining in the hydrodynamic wake is then

$$\langle f\rangle = \frac{1}{T}\int_0^T f\,dt \qquad (17)$$

where T is the period of oscillations.

The kinetic energy remaining in the hydrodynamic wake per unit path of the caudal fin is found by the equation

$$E = \frac{1}{2} m^*(\alpha_1) w_1^2 = \frac{1}{2} m^*(\alpha_1)\left(\frac{\partial h}{\partial t} - V\frac{\partial h}{\partial x}\right)^2_{x=x_1} \qquad (18)$$

The mean value of kinetic energy is

$$\langle E\rangle = \frac{1}{T}\int_0^T E\,dt \qquad (19)$$

The other part of the pulling force is realized in the form of suction force

$$P = -\int_{x_0}^{x_1} \frac{dm^*(x)}{dx}\,\frac{1}{2}\left(\frac{\partial h}{\partial t} - V\frac{\partial h}{\partial x}\right)^2 dx \qquad (20)$$

The mean active power of the pulling forces is

$$\langle N\rangle = (\langle f\rangle + \langle P\rangle)V \qquad (21)$$

The power expended to form the pulling force is as follows:

$$|\vec{W}| = |\vec{U}| + |\vec{V}| \cdot \vec{V} = |\vec{U}|\vec{V} \tag{22}$$

The hydrodynamic efficiency is then

$$(\eta_h) = \frac{|\vec{U}|}{|\vec{W}|}. \tag{23}$$

We note that the main formulas given above were first found by Academician of the Ukrainian SSR Academy of Sciences G. V. Lepikhovskiy [3].

Let us use the optimal method of estimating the efficiency of the caudal fin as a fin capable of the maximum feature of economy. In this case let us be given the law of deformation of a flexible body in the form of the function

$$y = y_0 \frac{x_0 - x}{x_0} \sin\left(\frac{\omega}{c} - \frac{x_0 - x}{\lambda}\right) \tag{24}$$

The linear law of variation of the oscillation amplitude of the propulsive wave along the flexible body is used in expression (24). Moreover the oscillation amplitude of the caudal fin, which is assumed to be known, is denoted by y_0. Moreover, let us assume that

$$\frac{\partial}{\partial x}(\rho U^2) = -\frac{\rho U^2}{x_0}, \tag{25}$$

i.e., the normal mass flow not vary along the body. Differentiating expression (24), we find

$$\frac{\partial y}{\partial x} = y_0 \frac{x_0 - x}{x_0} \frac{\omega}{c} \cos\left(\frac{\omega}{c} - \frac{x_0 - x}{\lambda}\right), \tag{26}$$

$$\frac{\partial^2 y}{\partial x^2} = -\frac{y_0}{x_0} \sin\left(\frac{\omega}{c} - \frac{x_0 - x}{\lambda}\right) + \frac{y_0}{\lambda} \frac{x_0 - x}{x_0} \cos\left(\frac{\omega}{c} - \frac{x_0 - x}{\lambda}\right). \tag{27}$$

It is then easy to calculate the normal velocity for the considered case

$$\left(\frac{x_0}{x_0 - x_0} - \frac{x}{x_0}\right) \omega \lambda \frac{y_0}{x_0} + \left(\frac{x_0}{x_0 - x_0} - \frac{x}{x_0}\right) \cos(\lambda - \eta \frac{x_0}{x_0 - x_0} \frac{x}{x_0} = v_0 \tag{28}$$

The mean value of the square of the normal velocity is

$$\overline{v^2} = \frac{1}{2}\left(\frac{y_0}{x_0}\right)^2 \omega^2 + \frac{1}{2}\left(\frac{y_0}{\lambda}\right)^2 \left(\frac{x_0 - x}{x_0}\right)^2 \omega - V^2 \tag{29}$$

Using expression (29), we find the mean value for the period of the exciting force for the case under consideration

$$(P) = -\frac{1}{T}\int_{t_0}^{t_0+T}\left[\frac{1}{2}\left(\frac{2\pi}{t_p}\right)^2 V^2 + \frac{1}{2}\left(\frac{2\pi}{t}\right)^2\left(\frac{s_1=s}{t_p}\right)(t-V)^2\right]\left(-\frac{m_1 s_1'}{t_p}\right)dt = -\frac{1}{8}m_1'\left(\frac{2\pi}{t_p}\right)^2 V^2 + \frac{1}{16}\left(\frac{2\pi}{t}\right)^2 V^2\left(\frac{c}{V}-1\right)^2 m_1' \tag{30}$$

The kinetic energy whose mean value is as follows per unit path for the considered case of the Scombridae method of swimming flows from the caudal fin into the wake:

$$(E) = \frac{1}{2}m_1'(v_*)^2 = \frac{1}{4}m_1'\left(\frac{2\pi}{t_p}\right)^2 V^2 + \frac{1}{8}\left(\frac{2\pi}{t}\right)^2\left(\frac{c}{V}-1\right)^2 V^2 m_1' \tag{31}$$

Further, let us calculate the mean value of the pulling force determined by the pulses remaining in the hydrodynamic wake:

$$(I) = m_1' V\,\frac{1}{T}\int_0^T\left[\frac{2\pi}{t}\,\frac{s_1=s}{t_p}\cos\left(\frac{\varphi t}{t}-\frac{s_1=s}{t_a}\right)(c-V) + \frac{2\pi}{t_p}V\sin\left(\frac{\varphi t}{t}-\frac{s_1=s}{t}\right)\right]\left[-\frac{2\pi}{t}\sin\left(\frac{\varphi t}{t}-\frac{s_1=s}{t_{min}}\right) + \frac{2\pi}{t}\,\frac{s_1=s}{t_p}\cos\left(\frac{\varphi t}{t}-\frac{s_1=s_1}{t}\right)\right]dt. \tag{32}$$

Integrating expression (32), we find

$$(I) = -\frac{1}{8}m_1' V^2\left(\frac{2\pi}{t_p}\right)^2 + \frac{1}{8}m_1' V^2\left(\frac{c}{V}-1\right)\left(\frac{2\pi}{t}\right)^2. \tag{33}$$

It is then obvious that the mean active power is

$$(A) = ((I)+(P))V = -\frac{1}{8}m_1' V^2\left(\frac{2\pi}{t_p}\right) + \frac{1}{16}m_1'\left(\frac{2\pi}{t}\right)^2 \times V^2\left(\frac{c}{V}-1\right)\left(\frac{c}{V}+3\right). \tag{34}$$

We find by simple calculations the mean expended power

$$(N) = \frac{1}{8}m_1'\left(\frac{2\pi}{t}\right)^2 V^2\left(\frac{c}{V}-1\right)\left(2\frac{c}{V}+1\right) \tag{35}$$

and the hydrodynamic efficiency for the case under consideration

$$(\eta_p) = \frac{1}{2\left(2\frac{c}{V}+1\right)}\left[\left(\frac{c}{V}+3\right) - \frac{3}{(2\pi St)^2\left(\frac{c}{V}-1\right)}\right]. \tag{36}$$

Based on limit theory

$$\lim_{\frac{c}{V}\to 1}(\eta_p)\to-\infty.$$

The dependence of the hydrodynamic efficiency on the relative velocity of the propulsive wave travelling along a deformed body on the assumption of Scombridae and eel fashion of swimming is presented in Figure 2. Calculations for the eel method of swimming were made by G. V. Logvinovich [3]. Comparative analysis of the data presented in Figure 2 permits one to make the following conclusions.

The hydrodynamic efficiency is less with the Scombridae fashion of swimming and at identical values of relative velocities of the propulsive wave than for corresponding values with the eel fashion of swimming. Moreover, the maximum efficiency is reached with the eel fashion of swimming at relative velocity equal to unity, whereas the corresponding maximum value with the Scombrida fashion of swimming depends on the number of propulsive waves contained on the length of the body and on relative velocity of the propulsive wave greater than unity.

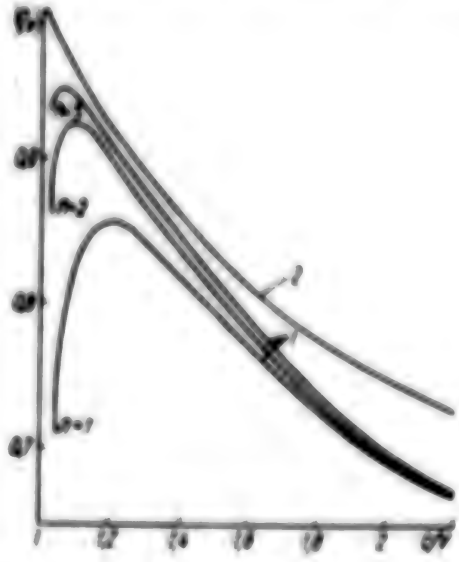

Figure 2. Dependence of Hydrodynamic Efficiency (η) on Relative Velocity of Propulsive Wave c/V Travelling Along Fish's Body: 1--Scombridae and 2--eel fashions of swimming; n--number of propulsive waves contained on length of fish's body

The efficiency in the Scombridae fashion of swimming with an increase of the number of propulsive waves approaches the corresponding value with the eel fashion of swimming.

Thus, formulas (30)-(36) which link the hydrodynamic and kinematic characteristics of aquatic animals swimming in Scombridae fashion, are found in final form as a result of simple calculations. Let us use the data on the kinematics of swimming of marine and freshwater fishes, obtained experimentally by V. Ye. Pyatetskiy and V. P. Kayan [6-11], to analyze the numerical values of the hydrodynamic characteristics. The main geometric characteristics of the tested fishes required for the

calculations are also presented in the mentioned papers. The values of the total thrust and the coefficients of hydrodynamic efficiency were calculated using a computer. It was assumed in the calculations that the total thrust during steady swimming is equal to the total hydrodynamic drag of the aquatic animal. The coefficient of total hydrodynamic drag was determined by the formula

$$\zeta = \frac{2R}{\rho V^2 S}, \tag{37}$$

where $R = (A)/V$ is the total hydrodynamic drag, ρ is the density of water, V is the swimming speed of the aquatic animal and S is the area of the wetted surface without regard to abdominal and dorsal fins. Moreover, the values of Reynolds numbers were calculated

$$Re = \frac{VL}{\nu}, \tag{38}$$

where ν is the kinematic coefficient of viscosity of the liquid.

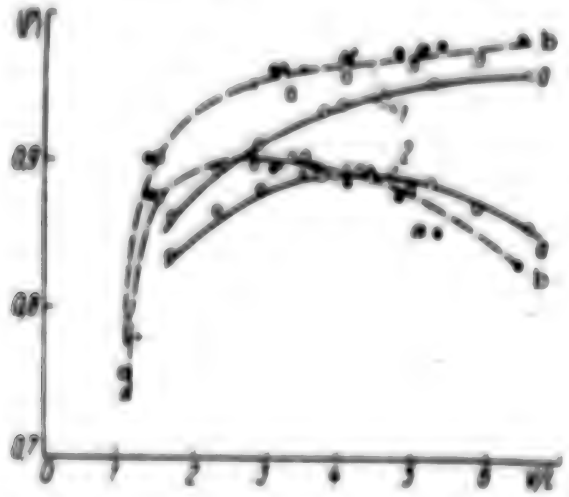

Figure 3. Dependence of Hydrodynamic Efficiency (η) on Relative Swimming Speed V/L of Fish: a--drum; b--trout; 1--eel and 2--Scombridae fashion of swimming

The dependence of the hydrodynamic efficiency (η) on relative swimming speed V/L for drum (a marine fish) and trout (a river fish) is presented in Figure 3. The efficiency was calculated on the assumption that the drum and trout swim in eel fashion, i.e., with constant amplitude of the propulsive wave travelling along the body (curve 1) and that these fishes swim in Scombridae fashion, i.e., the amplitude of the propulsive wave travelling along the body increases by linear law as this wave approaches the caudal fin (curve 2). Analysis of the movie films of the kinematics of swimming of the drum and trout recorded by V. Ye. Pyatetskiy and V. P. Kayan during experimental investigations, showed that the mentioned amplitude varies during motion of the propulsive wave along the body of the swimming fish.

Analysis of the data presented in Figure 3 permits one to make two conclusions. First, the values of efficiency calculated on the assumption of the eel fashion of

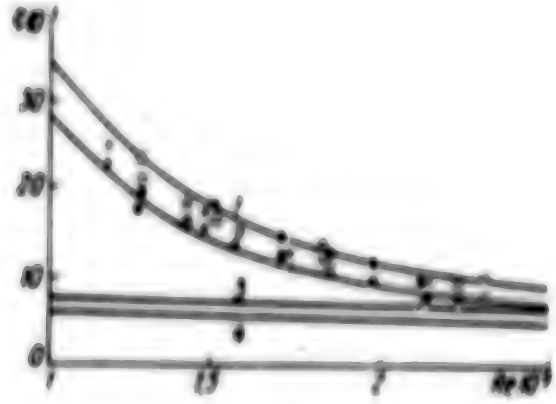

Figure 4. Dependence of Coefficient of Hydrodynamic Drag of Fish ζ on Reynolds Number Re: 1--eel and 2--Scombridae fashion of swimming; 3--turbulent and 4--laminar modes

swimming are always greater than the corresponding values determined on the assumption of the Scombridae fashion of swimming. Moreover, the numerical values of these differences are very significant. Thus, these differences comprise approximately 10 percent for the drum at relative swimming speed of V/l = 6-7 and they comprise 15 percent for the trout. Second, the dependence of the efficiency found on the assumption of the Scombridae fashion of swimming of the drum and trout is extreme in nature. Moreover, the maximum values of the efficiency coincide with "cruising" values of relative speeds more typical for these fish. Cruising speeds comprise from 3 to 5 for the drum (in relative values to the length of the fish) and from 1.5 to 3.0 for the trout. One must also keep the following concepts in mind when viewing the graph (Figure 3). The given data were calculated for an ideal impeller, i.e., without regard to viscous losses occurring as a result of the work of the fish's caudal fin as an impeller. It is for this reason that the efficiency has values comprising 0.85-0.90 in most cases. To estimate their real values with regard to viscous losses, one must multiply the data given in Figure 3 by a coefficient equal to approximately 0.6-0.7.

Special calculations of the efficiency of caudal fins of the drum and trout are general in nature. The fact is that these conclusions remain unchanged in the qualitative sense for all 10 fishes examined. Only the numerical values of the coefficient vary somewhat (and even then not significantly) for different fishes. Moreover, the relative cruising speeds in the sense mentioned above for mullet and bonito, when the efficiency has the greatest value, comprise 1.5-2.5 and 4-6, respectively.

A graph of the dependence of the coefficient of hydrodynamic drag ζ on Reynolds number Re on the basis of averaged data for four trout on the assumption of eel (curve 1) and Scombridae (curve 2) methods of swimming, is presented in Figure 4 as an example. The corresponding dependence for viscous drag of the trout body were calculated by using boundary layer theory [12] on the assumption of completely laminar (curve 3) and turbulent (curve 4) steady flow over the rigid part of the fish body installed along the flow.

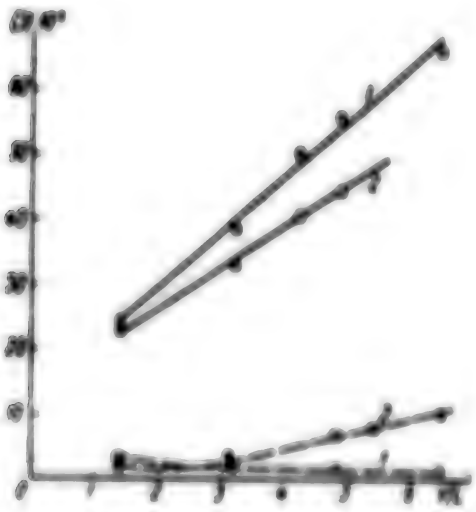

Figure 5. Dependence of Pulling (T) and Suction (P) Forces for Trout on Relative Velocity: (T)--solid line; P--dashed line; 1--eel and 2--Scombridae fashion of swimming

The following aspects are noteworthy upon analysis of Figure 4 and the similar graphs.

First, the coefficients of hydrodynamic drag of a fish are higher than the corresponding values for the rigid body of a fish during steady flow and completely turbulent flow. The coefficients of the hydrodynamic drag of a fish asymptotically approach the corresponding curve for a rigid body of a fish during turbulent flow as Reynolds number increases. This variation of the dependencies can apparently be explained in the following manner. Measurements of the degree of turbulence in the flow of a biohydrodynamic tube in which the kinematics of swimming of fishes was investigated, which were the basis for calculations of the hydrodynamic characteristics, showed that it comprises a very impressive value (several percent). Therefore, the mode of flow over a swimming fish at Reynolds numbers having value of approximately 200,000 was formed as turbulent flow. It should be said that this circumstance may not, as sometimes assumed, significantly affect the kinematics of swimming of fishes, most of which swim in a laminar or transient flow under natural conditions. As follows from Figure 4 (curves 3 and 4), the coefficients of hydrodynamic drag differ insignificantly during laminar and turbulent flow (by 10-20 percent) in the range of Reynolds numbers in which the fishes under investigation swim.

Second, the rather significant difference of the corresponding coefficients of hydrodynamic drag is obvious. For example, the difference reaches more than 100 percent at Reynolds numbers of approximately 100,000. It is difficult to completely explain the latter circumstance only by the significant transient [illegible] of the swimming motions of the fish under investigation at low speeds. Actual attentive observation possible during testing of the fish in the flow of a biohydrodynamic tube shows that the oscillation amplitudes of the body decrease all the time as the flow velocity increases and consequently as the swimming speed of the fish increases and only the caudal fin oscillates at maximum speeds. Therefore, the coefficient

of the hydrodynamic drag of a fish naturally asymptotically approaches a corresponding value for a rigid body during stead flow as Reynolds number increases.

At the same time observations of the swimming of fishes in a hydrodynamic tube show that fish usually employ the dorsal and especially the abdominal fins at low speeds apparently to create stability of the body in the incident flow. As speed increases, the dorsal and abdominal fins are usually brought closer and closer to the fish's body and thus reduce hydrodynamic drag. If this circumstance is taken into account and also the fact that the additional area of the dorsal and abdominal fins was not taken into account in the given calculations of hydrodynamic drag of fishes and of the corresponding coefficients, one can convincingly state that there is close agreement of the coefficients of hydrodynamic drag calculated, on the one hand, using approximate hydrodynamic theory of swimming of aquatic animals, and, on the other hand, using boundary layer theory.

The following circumstance must be analyzed. Some authors do not take into account the suction force calculated in Scombridae fashion of swimming by formula (30) in theoretical investigations of the hydrodynamic characteristics of aquatic animals. Actually, it follows from the general expression (4) for the element of suction force that this value has the order of the derivative of the semiaxis of the transverse section of the fish's body along the longitudinal coordinate. However, it is assumed in the theory of a thin body, which was used when analyzing the hydrodynamics of swimming of aquatic animals, that the mentioned derivative is a second-order value of smallness and is usually disregarded in calculations. It is therefore of interest to analyze the data on the comparative value of the suction and pulling forces. These calculated data found by formulas (30) and (32) for the trout are presented in Figure 5 as a function of the relative swimming speed. They indicate that the suction force in the range of relative speeds from 1 to 6 are an order less than the pulling force. Moreover, this conclusion does not depend on the assumption that the trout swims in eel or Scombridae fashion. It should be noted that similar conclusions were found for all of the investigated fish.

Thus, the hydrodynamic theory of aquatic animals swimming in Scombridae fashion, developed in this paper, permits one to analyze rather simply the swimming efficiency of some fast-swimming river and marine fishes.

BIBLIOGRAPHY

1. Kozlov, L. F., "Hydrodynamic Problems of Biomechanics," Abstracts of Reports of the Fourth All-Union Congress on Theoretical and Applied Mechanics, Kiev, 1976.

2. Kozlov, L. F. and R. A. Oleynik, "The Hydrodynamics of Aquatic Animals Swimming in Scombridae Fashion," DOKL. AN USSR, No 11, 1976.

3. Logvinovich, G. V., "The Hydrodynamics of a Thin Flexible Body (Analysis of the Hydrodynamics of Fishes)," BIONIKA, No 4, 1970.

4. Logvinovich, G. V., "The Hydrodynamics of a Thin Flexible Body (Analysis of the Hydrodynamics of Fishes)," UCHEN. ZAP. TSENTR. AEROGIDRODINAM. IN-TA, Vol 1, No 2, 1970.

5. Logvinovich, G. V., "The Hydrodynamics of Swimming of Fishes," Report Topics of the 13th International Congress on Theoretical and Applied Mechanics, Moscow, 1972.

6. Pyatetskiy, V. Ye., "The Kinematic Characteristics of Swimming of Some Fast-Swimming Marine Fishes," BIONIKA, No 4, 1970.

7. Pyatetskiy, V. Ye., "The Hydrodynamic Characteristics of Swimming of Some Fast-Swimming Fishes," BIONIKA, No 4, 1970.

8. Pyatetskiy, V. Ye. and V. P. Kayan, "The Characteristics of Swimming of the Lake Trout," BIONIKA, No 6, 1972.

9. Pyatetskiy, V. Ye. and V. P. Kayan, "A Closed Biohydrodynamic Installation to Investigate the Hydrodynamics of Swimming of Marine Animals," BIONIKA, No 5, 1971.

10. Pyatetskiy, V. Ye. and V. P. Kayan, "The Kinematics and Hydrodynamics of Swimming of Black Sea Garfish," BIONIKA, No 5, 1971.

11. Pyatetskiy, V. Ye. and V. P. Kayan, "Investigating the Kinematics of Swimming of Aquatic Animals," Abstracts of Reports of the Fourth All-Union Congress on Theoretical and Applied Mechanics, Kiev, 1976.

12. Shlikhting, G., "Teoriya pogranichnogo sloya" [Boundary Layer Theory], Moscow, Nauka, 1975.

13. Symposium on Swimming and Flying in Nature, edited by C. Brennen, Pasadena, California Institute of Technology, 1974.

UDC 532.51;533.601

A SOLID PREVIOUSLY DEFORMABLE PROFILE IN A LIMITLESS FLUID

Kiev BIONIKA in Russian No 12, 1978, pp 13-21

[Article by B. S. Berkovskiy and T. G. Puchkova, Irkutsk State University]

[Text] Development of the aerohydrodynamics of previously deformable bearing components (BE)--profiles, wings, bodies and so on--is of theoretical and practical significance since it is related to the development of one of the trends of transient aerohydrodynamics of bodies and to research in bionics and the dynamic stability of the designs of flexible BE. Papers are known [4, 6] in which the problem of thin previously deformable profiles is studied analytically on the assumptions of small perturbation theory. Moreover, these materials [4, §5, Chapter 6] are only conditionally related to research on prescribed deformations. Real objects have a definite solid nature and therefore it is desirable to know the properties of at least schematized models of these objects.

The transient problem on previously deformable bearing components in a plane flow is studied in the proposed paper. The investigation was carried out on the basis of the approach outlined in [1] and on the basis of consideration of deformations of the traveling wave type with generalization to solid bearing components. The main apparatus of the investigation was the theory of acceleration potential [5]. The method of solution sharing by the structure of th square of the operator of the relationship of the velocity potential to the acceleration potential in small perturbation theory [2], which is a development of methods of solution-sharing [4, 5], is used for effective construction of solutions. The results of steady and transient theories of rigid bearing components follow as maximum cases of the solutions found at $k_1 = 0$ and $R_1 = 0$.

1. A previously deformable thin profile. Let us consider flow over a thin flexible profile S, deformable by given law, moving horizontally, uniformly and linearly at velocity V_0 in a limitless quiescent ideal incompressible homogeneous fluid at a zero edge angle of attack $\alpha_k = 0$.

Let us introduce the rectangular coordinate system xOy bound to the BE, the x axis of which we direct along the main motion and the y axis of which we direct vertically upward.

Let us write the equation of a thin deformable profile in the selected coordinate system: $y = f(x,t)$ and let us write the boundary value problem of flow in terms of the acceleration potential:

$$\Delta\Theta(p, t) = 0, \quad p \in \Omega, \ t \in I,$$
$$\nabla\Theta(p, t) \to 0, \quad p \to \infty,$$
$$\{\Theta_y\}_{y=0} = D_1^1 f(x, t), \ x \in S_p, \tag{1}$$
$$[\Theta] = 0, \quad x = -a,$$
$$\Theta = 0, \quad t \leqslant t_0,$$

where $p = p(x, y)$, $D_1 = \partial/\partial t - V_0(\partial/\partial x)$ and S_p $(-a, a)$ is projection of the S profile onto the x axis, Ω is the region occupied by the fluid and I is the time interval.

Formally, the solution of the postulated problem (1) is given by the operator of a double layer [5]--$\Theta = A\bar{\gamma}$. Its properties and the boundary condition of flow over a thin deformable profile permit one to construct the integral equation

$$\bar{A}_0\bar{\gamma} = D_1^1 f(x, t), \quad x \in S_p,$$

or in inverted for n

$$\frac{1}{2\pi}\int_{-a}^{a} \bar{\gamma}(\xi, t)\frac{d\xi}{(x-\xi)^2} = \left(\frac{\partial}{\partial x^2} - 2V_0\frac{\partial}{\partial x\partial t} + V_0^2\frac{\partial}{\partial x^2}\right) f(x, t), \tag{2}$$

where the integral of the left side of equation (2) is understood in the sense of [5] and $\bar{\gamma}$ is the intensity of the characteristics in the space of the acceleration potential.

Based on the method of decision-sharing by the structure of operator D_1^2 (2), let us represent the solution of equation (2) as the sum

$$\gamma = \gamma_1 + \gamma_2 + \gamma_3. \tag{3}$$

where $\gamma_2 = \gamma_{21} + \gamma_{22}$ and γ_1 α_0^0 is the regular solution which takes into account irrotational effects, γ_{21} α_0^0 are regular solutions which take into account rotational effects and γ_3 α_0^∞ is a singular solution which takes into account rotational effects.

We note that equation (2) permits one to find only regular solutions [5]. According to (2) and (3), we find a number of integral equations of first kind to find regular solutions

$$\frac{1}{2\pi}\int_{-a}^{a} \bar{\gamma}_n(\xi, t)\frac{d\xi}{(x-\xi)^2} = \Phi_n(x, t), \quad n = 1, 21, 22. \tag{4}$$

the known specifics of singularity $\alpha = 2$ in equations (4) leads to the need to reduce the singularity by using operator

$$N_{01} = -\frac{1}{V_0} \times \int_{-\infty}^{x} [\ ]\,dx.$$

$$\frac{1}{\pi i}\int_{-a}^{a}\gamma_0(\xi,t)\frac{d\xi}{x-\xi}=N_{01}\Phi_0(x,t)+C_0(t). \tag{5}$$

where γ_0 is the intensity of the singularities in the space of the velocity potential. Thus, a number of singular integral equations of first kind with a Cauchy kernel is found. We find solutions of $\gamma_0(n = 1, 21, 22)$ of equations (5) by using the inversion operator [3]

$$\gamma_0(x,t)=-\frac{1}{\pi}\sqrt{a^2-x^2}\int_{-a}^{a}\frac{N_{01}\Phi_0(\xi,t)+C_0(t)}{\sqrt{a^2-\xi^2}\,(\xi-x)}\,d\xi \tag{6}$$

provided that

$$\int_{-a}^{a}\frac{N_{01}\Phi_0(x,t)+C_0(t)}{\sqrt{a^2-x^2}}\,dx=0 \tag{7}$$

The singular solution γ_3 is found in the space of the velocity potential from the equation

$$N_1\bar{\lambda}_3\gamma_3=D_1f(x,t)-N_1\bar{\lambda}_3(\gamma_1+\gamma_{21}+\gamma_{22}). \tag{8}$$

where $N_1 = D_1^{-1}$ is found from solution of the corresponding boundary value problem.

2. Deformations by travelling wave law. The foregoing is valid for arbitrary prescribed laws of small deformations--periodic and aperiodic. Let us consider prescribed deformations of the travelling wave type, i.e.,

$$f(x,t)=\delta e^{i(\omega t\pm kx)},$$

where δ is the amplitude of small deformations, $\omega = 2\pi\nu$ is the circular frequency, $k = 2\pi/\lambda$ is the wave number and λ is wavelength (the symbol $\pm$ indicate motion of the travelling wave along and opposite the flow, respectively).

Thus, the process under study is transient in time and space and, moreover, is periodic, i.e., one can assume that all the variable characteristics depend on time as $\bar{P}(x, t) = \bar{P}(x)e^{i\omega t}$ and the initial condition in the boundary value problem (1) is eliminated since

For generality of the investigation and of the results obtained, let us turn to a standardized coordinate system, introducing the transforms $x = a\bar{x}$, $y = a\bar{y}$ and $\bar{t} = V_0t/a$, which yield $D_1 = (V_0/a)\bar{D}_1$ and $N_{01} = (a/V_0)\bar{N}_{01}$.

$$\bar{f}(\bar{x},\bar{t})=\bar{\delta}e^{i(\bar{\omega}\bar{t}\pm\bar{k}\bar{x})}, \tag{9}$$

where

$$\bar{D}_1=\frac{\partial}{\partial\bar{t}}-\frac{\partial}{\partial\bar{x}},\quad \bar{N}_{01}=\int_{-1}^{1}(\;)\,d\bar{x},\quad \bar{f}=af,\quad \bar{\delta}=a\delta,$$

$$\bar{k}=\frac{ak}{V_0},\quad \bar{R}=\frac{2\pi}{\bar{k}},\quad \bar{\lambda}=\frac{\lambda}{a}.$$

The boundary value problem (1) assumes the form

$$\Delta\tilde{\Theta}(\tilde{\rho}, \tilde{t}) = 0, \quad \tilde{\rho} \in \tilde{\Omega}, \quad \tilde{t} \in (-\infty, \infty),$$
$$\nabla\tilde{\Theta}(\tilde{\rho}, \tilde{t}) \to 0, \quad \tilde{\rho} \to \infty,$$
$$(\tilde{\Theta}_{\tilde{\rho}})_{\tilde{\rho}=1} = \tilde{B}\tilde{\Theta}(\tilde{s}, \tilde{t}), \quad \tilde{s} \in (-1, +1),$$
$$[\tilde{\Theta}] = 0, \qquad \tilde{s} = -1,$$

where

$$\tilde{\Theta} = \frac{\Theta}{\gamma_0^2}, \quad \tilde{\rho} = \frac{\rho}{\rho_0}, \quad \tilde{B} = \frac{\partial^2}{\partial s^2} - 2\frac{\partial^2}{\partial s \partial t} + \frac{\partial^2}{\partial t^2},$$

and the integral equation (2) with regard to (9) assumes the form

$$\frac{1}{2\pi}\int_{-1}^{+1} \tilde{\gamma}(\zeta, t)\frac{d\zeta}{\zeta - \zeta^0} = -\tilde{\gamma}^0 e^{i(\omega t + \delta)} \pm 2ikRe^{i(\omega t + \delta)} - R^2 e^{i(\omega t + \delta)},$$

where $\tilde{\gamma} = \frac{\gamma}{\gamma_0}$

Reducing by $e^{i\omega t}$ and omitting the indices of normalization, we find

$$\frac{1}{2\pi}\int_{-1}^{+1} \tilde{\gamma}(\zeta)\frac{d\zeta}{\zeta - \zeta^0} = -\tilde{\gamma}^0 e^{i\delta} \pm 2ikRe^{i\delta} - R^2 e^{i\delta}, \tag{10}$$

where $\tilde{\gamma}^0$ is the amplitude value of γ.

Thus, equations (5) change in the considered case to equations

$$\frac{1}{2\pi}\int_{-1}^{+1} \tilde{\gamma}_n(\zeta)\frac{d\zeta}{s - \zeta} = N_{n1}\tilde{\Phi}_1(\tau) + \tilde{c}_n, \tag{11}$$

where $\tilde{\gamma}_n$ is the amplitude value of γ_n,

$$N_{n1}\tilde{\Phi}_1(\tau) = \mp\frac{\partial^2 \tilde{\Phi}}{\partial \tau^2}e^{i\delta\tau},$$

$$N_{n1}\tilde{\Phi}_{11}(\tau) = 2ikRe^{i\delta\tau},$$

$$N_{n1}\tilde{\Phi}_{12}(\tau) = \mp iR^2 e^{i\delta\tau}.$$

Solutions $\gamma_n \in a_0^0$ of equations (11), according to (6) have the form

$$\overset{\circ}{\gamma}_1(\xi) = \pm \frac{1}{\pi}\frac{\alpha\nu\theta}{\beta} i \sqrt{1-x^2}\int_{-1}^{1}\frac{e^{iR\xi}d\xi}{\sqrt{1-\xi^2}(x-\xi)}$$

$$\overset{\circ}{\gamma}_{21}(\xi) = -\frac{2}{\pi}(k\theta)\sqrt{1-x^2}\int_{-1}^{1}\frac{e^{iR\xi}d\xi}{\sqrt{1-\xi^2}(x-\xi)} \qquad (12)$$

$$\overset{\circ}{\gamma}_{22}(\xi) = \pm\frac{1}{\pi}(R\theta)\sqrt{1-x^2}\int_{-1}^{1}\frac{e^{iR\xi}d\xi}{\sqrt{1-\xi^2}(x-\xi)}$$

with regard to the fact that $\overset{\circ}{C}_n$, determined by condition (7) is

$$\overset{\circ}{C}_1 = \pm\frac{\alpha\nu\theta}{\beta} I_0(R), \quad \overset{\circ}{C}_{21} = -2ik\theta I_0(R), \quad \overset{\circ}{C}_{22} = \pm iR\theta I_0(R),$$

where $I_0(R)$ is a zero-order Bessel function of first kind.

We find solution $\overset{\circ}{\gamma}_3 \in h_1^*$ according to equation (8), where in the considered case

$$N_1 = -\frac{e^{ikx}}{\gamma_0}\int_{-\infty}^{x} e^{-ikx}(\ )dx,$$

from an equation of type

$$\frac{1}{2\pi}\int_{-1}^{1}\overset{\circ}{\gamma}_3(\xi)\left[\frac{1}{x-\xi} + ik e^{ikx}\int_{-\infty}^{x} e^{-ikx}\frac{dx}{x-\xi}\right]d\xi = i(k \mp R)\theta e^{ikx} -$$

$$-\frac{1}{2\pi}\int_{-1}^{1}\left[\overset{\circ}{\gamma}_1(\xi)+\overset{\circ}{\gamma}_{21}(\xi)+\overset{\circ}{\gamma}_{22}(\xi)\right]\left[\frac{1}{x-\xi}+ik e^{ikx}\int_{-\infty}^{x}\frac{e^{-ikx}dx}{x-\xi}\right]d\xi \qquad (13)$$

Assuming that $\overset{\circ}{\gamma}_3(x) = \overset{\circ}{a}_0\sqrt{\frac{1+x}{1-x}}$, by introducing all values of $\overset{\circ}{\gamma}_n$ (n = 1, 21, 22, 3) into equation (13) and carrying out integration, we find

$$\overset{\circ}{a}_0 = -2(k \mp R)\theta\{[iI_0(R) \pm I_1(R)]C(k) \mp I_1(R)\}, \qquad (14)$$

which yields

$$\overset{\circ}{\gamma}_3(x) = -2(k \mp R)\theta\{[iI_0(R) \pm I_1(R)]C(k) \mp I_1(R)\}\sqrt{\frac{1+x}{1-x}}. \qquad (15)$$

Thus, the general solution is as follows:

$$\gamma(x,t) = \Big\{\pm\frac{2i}{\pi}\frac{(k \mp R)\nu}{\beta}\theta\sqrt{1-x^2}\int_{-1}^{1}\frac{e^{iR\xi}d\xi}{\sqrt{1-\xi^2}(x-\xi)} -$$

$$-2(k \mp R)\theta\{[iI_0(R) \pm I_1(R)]C(k) \mp I_1(R)\}\sqrt{\frac{1+x}{1-x}}\Big\}e^{i\omega t}. \qquad (16)$$

where $I_{kn}(k)$ are special functions of first kind and $C(k)$ is a Theodorsen function [8]

Analysis of derived solutions (10) and (11) shows: 1) solution $v_{11}(x, t)$ is proportional to δ^2 and is dependent on number R; 2) $v_{21}(x, t)$ is proportional to δ and also dependent on R; 3) $v_{31}(x, t)$ is proportional to δ and is dependent only on R; 4) $v_{41}(x, t)$ has a more complex structure than the corresponding solution for a rigid oscillating profile and solutions (12) and 5) $\dot{v}_{51}(x)$ includes three types of distributed loads.

$$\dot{v}_{51}(x) = \dot{v}_{511}(x) + \dot{v}_{512}(x) + \dot{v}_{513}(x). \tag{17}$$

where $\dot{v}_{511}(x) = \alpha \Gamma(\beta \otimes R) A_1(R) \sqrt{\frac{1+x}{1-x}}$ is a singular quasi-steady solution,

$\dot{v}_{512}(x) = -\Gamma(\beta \otimes R) A_1(R) C(k) \sqrt{\frac{1+x}{1-x}}$ is a singular solution which determines the rotational damping of second kind and which "supports" loads of second kind, and

$\dot{v}_{513}(x) = \alpha \Gamma(\beta \otimes R) A_1(R) C(k) \sqrt{\frac{1+x}{1-x}}$ is a singular solution which determines rotational damping of third kind and which "supports" loads of third kind. 5) singular solution (17) on vector e_{51} of (18) determines the suction force on the leading edge and its structure, which is important from the viewpoint of analyzing the applicability of the bearing component under study as an impeller. General solution (18) contains combinations of the enumerated effects and determines the complex play of forces.

The lifting force Y and moment M_z of the bearing component are determined by known formulas

$$Y = \rho b^2 \omega^2 \int_{-1}^{1} \gamma(x, t)\, dx, \tag{19}$$

$$M_z = \rho b^3 \omega^2 \int_{-1}^{1} \gamma(x, t)(x - x_0)\, dx. \tag{20}$$

where the moment is taken with respect to some point of reduction of x_0.

In our case for $x_0 = 0$

$$Y = -\pi \rho b^2 \omega^2 (\alpha \otimes R) \left[i A_1(R) \otimes I_1(R) C(k) \otimes \frac{b}{2} I_1(R) \right] e^{i\omega t}, \tag{21}$$

$$M_z = -\pi \rho b^3 \omega^2 (\alpha \otimes R) \left[i A_1(R) \otimes I_1(R) C(k) \otimes I_2(R) \otimes i \frac{\alpha \otimes b}{2} I_2(R) \right] e^{i\omega t} \tag{22}$$

Here and further the final results are found by division of the real parts. Expressions (18), (20) and (21) for $\dot{x}_0$, lifting force and moment correspond to the solutions found by using an integral Laplace transform and methods of the theory of functions of the complex variable in [6] for a wave traveling along the flow.

3. A solid profile. Let a previously deformable closed solid profile C move horizontally at small local angles of attack, uniformly and linearly at velocity v_0

to region 6, described in paragraph 1. The deformations are small and are organized on both unperturbed boundaries of the profile according to certain laws, specifically by laws of traveling waves. The postulated problem of flow on assumptions of small perturbation theory in terms of acceleration potential is formulated omitting the indices of normalization) in the following manner in the aforedescribed coordinate system described above:

$$\begin{gathered}\Delta\Phi=0,\quad \rho\in\Omega,\quad t\in I,\\ \nabla\Phi\to 0,\quad \rho\to\infty,\\ (\Phi_n)_{y=0}=f_{1y}'(x,t),\quad x\in[-1,\ +1],\\ (\Phi_n)_{y=0}=f_{2y}'(x,t),\quad x\in[-1,\ +1],\\ [\Phi]=0,\quad x=-1,\end{gathered}\tag{22}$$

where

$$f_i(x,t)=f_{i0}(x)+f_{i1}(x,t)\tag{23}$$

are equations of the shapes of the upper ($i=1$) and lower ($i=2$) sides of the profile, respectively, $f_{i0}(x)$ are equations of undeformed boundaries,

$$f_{i1}(x,t)=h_i e^{i(\omega t+\varphi_i)}\tag{24}$$

are small prescribed deformations of the boundaries and h_i are the amplitudes of the deformations.

In view of the closed nature of the shape of the profile

$$f_1(-1)=f_2(-1),\quad f_1(1)=f_2(1)\tag{25}$$

For a profile with rounded leading and tapered trailing edges with zero angle of taper of the latter, which is determined by the developed theory, besides the conditions similar to (25), conditions of type $f_{10}'(1)=-\infty$, $f_{20}'(1)=\infty$ and $f_{10}'(-1)=f_{20}'(-1)=0$ make sense will occur for f_{i0}.

Two versions are possible in this case. The first--there are conditions for the product by f_1 that automatically place conditions on the type of shapes of f_{11} and is strictly necessary for the flow problem in accurate postulation, but significantly limits the possibilities of the investigation. Small perturbation theory 'softens' the conditions by derivatives and therefore a second version is possible--without conditions for derivatives f_1 and f_{11}.

In the general case we represent the shape of the deformable profile in the form of the sum of two shapes: 1) symmetrical which forms a thin deformable NP--Ω_0, located at some edge angle of attack $\alpha_0\neq 0$ and 2) symmetrical, which forms a symmetrically deformable closed profile Ω having a straight mid-line located at $\alpha_0=0$, i.e.,

$$f_1(x,t)=f'(x,t)+f^*(x,t),\quad f_2(x,t)=f'(x,t)-f^*(x,t),\tag{26}$$

where

$$\left.\begin{aligned} f^{+}(x,t) &= f_0^{+}(x) + f_1^{+}(x,t), \qquad f^{-}(x,t) = f_0^{-}(x) + f_1^{-}(x,t) \\ f_0^{+}(x) &= \frac{f_{10}(x) + f_{20}(x)}{2}, \qquad f_1^{+}(x,t) = \frac{f_{11}(x,t) + f_{21}(x,t)}{2}, \\ f_0^{-}(x) &= \frac{f_{10}(x) - f_{20}(x)}{2}, \qquad \gamma_1(x,t) = \frac{f_{11}(x,t) - f_{21}(x,t)}{2}. \end{aligned}\right| \tag{27}$$

Here f_0^0 is the equation of the shape of a thin "rigid" NE--S_{00}, f_1^0 is the equation of the shape of some thin previously deformable NE--S_{01}, f_0^c is the equation of the shape of the upper boundary of a solid "rigid" NE--$S_{\delta 0}$ and f_1^c is the equation of the shape of the upper boundary of some solid previously deformable NE--$S_{\delta 1}$. As follows from (26) and (27), two cases are possible: $f_{11} = f_{21}$ and $f_{11} \neq f_{21}$, to which correspond profiles of fixed and variable thickness and cross-sectional area.

Investigation of the aerohydrodynamics of a solid previously deformable profile in a limitless fluid in the case of variable thickness reduces to study of two independent problems: the problem of flow over a thin previously deformable profile S_0 located at $\alpha_k \neq 0$ and the problem of flow over a solid, symmetrically deformable profile S_δ, having a straight mid-line located at edge angle α equal to zero. Each of these problems is broken down into pairs of independent problems: 1) the problem of flow over a thin "rigid" profile S_{00} and a thin previously deformable profile S_{01} and 2) the problem of flow over a solid symmetrical rigid profile $S_{\delta 0}$ and a solid symmetrical previously symmetrically deformable profile $S_{\delta 1}$, which are arranged at $\alpha_k = 0$.

The investigation is simplified in the case of a profile of fixed thickness and problem (2) reduces to a problem of flow only over a rigid profile $S_{\delta 0}$.

Formally, solution of boundary value problem (22) is given by the sum of operators of simple and double layers [5]:

$$\theta = A_1\bar{\bar{\chi}} + A_2\bar{\bar{\gamma}}, \quad \rho \in \Omega. \tag{28}$$

The properties of operators (28) and the boundary conditions of flow over a solid profile reduce to two equations:

$$\begin{aligned} -\frac{1}{2}\bar{\bar{\chi}} + \bar{\bar{A}}_{2\omega}\bar{\bar{\gamma}} &= F_{+}(x,t), \\ \frac{1}{2}\bar{\bar{\chi}} + \bar{\bar{A}}_{2\omega}\bar{\bar{\gamma}} &= F_{-}(x,t). \end{aligned} \tag{29}$$

where

$$\bar{\bar{A}}_{2\omega}\bar{\bar{\gamma}} = \lim_{\substack{\omega \to 0 \\ \rho \to \omega}} \bar{\bar{A}}_{2\omega}\bar{\bar{\gamma}}$$

The sum and difference of equations (29) yield an integral equation with respect to $\bar{\bar{\gamma}}$ and the relationship for determination of $\bar{\bar{\chi}}$.

$$\bar{\bar{A}}_{2\omega}\bar{\bar{\gamma}} = F_{2\omega}(x,t). \tag{30}$$

$$\bar{\chi} = -[F(x, t)]. \tag{31}$$

where

$$F_{ср} = \frac{F_+ - F_-}{2}, \quad [F] = F_+ - F_-, \quad F_+ = D^2 I_+, \quad F_- = D^2 I_-, \quad \text{i.e.,} \quad F_{ср} = -D^2 \frac{I_+ + I_-}{2}, \quad \bar{\chi} = -D^2 [I_+ - I_-].$$

Thus, the structure of $\bar{\chi}$ in the transient problem, similar to the structure of $\bar{\gamma}$ in (3), is determined by several effects, which in turn determines the nature of the pressure and force components caused by the solid angle of the deformable profile in a limitless medium.

For illustration let us consider the special case--an initially nondeformable symmetrical profile located at $\alpha_k = 0$, i.e., $f_{10} = -f_{20}$. Then, with regard to 23 and 24, the integral equation (30) will have the form

$$\bar{\lambda}_{kl} \bar{\gamma} = -\frac{1}{2} [\delta_1 (k_1 \mp R_1)^2 e^{i(R_1 x \pm R_1 \alpha)} + \delta_2 (k_2 \mp R_2)^2 e^{i(R_2 x \pm R_2 \alpha)}], \tag{32}$$

and expression (31) assumes the form

$$\bar{\chi} = -2 f'_{10}(x) + \delta_1 (k_1 \mp R_1)^2 e^{i(R_1 x \pm R_1 \alpha)} - \delta_2 (k_2 \mp R_2)^2 e^{i(R_2 x \pm R_2 \alpha)}, \tag{33}$$

which permits one to determine the pressure along the profile in the symmetrical part of the problem. Moreover, $\bar{\chi} = \bar{\chi}_0 + \bar{\chi}_1$, where $\bar{\chi}_0 = -2f'_{10}(x)$ is the steady and $\bar{\chi}_1$ is the transient part of χ. The form of the right side of (32) permits one to find the solution of the equation as the sum $\gamma(x, t) = \sum_{m=1}^{2} \gamma^{(m)}(x) e^{iR_m t}$. Thus, we find two integral equations

$$\bar{\lambda}_{kl} \bar{\gamma}^{(m)} = -\frac{1}{2} \delta_m (k_m \mp R_m)^2 e^{\pm i R_m \alpha}, \quad x \in [-1, +1], \; m = 1, 2,$$

similar to equation (10), i.e., the problem broke down into two problems on travelling waves on thin profiles for which the solution was already found in paragraph 1 and, consequently, there is a solution of the problem under consideration

$$\bar{\gamma}^{(m)}(x) e^{iR_m t} = \left\{ \pm i \frac{(k_m \mp R_m)^2}{\pi R_m} \delta_m \sqrt{1 - x^2} \int_{-1}^{+1} \frac{e^{\pm i R_m \zeta}}{\sqrt{1 - \zeta^2}(x - \zeta)} - \right.$$
$$\left. - \delta_m (k_m \mp R_m) \{ [i I_0(R_m) \pm I_1(R_m)] C(k) \mp I_1(R_m) \} \sqrt{\frac{1 + x}{1 - x}} \right\} e^{iR_m t}. \tag{34}$$

Thus, in the case of $f_{10} = -f_{20}$, the problem of a closed profile previously deformable due to its own boundaries in a limitless medium reduced to one of two superimposed travelling waves at $\alpha_k = 0$ and to the problem of a closed symmetrical symmetrically deformable profile located at $\alpha_k = 0$, permeable in the general case, which does not correspond to the boundary conditions of flow of boundary value problem (22).

There are apparently two methods of eliminating this nonconformity. The first is to supplement the boundary conditions of flow over an NE by terms which take into

account the permeability of the closed profile from the bottom and top, which in the case of solid boundaries is relatively simple, but requires additional investigations with regard to the effect of permeability on the bearing properties of the profile. The second is to establish conditions for the parameters of travelling waves in which the condition of nonpermeability is fulfilled. We make use of the latter below to determine a number of special cases of nonpermeable profiles. A more general approach is also possible--removal of the condition of the closed nature of the profile.

On the whole the problem under consideration describes a number of cases formed by combinations of parameters k_k and R_m, including cases of eel-like, travelling-pulsating and "flapping" motions, and is easily generalized at $\alpha_k \neq 0$ and specifically at $f_{10} = -f_{20}$.

A generalization of the problems considered in paragrahs 1-3 is the problem of a solid profile previously deformable due to deformations of its own initial boundaries and the initial mid-line, which yields

$$f_1^0 = \frac{f_{11} + f_{21}}{2} + \Delta f_1^0, \tag{35}$$

where Δf_1^0 are the prescribed deformations of the mid-line. This case leads to consideration of the asymmetrical problem on three superimposed prescribed forms of deformations, specifically of travelling waves, and does not alter the symmetrical part of the problem. An additional possibility of controlling the aerohydrodynamic characteristics appears in this case due to the appearance of $\gamma^{(3)}$ and of the parameters contained in it. This generalization is equivalent to some problem with deformations only of the initial boundaries of the profile and namely: $f_j = f_{j0} + f_{j1} + \Delta f_{j1}$, where

$$\Delta f_{11} = \Delta f_{21}, \tag{36}$$

i.e., $\Delta f_1^0 = \Delta f_{j1}$ and $\Delta f_1^c = 0$ in (35).

The case of deformation of only the mid-line of a solid profile is also of interest.

4. Conditions of permeability. The case of a previously deformable closed profile of variable thickness and cross-sectional area, to which the presence of permeability of the profile corresponds, was investigated in paragraphs 2 and 3. Let us determine cases of an inpermeable profile, as that required by boundary value problem (22), i.e., let us determine what parameters of deformability impermeable profiles should have.

Since an incompressible fluid is being considered, two types of criteria of impermeability--geometric and hydrodynamic--are possible. The geometric criterion of impermeability consists in the requirement of constant values of cross-sectional area (of profile) in plane problems or of the volume of a body in three-dimensional problems. The hydrodynamic criterion requires that the total abundance of source distribution--flows--which simulate the solid angle--be equal to zero.

In the considered case of $f_{10} = -f_{20}$ and $f_{11} \neq f_{21}$, the first criterion yields the condition

$$\frac{\delta_1}{R_1}\cos k_1 l \cdot \sin R_1 + \frac{\delta_2}{R_2}\cos k_2 l \cdot \sin R_2 = 0. \tag{37}$$

Since $\delta_j \geq 0$, $k_j \geq 0$ and $R_j \geq 0$, then at $\delta_1 \neq \delta_2$, $k_1 \neq k_2$ and $R_1 \neq R_2$, the conditions of constant impermeability follow from (37)

$$\sin R_1 = 0, \quad \sin R_2 = 0 \tag{38}$$

or

$$R_1 = m\pi, \quad R_2 = n\pi, \tag{39}$$

where $m \neq n$ in the general case. Conditions (38) and (39) are equivalent to conditions

$$\lambda_1 = \frac{2}{m}, \quad \lambda_2 = \frac{2}{n}, \tag{40}$$

which denote that whole numbers of travelling waves λ_j should be added on the geometric chord of the profile, i.e., the specific range of wavelengths is determined.

The second hydrodynamic criterion of impermeability has the known form $\int_{-1}^{+1} \chi(x, t)\,dx = 0$, where $\chi(x, t) = -D_1[f_1(x, t) - f_2(x, t)]$. In the case under study $\chi(x, t) = [f_{10}(x) - f_{20}(x)]' - i(k_1 \mp R_1)\delta_1 e^{i(k_1 x \pm R_1 n)} + i(k_2 \mp R_2)\times\delta_2 e^{i(k_2 x \pm R_2 n)}$, which yields the condition (with appropriate selection of f_{10} and f_{20})

$$(k_1 \mp R_1)\delta_1 e^{ik_1 x}\cdot\sin R_1 - (k_2 \mp R_2)\delta_2 e^{ik_2 x}\cdot\sin R_2 = 0, \tag{41}$$

equivalent to condition (37) and conditions (38)-(40) which ensue from it. Various special cases follow from condition (37) and (41).

Generalization of the problem of the solid profile previously deformable due to its own initial boundaries for the case of prescribed deformations of the mid-line does not alter the conditions of impermeability since (36) corresponds to this problem.

5. Lifting force and moment. The total aerohydrodynamic characteristics for a previously deformable impermeable profile are determined by formulas (18) and (19) and in the case of prescribed deformations of boundaries and of the mid-line at $f_{10} = -f_{20}$ are described by the equation

$$Y = -\pi\rho V_\infty^2 \left\{\sum_{n=1}^{\infty} \delta_n(k_n \mp R_n)\left([iI_0(R_n) \pm I_1(R_n)]C(k_n) \pm \frac{k_n}{R_n} I_1(R_n)\right)\times\right. \tag{42}$$
$$\left.\times e^{ik_n x} + 2\delta_1(k_1 \mp R_1)\left([iI_0(R_1) \pm I_1(R_1)]C(k_1) \pm \frac{\delta_1}{R_1} I_1(R_1)\right)e^{ik_1 x}\right\}$$

and specifically, for $x_0 = 0$

$$M_z = -\frac{1}{2}\pi\rho V_\infty^2 \left\{\sum_{n=1}^{\infty} \delta_n(k_n \mp R_n)\left([iI_0(R_n) \pm I_1(R_n)]C(k_n) \mp I_1(R_n) \mp\right.\right.$$

$$\mp i\frac{\lambda_m \mp R_m}{R_m} I_1(R_m)\Big) e^{i\lambda_m x} + 2\lambda_0(\lambda_0 \mp R_0)\left(\left[i I_0(R_0) \pm I_1(R_0)\right] C(\lambda_0) \mp \right.$$

$$\left. \mp i\frac{\lambda_0 \mp R_0}{R_0} I_1(R_0)\right) e^{i\lambda_0 x}\Bigg\}. \qquad (43)$$

From (42) and (43) we find coefficients C_γ and m_β and the coordinates of the points of application of equivalent loads of different nature. The latter is necessary to investigate the problem of thrust.

6. Remarks. The problem of previously deformable thin and solid profiles, specifically deformable by laws of travelling waves, is studied in the paper on the assumptions of small perturbation theory. Based on the method of solution-sharing with respect to the structure of operator D_1, an approach is outlined for investigating problems for previously deformable solid bearing components and precise analytical solutions of integral equations of a thin flexible profile and a solid profile previously deformable due to its own initial boundaries--transient distributed characteristics--were found and analyzed. The problem is generalized for the case of prescribed deformation of the initial mid-line of the profile. The conditions of impermeability of a solid profile previously deformable according to laws of travelling waves were constructed. The total transient aerohydrodynamic characteristics were found. The results of steady and transient theory of a rigid profile follow from the results of the paper as special cases.

BIBLIOGRAPHY

1. Berkovskiy, B. S., "Investigating the Aerohydrodynamics of Rigid and Deformable Wings in a Limited Fluid," PRIKL. MATEMATIKA, No 2, 1971.

2. Berkovskiy, B. S., "Investigating the Transient Hydrodynamics of a Flexible Wing in a Limited Fluid," Report Topics of the All-Union Symposium on the Aerohydrodynamics of Ships With Dynamic Principles of Support (Krilov Lectures, 1972), SB. NAUCH.-TEKHN. O-VA SUDOSTROIT. PROM-STI, No 177, 1972.

3. Gakhov, F. D., "Boundary Value Problems," Moscow, Fizmatgiz, 1963.

4. Nekrasov, A. I., "Teoriya kryla v nestatsionarnom potoke" [The Theory of a Wing in a Transient Flow], Moscow, Izd-vo AN SSSR, 1962.

5. Panchenkov, A. N., "Teoriya potentsiala uskoreniy" [The Theory of Acceleration Potential], Novosibirsk, Nauka, 1975.

6. Wu, T. Y., "Hydromechanics of Swimming Propulsion," Part 1, JOURNAL OF FLUID MECHANICS, Vol 46, No 2, 1971.

UDC 62-50+597+591.173

THE PROBLEM OF SWIMMING OF FISH

Kiev BIONIKA in Russian No 12, 1978 pp 22-33

[Article by N. N. Gvozdkov, S. M. Zil'bershteyn and O. V. Miklyaeva, Voronezh Polytechnical Institute]

[Text] The dynamics of motion of aquatic animals and fishes has long attracted the attention of investigators. However, as can be seen from a recently published survey [3], there are as yet no adequately precise concepts on the mechanism of the interaction of the fish's body with the fluid medium during motion. At the same time it is clear that optimum mechanisms of body-fluid interaction should be developed during evolutionary development of organisms. Thus, the motion of fish is a complex process of optimum interaction of a multilevel system with the external environment. Unfortunately, the dynamics of the systems of organisms is insufficiently developed and therefore it is still impossible to solve the complete problem of the motion of fish. One is usually distracted from internal self-control of the organism and the attention is concentrated on the external hydrodynamic interaction of the fish's body and the fluid, simplifying in this case the concepts on the shape of the fish's body and its external organs of locomotion and the viscous effects in the fluid are sometimes disregarded.

Existing approaches of describing mechanisms of swimming utilize analytical ideas constructed with respect to problems of the transient vortex theory of a thin wing or the source theory of a body [4, 5, 8-10]. Both of the indicated analytical methods of aerodynamics yield approximately identical values for the force of thrust of a model of a moving fish, but these methods are still hardly adaptable to description of the mechanisms of interaction of the fish's body and the fluid medium. Specifically, it is unclear which parameters that change the shape of the model of the body of an aquatic animal have a more significant effect on the thrust and energy of motion.

Thus, a low-aspect wing or even simpler, an oscillating plane fin wing moving in an ideal fluid, can be used in the most simplified postulation as a model of a moving fish. Obviously, a low-aspect wing is a more suitable model. However, one should bear in mind that the model of a plane wing, on the basis of the hypothesis of plane cross-sections, is an integral part of a wider model of a finite-span wing. The parameters which optimize the thrust of a thin wing will also apparently optimize the thrust of a low-aspect wing. There are similar methods of calculations using a computer for calculating the thrust of a plane profile [4, 5], whereas methods of calculating the thrust are much more complex for a low-aspect wing and

require development of the suitable algorithms for computer application. All the foregoing led to the adoption of the simplest model of a fish--a plane wing--for analyzing in first approximation the effect of bending parameters on thrust.

The results of applying an algorithm [2] developed for transient motion of a thin wing to calculation on a digital computer of the thrust of a profile which simulates a swimming fish are presented in the given paper.

The main method of locomotion of fish in water is so-called undulation swimming--bending of the body in which the deformation wave travels from head to tail. Two extreme conditions are possible: eel-like (the wave amplitude is constant along the body) and mackerel-like (the wave travels along the extremity of the body to the tail).

The results of calculating the thrust coefficient for eel-like swimming conditions of a model using experimentally established parameters for bluefish are presented in the paper [6]. The calculating algorithm was calculated under the following conditions [2]:

1. The initial motion of a thin profile which simulates a swimming fish is assumed steady and accomplished at velocity $V^0(s, t_0)$ with respect to the reading system in which the fluid is quiescent at infinity. One can then determine the initial vorticity $\gamma(s, t_0)$ at the points of the profile l from the condition of nonflow of the fluid through the profile

$$Im\left\{e^{i\theta(s,t)}\left[\frac{1}{2\pi i}\int_0^l \frac{\gamma(\sigma)\,d\sigma}{z(s,t_0)-z(\sigma,t)} - V^0(s,t)\right]\right\} = 0, \qquad (1)$$

where s is the point of the profile, l is the length of the moving profile and θ is the angle between the tangent to the profile and the x axis.

2. For numerical calculation the profile is divided by points σ_k into N equal segments with length $\varepsilon = l/N$. The vortex layer with continuous intensity $\gamma(\sigma)$ on each segment $\sigma_{j+1} - \sigma_j$ is replaced by the total discrete vortex located at its center of gravity z_j, while the condition of nonflow is placed at point Z_k, where the normal velocities induced by the continuous vortex layer of segments and the system of discrete vortices are identical. It is noted [2] that the position of the coordinates of points Z_k and z_j on segments of the profile of a thin wing is hardly dependent on the type of shape of the profile, but it may be assumed fixed for the division when $N \geq 15$. Equation (1) then forms a system of linear algebraic equations for intensity Γ_j of discrete vortices

$$Im\left\{e^{i\theta_k}\frac{1}{2\pi i}\left[\sum_{j=1}^{N}\frac{\Gamma_j}{Z_k - z_j} - \int_0^l \frac{\gamma(\sigma)\,d\sigma}{Z_k - z(\sigma)}\right]\right\} = 0. \qquad (2)$$

3. In time the motion of the profile becomes quasi-steady and a free vortex layer then comes off its trailing edge. It is further assumed that the generatrix of thrust with subsequent average motion provides motion of the profile. The elementary segment of the flowing layer is assumed linear at the moment of departure

and oriented by the rate of departure. The discrete vortices equivalent to a free layer are regarded at discrete moments of time t_n by steps of development $t_{n+1} - t_n$ as determined by the condition $t_{n+1} - t_n = \varepsilon/U(t_n)$, where $U(t_n)$ is the relative velocity of the flowing layer at the point of departure from the profile. The centers of the vortices equivalent to the free layer at the moments of departure correspond to their position on the profile prior to departure and then shift to the middle of the segment by step $n \geq (1/2)N$. The points of nonflow are transformed in the free layer to points of continuity and approach the centers of the distances between adjacent vortices.

The intensity of the system of vortices Γ_k and γ_n on the profile and in the wake formed by the end of the n + 1 time step and also the intensity γ_{n+1} of the vortex formed during this time step is determined from the linear equations

$$\begin{gathered} Im\left\{e^{i\theta_k}(v_{n+1}-iv)\left|\frac{1}{2\pi i}\sum_{m=1}^{N}\frac{\Gamma_m}{z_k-z_m}+\frac{1}{2\pi i}\sum_{j=1}^{n+1}\frac{\gamma_j}{z_k-z_j}+V(z_k,t_{n+1})\right|\right\}=0, \\ \sum_{m=1}^{N}\Gamma_m(t_{n+1})+\gamma_{n+1}=\sum_{m=1}^{N}\Gamma_m(t_n). \end{gathered} \tag{3}$$

The coefficients of system (3) are calculated according to the law of variation of the profile and its motion.

4. The thrust of the profile consists of the resulting pressure along both sides of the profile added along its components of length and suction force. The coefficient of pressure $C_{T_n}^{(1)}$ on step n, found by relating the force of total pressure to $(1/2)\rho V^2 l$, is represented by the expression

$$C_{T_n}^{(1)}=\varepsilon\sum_{k=1}^{N}\Gamma_k\left[v_{ex}(\sigma_k)-v_{ex}(\sigma_k)\right]+Q_n, \tag{4}$$

where

$$v_{ex}(\sigma_k,t_n)=Re\left\{e^{i\theta_k}\cdot\overline{(\cdot)}\frac{1}{2\pi i}\left[\sum_{m=1}^{N}\frac{\Gamma_m}{z_k-z_m}+\sum_{j=1}^{n}\frac{\gamma_j}{z_k-z_j}\right]\right\}.$$

Q is a term determined by contribution of the n-th step to the value of the coefficient of thrust, determined by variation of the intensity of vortices on the profile.

The coefficient of thrust of the suction force $C_{T_n}^{(2)}$, according to [2, 7], after being related to $(1/2)\rho V^2 l$, assumes the form

$$C_{T_n}^{(2)}=\frac{\pi\cos\theta_0}{2\varepsilon}\left[\Gamma_1(2\sqrt{2}-1)-\Gamma_2\right]^2, \tag{5}$$

where θ_0 is the angle of inclination of the profile at the leading point and Γ_1 and Γ_2 are the intensity of the vortices on the first two segments of the profile.

Some procedure of establishing the conformity of the arc coordinate s and coordinate x is introduced for the calculations. The velocity components at points k (points of nonflow), formed by a singular vortex located at point σ_j, are then determined. These values are coefficients at unknown values of Γ_j in system (2) Calculation of Γ_n and γ_j of system (3) is prepared in similar fashion. The contour of the profile was divided in 15 parts and 30 time steps were considered in subsequent motion.

The program of calculations consists of two parts. The initial values of discrete vortices on Σ_1 are found in the first part and the values of Γ_k on each time step, the thrust and total coefficient of thrust are found in the second part.

The calculations were carried out for deformations of a profile which simulate eel-like motion in two modes:

$$1.\ y = A\sin(kx - \omega t). \tag{6}$$

$$2.\ y = Ax\sin(kx - \omega t). \tag{7}$$

The initial (dimensionless) parameters contained in (6) and (7) were assumed, according to mean experimental data of [6], as follows for the bluefish: $A = 0.066$, $k_0 = 2\pi/\lambda_0 = 8.4$, $\omega_0 = c_0 k_0 = 12.35$, where λ_0 and c_0 are the mean length and velocity of the deformation wave of the profile, respectively. The calculations were carried out on the M-222 computer. Approximately 30 minutes of machine time was expended to calculate a single value of C_T. The calculations showed that both the suction force and the pressure on the profile, by retaining the sign, fluctuate by time steps. The coefficient of thrust has a greater value during the first steps, then, decreasing, approaches the value indicated in the table by the 5th-10th step. The value of C_T fluctuates for mode 1 during initial time steps and decreases monotonically for mode 2.

Values of C_T

λ/λ_0	c/c_0				
	2/3	1	4/3	2	3
1/3	0.002	—	—	0.144	0.018
2/3	(0.070)	(0.184)	—	—	—
	0.070	0.016	—	—	—
3/4	—	—	0.028	0.100	0.312
1	—	(0.028)	(0.085)	—	—
		0.002	0.007	—	—
3/2	0.000	—	—	0.005	0.013

The table of values of coefficient C_T, established during the final time steps of calculation with variation of the value of wavelength and the rate of propagation, is presented.

The values of C_T for mode 1 are indicated in the parentheses in the table. The values of C_T are close to those found for a thin body in [5, 9, 10] for mode 1 at

$\lambda/\lambda_0 = c/c_0 = 1$. There is a twofold increase of C_T with "normal" rate of deformation ($c = c_0$) and truncation of wavelength ($\lambda = (2/3)\lambda_0$ and also with "normal" wavelength ($\lambda = \lambda_0$) and with an increase of the rate of deformation ($c = (4/3)c_0$), while one-time truncation of wavelength ($\lambda = (2/3)\lambda_0$) and an increase of the rate of deformation lead to a fourfold increase of the thrust coefficient.

The value of C_T decreases by 1.5 orders in mode 2 for $c/c_0 = \lambda/\lambda_0 = 1$ compared to the value in mode 1, and at $\lambda = (3/4)\lambda_0$ coincides with the value for mode 1 at $c/c_0 = \lambda/\lambda_0 = 1$.

The effect of variation of wavelength and rate of deformation on the thrust coefficient is noted inboth modes and the values of C_T increase at wavelength of $\lambda \leq \lambda_0$ with an increase of c/c_0 in the range $(2/3)c_0 \leq c \leq c_0$, revealing a tendency to form a maximum at $\lambda = (1/3)\lambda_0$ and a minimum at $\lambda = (3/2)\lambda_0$.

The values of C_T significantly exceed those at $c/c_0 = \lambda/\lambda_0 = 1$ at fixed rates of deformation in the range of $(4/3)c_0 \leq c \leq 3c_0$ and wavelengths $\lambda \geq \lambda_0$.

Thus, the thrust coefficient depends on the relationship between wavelength and rate of its motion along the profile in eel-like motion in modes 1 and 2. Obviously, there are optimum modes of bending of the profile in which the thrust coefficient significantly exceeds the values found in [5, 9, 10].

BIBLIOGRAPHY

1. Belotserkovskiy, S. M. "Krylo v nestatsionarnom potoke gaza" [A Wing in a Transient Gas Flow], Moscow, Nauka, 1974.

2. Gorelov, D. N. and R. L. Kuliyev, "The Nonlinear Problem of Transient Flow of an Incompressible Fluid Over a Thin Profile," MEKHANIKA ZHIDKOSTI I GAZA, No 6, 1971.

3. Kokshayskiy, N. V., "Ocherk biologicheskoy aerodinamiki" [Essay on Biological Zerodynamics], Moscow, Nauka, 1974.

4. Lighthill, M. J., "The Hydrodynamics of Motion of Aquatic Animals;" MEKHANIKA, No 1, 1972.

5. Logvinovich, G. V., "The Hydrodynamics of a Thin Flexible Body," BIONIKA, No 4, 1970.

6. Pyatetskiy, V. Ye., "The Hydrodynamic Characteristics of Swimming of Some Fast-Swimming Fishes," BIONIKA, No 4, 1970.

7. Sedov, L. I., "Ploskiye zadachi gidrodinamiki i aerodinamiki" [Plane Problems of Hydrodynamics and Aerodynamics], Moscow, Nauka, 1966.

8. Lighthill, M. J., "Mathematics and Aeronautics," J. ROY. AERONAUT. SOC., Vol 64, No 595, 1960.

9. Wu, T. Yao-Tsu, "Hydromechanics of Swimming Propulsion, Part 1, Swimming of a Two-Dimensional Flexible Plate," JOURNAL OF FLUID MECHANICS, Vol 46, No 2, 1971.

10. Wu, T. Y., "Hydromechanics of Swimming Propulsion, Part 3, Swimming in Optimum Moments of Slender Fist Side Fins," JOURNAL OF FLUID MECHANICS, Vol 46, No 3, 1971.

UDC 517.4

THE PARAMETRIC METHOD OF INTEGRATING EQUATIONS OF MOTION OF A TURBULENT FLUID

Kiev BIONIKA in Russian No 12, 1970 pp 26-33

[Article by Yu. T. Borshchevskiy, A. D. Dyachuk and E. N. Litvinenko, Voronezh Polytechnical Institute]

[Text] 1. Following [1-3], solution of the system of equations

$$\omega_0 \frac{\partial v_i}{\partial t} + v_j \frac{\partial v_i}{\partial x_j} = -\frac{\partial p}{\partial x_i} + \frac{\partial \sigma_{ij}}{\partial x_j \rho}, \tag{1}$$

$$\frac{\partial v_j}{\partial x_j} = 0 \ (i, j = 1, 2, 3); \tag{2}$$

$$x_i = \frac{\tilde{x}_i \tilde{\omega}_0}{\tilde{v}}, \ t = \tilde{\omega} \tilde{t}, \ \omega_0 = \frac{\tilde{\omega}}{\tilde{\omega}}, \ v_j = \frac{\tilde{v}_j}{\tilde{v}_0}, \ p = \frac{\tilde{p}}{\tilde{\rho} \tilde{v}_0^2}$$

(where, besides the generally accepted terms, $\tilde{\omega}$ is typical frequency and the tilda is a sign of dimensionality) for a strongly sheared flow can be represented in the form

$$v_j \approx \frac{2m}{c_1 - \eta} \frac{\partial \eta}{\partial x_j} \quad (\eta = c_2 - 2m \ln (c_1 - \eta)), \tag{3}$$

where parameter η is determined from

$$\omega_0 \frac{\partial \eta}{\partial t} - \frac{\partial^2 \eta}{\partial x_j \partial x_j} = \delta (x, t) f_0 (x, t). \tag{4}$$

c_1 and c_2 are integration constants $f_0(x, t)$ is a function of the distribution density of pressure fluctuations and $\delta(x, t)$ is a unit functional. According to (3), components $v_j(x, t)$ are determined with accuracy up to components $v_j^{(n)}(x, t)$ of isotropic turbulence.

2. At $c_1 = 0$, based on (3) we have

$$v_j = -2m \frac{1}{\eta} \frac{\partial \eta}{\partial x_j}. \tag{5}$$

Or, following [2], after integration with respect to x_j

$$\eta = C(t)\exp\left[-\frac{1}{2\mu}\int_0^{x_j}(\theta_1 + v_1' + v_1'' + \dots)\,dx_j\right] = \tag{8}$$

$$= C(t)\exp\left[-\frac{1}{2\mu}(\Delta\eta_1 + \Delta\eta_2 + \dots)\right] = \eta_1\eta_2\dots\eta_{n-1}.$$

where η_j and $\Delta\eta_j$ are functions which take into account the corresponding contributions of velocity to the total field and $C(t)$ is an integration constant which is a function of time t. The derived expression indicates that the method of superposition of partial solutions can be used when investigating three-dimensional turbulent flows. Partial solutions can be regarded not only as solutions of $\eta_j(v_j^{(j)})$ or $v_j^{(j)}(\eta_j)$ related to scales, but also contributions of a more general type related, for example, to flow of expulsion from a body moving in a fluid, variation of pressure gradient and so on.

If the initial flow $v_j(x, 0)$ is given at $t = 0$, then according to (8)

$$\eta_0(x, 0) = C_0\exp\left[-\frac{1}{2\mu}\int_0^{x_j} v_j(x, 0)\,dx_j\right] \tag{7}$$

Based on (1) and (4), we have

$$\eta = 1 - \epsilon_0\frac{e^{\alpha t}}{(t)^{3/2}}\,e^{-\frac{r^2}{4\mu t}}, \tag{8}$$

where ϵ is the solution of a homogeneous equation of thermal conductivity corresponding to an instantaneous point source with intensity $\alpha_0 \neq 1$. It is obvious that to satisfy the given initial condition, there should be

$$\eta = \epsilon_0\eta_0 = C_0\frac{e^{\alpha t}}{(t)^{3/2}}\int_\Omega\exp\left[-\omega_0\frac{r^2(x, \xi)}{4\mu t} - \right.$$

$$\left. -\frac{1}{2\mu}\int_0^{x_j} v_j(x, 0)\,dx_j\right]d\xi_1\,d\xi_2\,d\xi_3 \tag{9}$$

$$r^2(x, \xi) = (x_1 - \xi_1)^2 + (x_2 - \xi_2)^2 + (x_3 - \xi_3)^2.$$

where Ω is the range of distribution of $v_j(x, 0)$. Accordingly, the parametric function η may be very convenient when solving problems with initial conditions.

Let us point out that the parametric function η determines the flow from transient vortices. Indeed, for a steady point source (a vortex), we find the following methods of descent by the variable t from (9)

$$\varphi(x) = \varphi(x) = -\int_{-\infty}^{\infty} \varphi(x, t)\, dt =$$

$$= -\left(\frac{\rho}{\pi}\right)^{\frac{1}{2}} \int_{-\infty}^{\infty} \frac{1}{(t^2+x^2)^{\frac{1}{2}}} e^{-\frac{x^2}{t^2}}\, dt = -\frac{\Gamma\left(\frac{1}{2}-1\right)}{\pi |x|^{1}}$$

Using this expression, we have

$$\varphi = c_0 + 2m \ln|x| + 2m \ln(kx) + 2\pi m \tag{10}$$

Comparing this formula with relation

$$\varphi = -\frac{\Gamma}{2\pi} \ln|x| + \text{const} \tag{11}$$

(where Γ is rotation of a steady point vortex), well-known in hydrodynamics, we note that the velocity field of the fluid induced by transient vortices is determined by using (3) and function φ.

Further favorable properties of the outlined method are the possibility of satisfying the variation principle using (3) and (8) and simple achievement of transient solutions using the same expressions in an arbitrary system of curvilinear orthogonal coordinates.

3. We assume that the considered flow moves along an elastically deformable boundary surface. We understand an elastically deformable surface as one on which local "depressions" which disappear due to elastic restoration of the surface material after cessation of the pressure pulse, may appear due to the effect of pressure pulses (as is known, which inevitably occur in a fluid in the vicinity of any surface). The properties of the material should determine the nature of surface deformation which satisfies the equation

$$\begin{aligned} &\sigma_0 \gamma(h) \frac{\partial h}{\partial t} = \frac{\partial}{\partial x_1}\left[\sigma(h) \frac{\partial h}{\partial x_1}\right] - k_1(h) \frac{\partial h}{\partial x_1} + \\ &+ Q \int_{-\infty}^{t} e^{-\frac{t-\tau}{t_0}} \frac{\partial}{\partial x_1}\left(\sigma \frac{\partial h}{\partial x_1}\right) d\tau + p'(x, t) \end{aligned} \tag{12}$$

$$\left(h = \frac{h'}{l},\ k_1 = \frac{k_1}{\rho' c_0^2},\ \sigma = \frac{\sigma'}{\rho' c_0 l}\right).$$

where $h(x, t)$ is the absolute deviation of the surface from its initial position in the region of the pressure pulse $p'(x, t)$ (Figure 1), $\sigma(h)$ is a function which has properties of the coefficient of surface tension, $k_1(h)$ is the coefficient of deformation resistance, $\gamma(h)$ is a converting function and Q and t_0 are constants which characterize the relaxing properties of the surface material. Let us assume that solution of equation (12) is known and is given by the function

$$h = h(x_1, x_2, t) = h(p') \tag{13}$$

It is obvious that the vertical velocity component of the fluid immediately adjacent to the surface is known during evolution of the depression on the surface due to the effect of p':

$$v_3(h) = u_n \frac{\partial \eta(x, t)}{\partial x} = v_3(p'). \tag{14}$$

The velocity components $v_1(h)$ and $v_2(h)$ approach zero, i.e., they have a higher order of smallness. If the pressure pulse in the fluid is sufficient to cause surface deformation, a unique "expulsion flow" should inevitably occur upon formation of the depression which will be superimposed on the entire flow at $x_3 > 0$. In this case one must take into account when determining parametric function η that the movable surface of any of the depressions of a boundary surface should be regarded as a movable system of sources which induces "expulsion flow" from the viewpoint of hydrodynamics. Therefore, the following expression is valid for the flow of an n-th depression on a surface [4]

$$\eta_n = \varepsilon_n' / \varepsilon_n = \int_0^t \int_S \frac{\Theta(x^*, t^*)\, a_0^{1/2}}{(2\sqrt{\pi})^3 (t - t^*)^{3/2}} e^{-\frac{a_0 r^2}{4(t-t^*)}} r \cos\alpha \frac{dS\, dt^*}{2(t - t^*)}. \tag{15}$$

where (x^*, t^*) are the four-dimensional coordinates of a movable surface S, $r = |x - x^*|$ and α is the angle between vector $\vec{xx^*}$ and the normal $\vec{n}$ to surface S at point x^*. In our case density is given by expression (14). The density on an arbitrary movable surface (for example, on the surface of a deformed bubble) is determined by using the integral Volterra equation

$$\Phi(t) = \frac{\Theta(x^*(t^*), t^*)}{2} + \int_0^t \int_S \frac{a_0^{1/2}\, \Theta(x^*(t), t^*)}{(2\sqrt{\pi})^3 (t - t^*)^{3/2}} \times \exp\left[-\frac{a_0 r^2}{4(t - t^*)}\right] r \cos\alpha \frac{dS\, dt^*}{2(t - t^*)}. \tag{16}$$

Based on the principle of superposition for a "expulsion flow" induced by a system of N transient perturbation sources with movable boundaries, we will have

$$\Delta\varphi^* = \varepsilon_1 - 2m \ln \prod^N (\varepsilon_1 - \eta_n) \tag{17}$$

and accordingly

$$\Delta v_i' = -\sum^N \frac{1}{\varepsilon_1 - \eta_n} \frac{\partial \eta_n}{\partial x_i}. \tag{18}$$

4. The solutions found above determine only the "vortex" component of the velocity field of a turbulent fluid. To describe the flow field directly in the wall region of the boundary layer, one must determine the still "laminar" velocity component of the fluid on the elastically deformable wall. Satisfying the condition of adhesion on the wall, we have

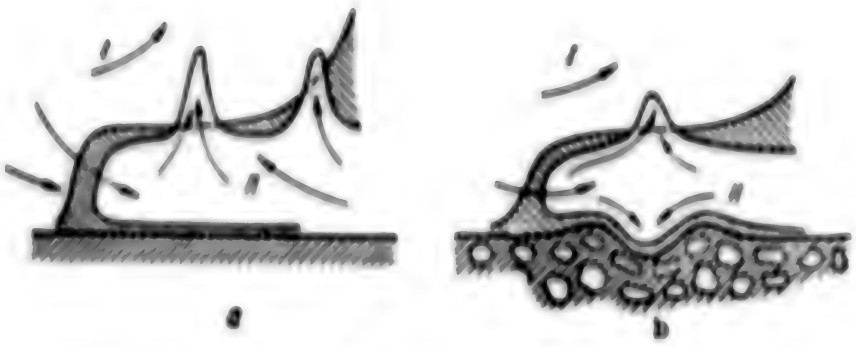

Figure 1. Diagram of Formation of Discharges During Motion of Turbulent Fluid Over Rigid (a) and Elastically Deformable (b) Surfaces

$$v_i = kx_i\varphi_0 + (\Delta v_{i\omega} + \Delta v'_{i\omega})(1 - \varphi_0), \tag{19}$$

where $\Delta v_{i\omega}$ is the vortex component of the velocity vector induced by the vortices distributed above the separation surfaces adjacent with respect to the resulting surface, $\Delta v_{i\omega}$, is the addition to the vortex component due to the mobility of local sections of the boundary surface and k is a proportionality constant. The function φ_0 related to pressure pulses is determined from the equation

$$\omega_0 \frac{\partial \varphi_0}{\partial t} + v'_j \frac{\partial \varphi_0}{\partial x_j} - \frac{\partial^2 \varphi_0}{\partial x_j^2} = \delta(x, t), \quad v'_j = v_j - \Delta v'_j, \tag{20}$$

in which $\delta(x, t)$ is a unit delta-function concentrated on the vortex surfaces $\sigma(x, t)$. When solving equation (20), let us introduce new variables

$$\varphi_0 = \varphi'_0(\xi_i), \quad v_0 = \frac{\Delta\varphi}{d\xi_i}, \quad \xi_i = \frac{x_i}{2\sqrt{t}} \tag{21}$$

(where ϕ as before is an analog of the velocity potential, $\Delta v_j = \partial\phi/\partial x_j$, $j = 1, 2, 3$) by means of which equation (20) reduces to the following

$$-\xi_i \frac{d\varphi'_0}{d\xi_i} + \frac{d\varphi}{d\xi_i}\frac{d\varphi'_0}{d\xi_i} - \frac{d^2\varphi'_0}{d\xi_i^2} = \delta(x, t). \tag{22}$$

Solution of this equation, which satisfies the condition of adhesion to the wall, has the form

$$\varphi'_0 = 1 - \frac{2}{\sqrt{\pi}} \int_0^{\xi_i} e^{-\frac{\xi_i^2}{4} + \omega\xi_i} d\xi_i. \tag{23}$$

Since transverse velocity v_j decreases due to the contribution of $\Delta v'_j$, the following expression should be placed in this expression according to (20) and (21)

$$\varphi(\xi_i) = \Delta\varphi(v_0) - \Delta\varphi^*(\Delta v'_j), \tag{24}$$

where the asterisk denotes the value induced due to partial surface mobility. At $\Delta v_1^* = 0$, i.e., in the absence of movable sections of the boundary surface, function $\phi \neq 0$ changes to a solution for an ordinary boundary layer. The following transformation is possible [2]:

$$\Delta\varphi^*(\Delta v_1^*) = \Delta\varphi^*(\xi), \quad \xi = \omega_*^{1/n} x_3 \rho \left(\int \rho^n d\eta\right)^{1/n}. \tag{25}$$

Therefore, we can write

$$\varphi_0^* = 1 - \operatorname{erf}\xi \cdot \exp\left[-f(\eta^*)\right], \tag{26}$$

where $f(\eta^*)$ is some function, the type of which depends on the solution for (12). As a result, for the profile of the longitudinal velocity of a fluid moving above an elastically deformable surface, we find the formula

$$v_1^* = \frac{\bar{v}_1}{\bar{v}_*} = kx_3\left(1 - e^{-\beta\eta^*}\right) + \left[v_1 - 2m\ln\left(c_1^* - \eta^*\right)\right]e^{-\beta\eta^*}. \tag{27}$$

In this formula the value

$$v_1 = kx_3\left(1 - \operatorname{erf}\xi\right) + \left(c_2 + c_1 \lg\eta\right)\operatorname{erf}\xi \tag{28}$$

is the velocity component in an ordinary turbulent boundary layer moving above a rigid surface. The constants in (28) are universal: $k = 0.4$, $c_2 = 5.2$ and $c_1 = 5.75$ and for an averaged flow $\langle\xi\rangle = 0.08\, x_3$. According to (18) and (24), one can also state that $\langle f(\eta^*)\rangle = \text{const}\cdot\text{Re}$, where Re is Reynolds number. In this case for the drag coefficient c_D for the case of motion of a flow along a plate on the basis of (27), following [5], it is easy to find the expression

$$c_D = 0{,}427\left(\lg \mathrm{Re} - 0{,}407\right)^{-1{,}64} e^{-c_3 \mathrm{Re}} + \left(1 - e^{-c_3 \mathrm{Re}}\right)\frac{1{,}328}{\sqrt{\mathrm{Re}}}, \tag{29}$$

which may change to a formula for c_D in either the laminar or turbulent flow mode over an elastically deformable surface under corresponding conditions.

We note that the Re number in (29) is compiled by the distance from the leading edge of the plate and the averaged contribution of $\langle\ln(c_1^* - \eta^*)\rangle$ is disregarded due to its smallness.

The values of coefficient c_D, found by using (29) at $c_3 = 8 \times 10^{-8}$, are shown in Figure 2 (curve 3); the presence of a transition region for an initial rigid surface was taken into account when constructing the left branch of this curve at $\mathrm{Re} < 10^7$. The experimental points on this figure were borrowed from the paper of M. O. Kramer [6].

A velocity profile $\bar{v}_1^*$, constructed by using (27) for an elastically deformable surface at $\mathrm{Re} = 16 \cdot 10^6$, is shown in Figure 3 (curve 3). Profile $\bar{v}_1$, which satisfies formula (28) (curve 1), profile $\bar{v}_1$ for a polymer solution (curve 2) and profile v_1 for a laminar flow (curve 4) are shown on the same figure for comparison. The formula for c_D, upon consideration of flow in a tube, unlike 29, has the form

$$\frac{1}{\sqrt{c_D}} = \left|2\lg \mathrm{Re}\sqrt{c_D} - 0{,}8\right| e^{-c_3 \mathrm{Re}} + c_1 \mathrm{Re}\sqrt{c_D}\left(1 - e^{-c_3 \mathrm{Re}}\right). \tag{30}$$

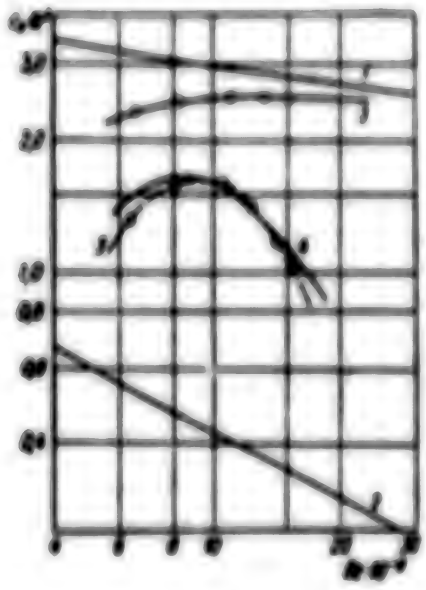

Figure 2. Drag Coefficient C_D: 1 and 2--during turbulent and laminar flow over a flat plate, respectively; 3 and 4--experimental curves for a cigar-shaped body with rigid and elastically deformable surface; 5--according to (29) for an elastically deformable surface

The latter formula has the same properties as (29) and both (30) and (29) indicate an "automodel" elastically deformable surface may contribute to a significant reduction of frictional drag due to partial extinction of turbulence.

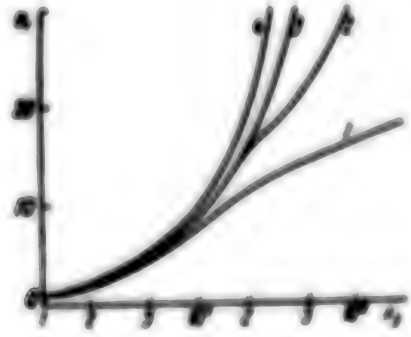

Figure 3. Velocity Profiles in Wall Layer: 1--according to (28) for ordinary turbulent boundary layer; 2--during motion of a polymer solution with concentration $\theta = 2 \cdot 10^{-5}$ g/cm^3; 3--according to (27) for an elastically deformable surface at $Re = 16 \cdot 10^6$; 4--profile $v_1 = x_3$

5. To take into account the relaxing properties of the fluid, the following value must be added to the right side of (1) [7]

$$\Delta\tau_{ij} = A \int_{-\infty}^{t} e^{-\frac{t-\tau}{\tau_0}} \frac{d}{dt_1}\left(\frac{\partial v_i}{\partial x_j}\right) dt_1. \qquad (31)$$

where A is a rheological constant and t_q is relaxation time. It is obvious from expression

$$-\nabla^2 p = \frac{\partial^2 \rho_0 v_i v_j}{\partial x_i \partial x_j} - A \int_{-\infty}^{t} e^{-\frac{t-\tau}{t_q}} \frac{\partial^2}{\partial x_i \partial x_j} \left(v, \frac{\partial v_i}{\partial x_j} \right) d\tau \tag{32}$$

that term (31) makes a contribution only in the presence of transient effects. It is difficult to find solution (1) with regard to (31) by the method of sequential approximations, having taken (3) and (4) as the initial values. Carrying out the corresponding calculations, we will have (Figure 3, curve 2)

$$v_1 = (1 - M) k x_1 (1 - \operatorname{erf} \xi) + \sqrt{c_1 + c_1 \lg \eta} \operatorname{erf} \xi + k M x_1 \tag{33}$$

and accordingly

$$\frac{1}{\sqrt{c_f}} = (2 \lg \mathrm{Re} \sqrt{c_f} - 0.8)(1 - M) + M (c_1 \mathrm{Re} \sqrt{c_f} + c_2). \tag{34}$$

At M = 0.148, c_1 = 0.0067 and c_2 = 26.7, the calculating values of the drag coefficient c_f are in good agreement with the "maximum" (least) values found when investigating the motion of polymer solutions in tubes of different diameter.

BIBLIOGRAPHY

1. Borshchevskiy, Yu. T., E. M. Litvinenko and V. G. Makhaychuk, "The Kinematics of a Turbulent Boundary Layer," IZV. AN SSSR, MEKHANIKA ZHIDKOSTEY I GAZOV, No 5, 1973.

2. Borshchevskiy, Yu. T. and E. M. Litvinenko, "The Structure of Turbulence in a Boundary Layer," IZV. AN SSSR, MEKHANIKA ZHIDKOSTEY I GAZOV, No 1, 1975.

3. Cowle, J., "A Quasilinear Parabolic Equation Found in Aerodynamics," MEKHANIKA, No 2, 1953.

4. Polozhiy, G. N., "Uravneniya matematicheskoy fiziki" [Equations of Mathematical Physics], Moscow, Vyssh. shkola, 1964.

5. Frenkel', Ya. I., "Kinematicheskaya teoriya zhidkostey" [The Kinematic Theory of Fluids], Moscow, Izd-vo AN SSSR, 1945.

6. Shlikhting, G., "Teoriya pogranichnogo sloya" [Boundary Layer Theory], Moscow, Izd-vo inostr. lit., 1956.

7. Kramer, M. O., "Boundary Layer Stabilization by Distributed Damping," ASME JOURNAL, No 2, 1960.

UDC 532.526-597.31

DEVELOPMENT OF TURBULENCE DURING FLOW OVER AN ELASTIC PLATE

Kiev BIONIKA in Russian No 12, 1978 pp 33-40

[Article by V. V. Babenko, Institute of Hydromechanics of the Ukrainian SSR Academy of Sciences]

[Text] Most birds and fishes are exposed to laminar flow over them during motion with regard to short body length. In those cases when turbulent flow occurs during motion of animals, mechanisms were developed during evolution which permit the animal to retain a quasi-transient flow mode in the boundary layer up to specific limits [1].

The hydrodynamic stability on rigid and elastic plates in a water flow were investigated to understand the principles of evolution of the structure of the external coverings of fast-swimming marine animals and also the study the physical pattern of fluid flow during the initial phase of transition of the laminar boundary layer to a turbulent boundary layer [2, 3]. The results of the investigations made it possible to conclude that the damping surfaces with proper selection of their mechanical properties, regardless of the type of disturbing motion, permit one to achieve at least one of the following effects: an increase of Reynolds number of the loss of stability, an increase of the transient zone and of the Reynolds number of transition, a decrease of the region of unstable oscillation frequencies of the laminar boundary layer, a decrease of the phase velocity of the disturbing motion, an increase of wave numbers and a decrease of the coefficients of increase, a decrease of the ordinate of the critical layer and a decrease of the kinetic energy of the disturbing motion.

Simultaneous action of several of the effects indicated above was usually observed during flow over damping surfaces since they are interrelated. The investigations also showed that the previously adopted criteria of similarity [4] simulate rather correctly the characteristics of flow over damping surfaces.

The telluric method [2-4] also made it possible to achieve, along with quantitative qualitative results which were not previously published and which will be partially presented below. The characteristics of damping surfaces are given in [4] according to the numbers of experiments. A graph copy of the photograph of three telluric streams which characterize development of perturbing motion along a simple damping surface (experiments V1 and V3) and for comparison along a rigid surface (experiments B7 and B10) is presented in Figure 1. The Ox axis is aligned along the surface of the working section along the longitudinal axis of symmetry, the Oy

axis is aligned vertically upward and the Oz axis is aligned to the right along the flow. The origin coincides with the beginning of the working section.

It should be noted that the physics of fluid flow along a surface is different in both cases. Comparison of the perturbing motion during flow over both surfaces in the region of the point of buckling is presented in Figure 1, a and b. The oscillation amplitude of the vibrator tape comprised 0.32 mm in experiments on a rigid surface and 0.24 mm during flow over a damping surface. However, this difference of amplitudes is insignificant. Oscillations at frequency close to that of the second neutral oscillation are recorded in the figures: 0.74 Hz for a rigid surface (Figure 1, a) and 0.98 Hz (Figure 1, b) for a damping surface. The perturbing motion near a rigid surface is three-dimensional for the entire thickness of the boundary layer and has all the features typical for the point of buckling [2]. The perturbing motion forms near the surface during flow over a damping surface. The shape and type of wave differ from similar waves during flow over a rigid surface. Moreover, the difference in the tendency toward twisting of the wave crest is obvious.

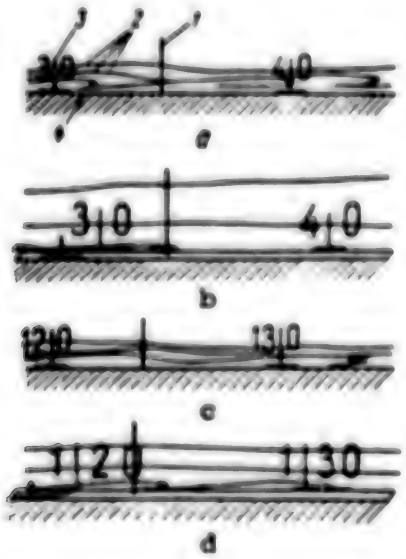

Figure 1. Development of Perturbing Motion Through Thickness of Boundary Layer During Flow Over a Rigid (a, c) and Simple Membrane Surfaces (b and d): 1--tellurium wire for photographing of profile; 2--telluric stream; 3--distance marks along working section, cm; 4--surface along which measurements are made

The same differences were found, only the amplitude of the oscillation on a flexible surface was still less, when the characteristics of the perturbing motion were compared to a frequency close to the first neutral frequency during flow over a rigid surface.

Comparison of the perturbing motion during flow over both surfaces in the region of $x = 120$ cm showed that the wavelengths are greater on a rigid surface (Figure 1, c), the shape of the wave is sloping, twisting of the wave crest occurs in a manner typical for a rigid surface and the perturbing motion is applied to the entire thickness of the boundary layer. During flow over a damping surface (Figure 1, d)

the wavelength λ increased compared to λ at x = 30 cm, but decreased compared to λ on a rigid surface at x = 120 cm. The shape of the wave also varied but remained the same as at x = 30 cm. The perturbing motion was observed approximately in the same section of the boundary layer as during flow over a rigid surface (Figure 1, c and d). The oscillation frequency of the wave comprised 0.60 Hz on a rigid surface and 1.1 Hz on a damping surface.

As can be seen from Figure 1, the perturbing motion during flow over a simple membrane surface becomes clearer but is more similar in shape to the perturbing motion with a positive pressure gradient, the results of investigation of which will be outlined separately.

It was found during study of the hydrodynamic stability on a rigid surface that there is a specific distance between the appearance of visible oscillations and "folding" of the wave for each oscillation frequency. This distance was arbitrarily named the stabilization zone. The stabilization zone initially decreases and then increases as the oscillation frequency increases. The stabilization zone is minimum near the second neutral oscillation and shifts opposite the flow to the vibrator strip as frequency increases. The principles of wave "folding" during flow over damping surfaces were essentially the same. The stabilization band seemingly characterizes the rate of increase of the perturbing motion. Thus, the stabilization band on practically all the testing damping coatings was less than during flow over a rigid surface. For example, the stabilization band comprised 20 cm during flow over a rigid surface at x = 70 cm and oscillation frequency of 0.74 Hz (a frequency close to the second neutral oscillation) (oscillations appeared at x_n = 60 and the wave was folded at x_k = 80). The stabilization band comprised 18 cm (x_n = 67 cm and x_k = 85 cm, respectively) during flow over a simple membrane surface at the same location (experiments V2) at oscillation frequency of 0.76 Hz, it comprised 10 cm (x_n = 70 cm and x_k = 80 cm) at 0.96 Hz and it comprised 6 cm (x_n = 72 cm and x_k = 78 cm) at 1.09 Hz close to the frequency of the second neutral oscillation. The stabilization band increased with a subsequent increase of frequency.

The shape of the perturbing motion is similar to the shape of this motion in experiments without heating during flow over a simple membrane surface with heating, but the perturbing motion was observed even closer to the surface in this case. Moreover, a stabilization band was not found. After a peak wave was formed, the perturbation with this shape of wave moved downward along the flow without being deformed, as in a solidified type.

Photographs of the perturbing motion perpendicular to the boundary layer during flow over a simple membrane surface are presented in [3]. It is obvious that the perturbing motion moved toward the outer boundary of the boundary layer at constant value y of the vibrator as the frequency increased.

The nature of the perturbing motion varied during flow over complex membrane surfaces, combining the characteristics of perturbing motion during flow over rigid and simple damping surfaces. A graph copy of the photograph of perturbing motion at frequency of n = 0.8 Hz and flow velocity of 13.6 cm/s (experiments P11) is presented in Figure 2, a and a diagram of the behavior of the perturbing motion of these surfaces is presented in Figure 2, b.

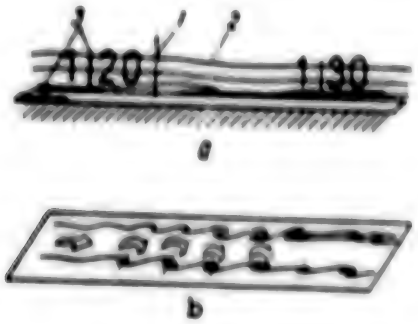

Figure 2. Perturbing Motion (a) and Diagram of Its Development (b) During Flow Over Complex Membrane Surface: 1, 2 and 3--the same as in Figure 1

Three characteristics of perturbing motion were found. The stabilization band behaved the same as during flow over a rigid surface. The stabilization band, approaching the vibrator, became constricted and then expanded as frequency increased. At the same time, unlike a rigid surface, double folding of the wave was observed. Part of the wave crest was "folded" while the upper part, not breaking down, continued to move above it. The upper part of the crest was then "folded" and two stabilized crests moved parallel to each other downward along the flow. The second characteristic included the fact that the perturbing motion was not immediately stabilized with a further increase of oscillation frequency, but was rotated inside so that if the axis around which the crest was twisted were previously parallel to the flow surface, this axis became perpendicular to the surface lower down the flow. The crest was twisted so rapidly at these frequencies and the wavelength decreased so much that seemingly small vortices parallel to the surface were initially formed which became stabilized after their rotational axis was turned by 90°. Moreover, the impression was created during motion of the perturbing motion downward along the flow that the lower layer of the fluid lying under the oscillating layer moved opposite the flow so much that it was strongly retarded, while waves moved above this layer, without increasing and without being damped immediately, but were stabilized considerably lower down the flow compared to a rigid surface.

The nature of the perturbing motion during flow over a viscoelastic surface also differed from the nature of that during flow over a rigid surface. A graph copy of a photograph of the behavior of perturbing motion during flow over a thick plate of polyurethane foam at velocity of 14.9 cm/s and oscillation frequency of 0.83 Hz (Figure 3, a, experiments P23), with the same velocity and oscillation frequency of 0.77 Hz (Figure 3, b, experiments P24), with velocity of 12.4 cm/s and oscillation frequency of 0.67 Hz (Figure 3, c, experiments P19), with velocity of 11.7 cm/s and oscillation frequency of 1.4 Hz (Figure 3, d, experiments P27) and with velocity of 10.0 cm/s and oscillation frequency of 1.0 Hz (Figure 3, e, experiments P35) is presented in Figure 3. Everywhere the oscillation frequencies are similar to the frequency of the second neutral oscillation. The oscillation amplitude decreases strongly compared to that on a rigid surface, the shape of the wave is similar to that during flow over a simple membrane surface, but the lower layer adjacent to this surface is strongly retarded as in the case of flow over complex membrane surfaces (Figure 3, a). The perturbing motion propagates in the immediate vicinity of the damping surface.

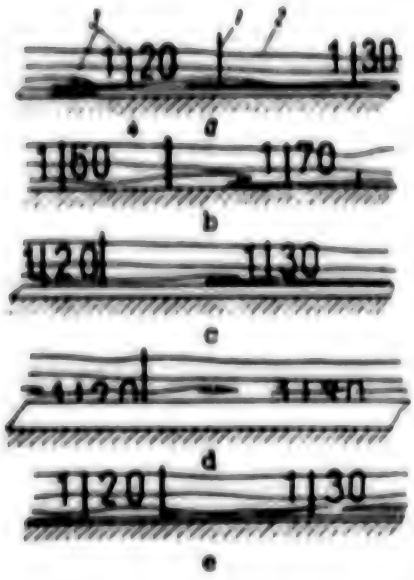

Figure 3. Perturbing Motion During Flow Over Viscoelastic Surface: 1, 2, 3 and 4--the same as in Figure 1

It is interesting to compare the behavior of the perturbing motion in the region of the point of buckling (Figure 3, a) to a similar situation for a rigid surface (Figure 1, a). The behavior of the non-sine-wave perturbing motion during flow over a sheet of polyurethane foam (Figure 3, c) is the same as during flow over a rigid surface, with the exception that the wave crest folds almost immediately behind the vibrator without development of oscillation.

The process of wave folding is the same as on a rigid surface and is similar to the process of double folding of the wave on a complex damping surface. The difference from double folding includes the fact that the beginning oscillation in yOx plane breaks down very rapidly almost immediately behind the vibrator with rotation to the zOx plane. All the oscillations in the yOx plane then stop and oscillation in the zOx plane continues for some time until complete stabilization. The behavior of the telluric stream after double folding is easily visible in the region of x = 120 cm, while separation of the stream in the zOx plane is visible in the region of x = 130 cm (Figure 3, c).

The oscillation amplitude of the vibrator tape comprised 0.24 mm during sine-wave perturbation on viscoelastic surfaces and comprised 0.3-0.4 mm during non-sine-wav oscillations. The oscillation was damped immediately behind the vibrator (experiment P17) in the first series of measurements in the region of x = 30 cm. The amplitude increased to 0.7 mm (experiments p18) in the second series at x = 80 cm. However, the oscillations are damped rather well even in this case. It was found that the fluid near the surface was severely retarded at frequencies close to the frequency of second neutral oscillation, but it seemingly slid over the lower layer of fluid so that an impression was created that the boundary layer of the fluid moved opposite the flow. A similar pattern was observed during flow over complex membrane surfaces.

When the oscillation amplitude of the vibrator tape decreased to 0.4-0.5 mm, the oscillation amplitude of the fluid was less than that during flow over a rigid surface and the perturbing motion itself was concentrated immediately near the surface.

The structure of the perturbing motion during flow over a polyurethane foam surface coated on the outside with film is shown in Figure 3, d. Although the nature of the perturbing motion was similar to the nature of this motion in experiments on a surface not covered with film, the frequency and oscillation amplitude increased. The same was observed in experiments on a thin sheet of polyurethane foam having worse stabilizing properties than a thick sheet (Figure 3, e).

Measurements were made in region 3 of natural transition during flow over a simple membrane surface (experiments VS45) similar to measurements during flow over a rigid surface (Figure 4).

It turned out that the shape of the flow in regions 2 and 3 of the transition of laminar to turbulent boundary layer varies the same as in region 1 compared to a rigid surface during flow over a membrane surface. If the flow structure during flow over a rigid surface is compared to a zero and positive pressure gradient, it is obvious that the rate of deformation of a plane Tollmin-Schlichting wave (transition zone 2) is considerably greater with a positive pressure gradient than with a zero gradient, i.e., hydrodynamic stability deteriorates. However, the wavelength of hertler vortices decreases somewhat in this case, which indicates an increase of flow stability in transition zone 3.

The rate of deformation of a plane wave increased during flow over a simple membrane surface, the stabilizing properties of which were nonoptimum, compared to a rigid surface with zero pressure gradient, but decreased compared to a rigid surface with positive pressure gradient. The wavelength of hertler vortices decreased significantly during flow over a damping surface.

Taking the foregoing into account, one can present the integral result of flow interaction with damping surfaces in the form of the dependence of the drag of the plate on Reynolds number (Figure 5). The solid lines and numbers 1-3 denote the curves for laminar, transient and turbulent modes of flow, respectively, along the plate [6]. Points A, B and C denote the typical Reynolds numbers during flow over a rigid plate and the dashed lines denote the principles of drag of damping surfaces. The remaining notations will be explained below.

Investigations on simple membrane surfaces showed that the hydrodynamic flow stability along the surfaces deteriorates with nonoptimum mechanical properties of them. If the results found in experiments V1-V5 are interpolated, the Reynolds number of buckling calculated with respect to x comprises $Re^{g}_{p.u} = 1.35 \cdot 10^4$. The point of buckling in Figure 5 is denoted by the letter G under these conditions. The $Re_{p.u}$ number decreased by a factor of 4 with respect to point A during flow over a rigid surface. Let us assume that deterioration of hydrodynamic stability leads to a decrease of the transition zone and to Re_{kl} approaching $Re_{p.u}$ (similar changes occur during flow over a rigid surface under unfavorable conditions). In fact, oscillations which do not coincide in phase with oscillations of the boundary layer occur in a destabilizing boundary layer of a damping surface due to the effect of flow pressure fluctuations, while the oscillation amplitude of the damping surface may exceed even the permissible height of the roughness.

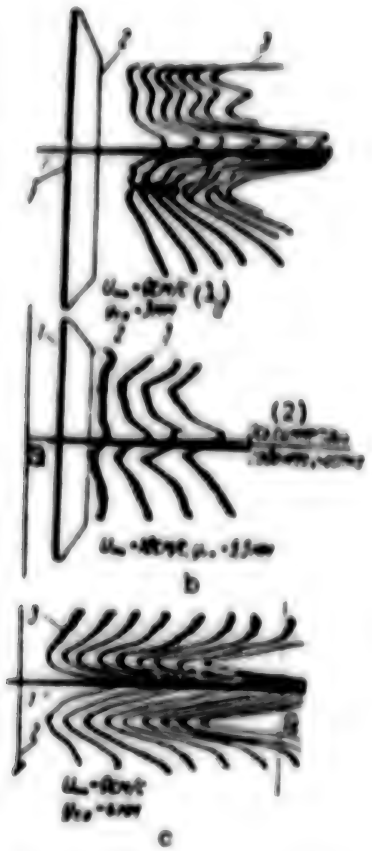

Figure 4. Deformation of Velocity Profile During Flow Over a Simple Membrane Surface (a) and Rigid Surface With Zero Pressure Gradient (b) and With Positive Pressure Gradient (c): 1--support for tellurium wire; 2--tellurium wire; 3--velocity profile in xOy plane

Key:

1. cm/s
2. Axis of symmetry of working section

Thus, the effect on the flow of the destabilizing surface can be similar to that of a rough or wavy rigid surface. Let us assume that the transition steps 1-5 denoted according to the classification suggested in [5, 9], are reduced during flow over a destabilizing surface and point B, corresponding to Re_{x1} of a rigid surface, is shifted upward along the flow to point D by a value proportional to the ratio $Re^{a}_{p.u}/Re^{g}_{p.u}$. The critical Reynolds number during flow over a destabilizing flexible surface then comprises $Re^{d}_{x1} = 1.25 \cdot 10^{5}$. The drag durve from point D to point E is shifted above the solid curve with strongly destabilizing properties of the flexible surface due to the fact that the pressure and velocity fluctuations in the laminar boundary layer will be greater than those during flow over a rigid surface. Step 6 of turbulence generation occurs from point E to point F during flow over a flexible surface. The drag of this surface, due to the factors indicated above, will be greater than that of a rigid smooth plate and corresponds to curve 4 in Figure 5. The nature of curve 4 may differ from that indicated in this figure as a function of the degree of destabilization of the boundary layer by the flexible surface.

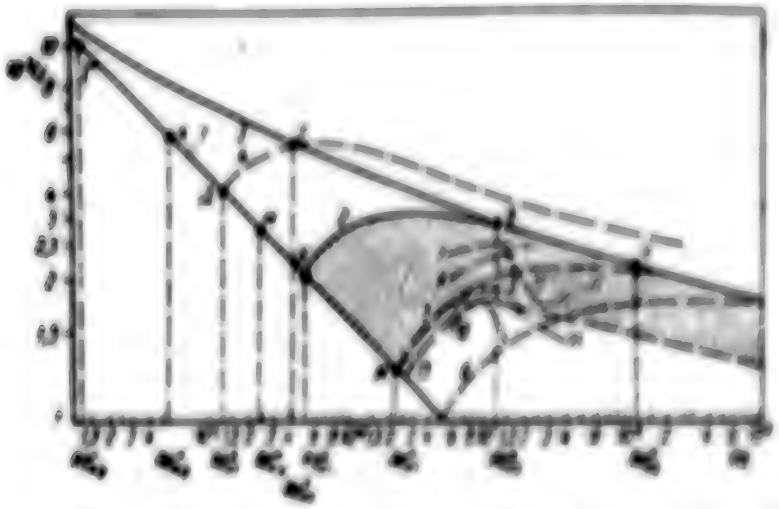

Figure 5. Dependence of Drag of Longitudinal Flow Over Rigid and Damping Plates on Reynolds Number

The Reynolds number of buckling comprised $Re^{*}_{1} = 650$ or $Re_{p,w} = 2.4 \cdot 10^{6}$ during investigations on the best damping surface. The point corresponding to this value of Reynolds number is denoted by the letter Zh in Figure 5. Due to the main effects enumerated above and found during investigations on a flexible surface, one may assume that not only the point of buckling is shifted downward along the flow but the entire transition zone increases as well.

Let us assume that steps 1-5 during flow over the best stabilizing surface increase their length compared to a rigid surface in proportion to the ratio $Re^{Zh}_{p,w}/Re^{3}_{p,w} = (2.4 \cdot 10^{5})/(5.4 \cdot 10^{4}) = 4.45$. Then Re^{*}_{1} accordingly increases during flow over a flexible surface and comprises $2.22 \cdot 10^{6}$.

Let us denote in Figure 5 the origin of step 6 of turbulence generation by the letter I during flow over this damping surface. Let us denote the end of this step by the letter K and let us denote the drag curve on this step by the number 5.

An advantage in reducing drag during flow over these damping surfaces compared to a rigid surface can be evaluated by using the cross-hatched zone 1 in Figure 5. The method of reducing hydrodynamic drag by using flexible surfaces, based on drawing the transition of laminar boundary layer to a turbulent boundary layer, is called the distributed damping method.

According to the results of the investigations, the coefficient of increase of Re^{*}_{1} number or the laminarization coefficient, comprised 4.45. The use of flexible surfaces may increase this coefficient to 10 [7]. The drag curve of a damping plate, constructed in Figure 5, is denoted by the number 6 with this coefficient. Judging from the results of these calculations, curve 6 characterizes the maximum effect of laminarization of the boundary layer by using flexible surfaces.

The results of tests by M. O. Kramer [8], who investigated the drag of a large-aspect body of rotation with different damping surfaces attached to the cylindrical part, towed by a launch, are denoted by curves 7-10 in Figure 5 (7--results of tests of a rigid standard; 8--of a damping surface having stiffness

E = 1.63·10^8 N/m^2, damping of δ = 57 percent and viscosity of the damping fluid of η = 10-600 cSt; 9--of a surface with parameters of E = 4.34·10^8 N/m^2, δ = 44 percent and η = 1,000 cSt; and 10 -- of a surface with parameters E = 2.17·10^8 N/m^2, δ = 67 percent and η = 300 cSt). The best results were found during tests of the latter surface. Drag was reduced in this case by 59 percent compared to the rigid reference. This means that 63 percent of the length of the model had a laminar flow over it.

Curves 11 and 12 of Figure 5 were plotted from the results of testing a supernatant rigid model of a body of rotation having laminarized shape. This shape permitted preservation of the laminar flow in the boundary layer over a long length of the body. Curve 12 characterizes testing of a model at different speeds of motion. It is obvious that the given shape of the body permits one to have different length of the laminar boundary layer at different velocities. Curve 11 was plotted from the results of testing a model with regard to the fact that 60 percent of its surface has a laminar boundary layer flowing over it at any speed.

Comparing curves 7-10 and 11-12 of Figure 5, one can conclude that damping surfaces reduce hydrodynamic drag not only by extending the transition, but also by laminarization of the boundary layer. If the envelope of the curve can be drawn by curves 10 and 11 and if it can be interpolated in both directions, then curve 13 is found. This curve characterizes zone 2 of reduction of hydrodynamic drag and includes zone 1.

The distributed damping method actually excludes mixed flow over the body if it is completely covered by a damping surface with correctly selected mechanical characteristics. In this case there is significant extension of the transition on the initial section of the body and the flow structure in steps 1-6 differs from a similar structure along a rigid surface. The boundary layer is then formed along the damping surface and differs in its structure from a turbulent boundary layer which would occur at the same values of x along a rigid surface.

It is known that damping surfaces have optimum stabilizing properties in a limited range of flow velocities. Therefore, if the mechanical properties of a damping surface are constant, the value of C_f begins to increase with an increase of Re number and may not only reach but also exceed the parameters of curve 3. In order for the right branch of curve 11 to be parallel to curve 3, one must regulate the mechanical properties of the damping surface with an increase of Reynolds number so that its stabilizing properties are optimum all the time.

Thus, the given results of investigating the development of perturbing motion in a laminar boundary layer indicate that the nature of perturbation is different in structure during flow over rigid and damping surfaces. Moreover, this difference is greater, the better the stabilizing properties of the latter.

BIBLIOGRAPHY

1. Babenko, V. V. and O. G. Nikitcheva, "Some Hydrodynamic Principles of Construction of the Skin of Marine Animals," BIONIKA, No 10, 1976.

2. Babenko, V. V. and L. P. Kozlov, "Experimental Investigation of Hydrodynamic Stability on Rigid and Elastic-Damping Surfaces," MEKHANIKA ZHIDKOSTI I GAZA, No 1, 1973.

3. Babenko, V. V., "Experimental Investigation of the Perturbing Motion in a Laminar Boundary Layer During Flow Over Damping Surfaces," BIONIKA, No 10, 1976.

4. Babenko, V. V., "The Main Characteristics of Flexible Coatings and the Criterion of Similarity," BIONIKA, No 5, 1971.

5. Nepp, K. P. and P. J. Roach, "Investigation of the Transition of a Boundary Layer By the Visual Method and Using a Thermoanemometer," RAKETNAYA TEKHNIKA I KOSMONAVTIKA, Vol 6, No 1, 1968.

6. Schlichting, H., "Teoriya pogranichnogo sloya" [Boundary Layer Theory], Moscow, Nauka, 1969.

7. Gyorgyfalvy , D., "The Possibilities of Drag Reduction by the Use of Flexible Skin," AIAA PAPER, No 430, 1966.

8. Kramer, M. O., "Boundary Layer Stabilization by Distributed Damping," JOURNAL OF AERONAUTICAL AND SPACE SCIENCES, Vol 27, No 1, 1960.

9. Stuart, J. T., "Hydrodynamic Stability," APPLIED MECHANICS REVIEWS, Vol 18, No 7, 1965.

UDC 532.526-597.587.5

THE BIONYDRODYNAMIC PHENOMENON OF THE SWORDFISH AS A LIMITING CASE OF HIGH-SPEED HYDROBIONTS

Kiev BIONIKA in Russian No 12, 1978 pp 40-48

[Article by S. V. Pershin, Leningrad]

[Text] The swordfish Xiphias gladius is known as the fastest hydrobiont. Its maximum swimming speed in short bursts V_{MAX} reaches 130 km/hr [1] (determined during unwinding of a spinning reel). The highest Reynolds number of the swordfish, calculated by the total length, approaches $Re_{MAX} \sim 1 \cdot 10^8$ [9]. There have repeatedly been attempts to explain the high swimming speed of the swordfish on the basis of investigating schematized models.

In [9], we considered the problems of optimization of body shape and caudal impeller in low-drag high-speed fish, we determined the external features of these fish and proposed a hydrodynamic classification and characteristics of low-drag high-speed fish, including Xiphoids. The possibility of cavitation flow over the swordfish on the basis of an original hydrodynamically correct diagram with observance of the biological condition of continuous gill respiration is considered in [10]. The inducer of the cavitation zone is assumed to be the wedge-shaped beak--the sword, arranged at a small positive angle of attack (in this case the cavity encompasses the upper greater part of the body while the swordfish glides on the water with the lower smoothly streamlined part of the body while retaining Archimedes buoyancy).

Other papers have also been devoted to the hydrodynamic function of the protruding beak of the swordfish. It is shown in [6] as a result of quasi-steady calculation that hydrodynamic drag may be reduced to 12 percent by thickening the boundary layer on a narrow attachment to a body of rotation. The conclusion was confirmed experimentally during towed testing of an elongated body of rotation with a tip [7]. However, this does not explain the high swimming speed of the swordfish. Quasi-steady calculations of the boundary layer in [3] and experiments permitted the conclusion that the optimum region of Reynolds numbers where the positive "swordfish effect" is manifested, comprises $Re \sim 4 \cdot 10^6$ to $8 \cdot 10^7$. This conclusion agrees with reality but even so does not completely explain the mystery of the swordfish.

On the other hand, the functions of the beak of Xiphoid fishes, including the swordfish, are not considered in the extensive survey on the hydromechanics of motion of aquatic animals [19]. Main significance in reaching high swimming

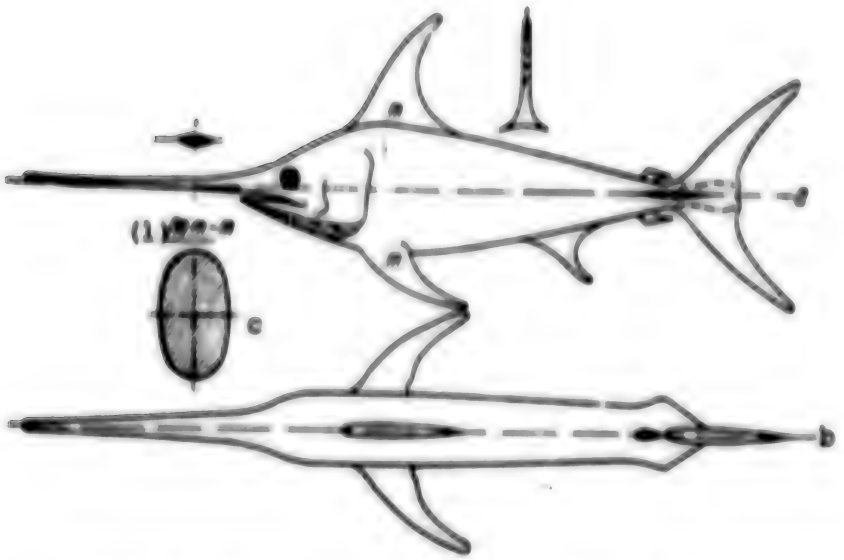

Figure 1. Swordfish Xiphias gladius (total length of approximately 2 meters): a--side view; b--top view; c--cross-section

Key:
1. Through t-t

speeds by aquatic animals is given to ahighly efficient caudal fin of "half-moon" shape in this survey on the basis of the theory of transient motion of an elongated body in an ideal fluid.

It should be noted that the body of a swordfish does not have the shape of a body of rotation (Figure 1), as is usually assumed.

Hydrobionic analysis. The entire complex of presently known reliable factors about the swordfish, considered partially in the papers mentioned above and also in [4, 5, 8, 12 and 16], is analyzed sequentially below for the first time in the hydrodionic aspect. The swordfish is regarded as a limiting case of high-speed hydrobionts and both hydrodynamic and biological principles are brought in when it is compared to these hydrobionts. To carry out the analysis, the factors which determine the high swimming speed of the swordfish and their hydrodynamic significance are systemized in the following manner:

Feature	Hydrodynamic Significance
Powerful Locomotive-Impeller Complex	High Thrust and High Swimming Speed
1. High power to weight ratio of body	Powerful muscular motor
2. High efficiency of caudal fin	Efficient flapping impeller
Unique Shape of Body and Protruding Parts	Optimization in Locomotion and Stability of Motion
3. Protruding beak-sword	Multifunctional designation
4. Steep tapered termination of confuzor part of body	Optimum configuration with diffusor part of body

Feature	Hydrodynamic Significance
5. Stiff dorsal fin	Rigid course stabilizer
Morphofunctional Characteristics of Skin	Reduction of Hydrodynamic Drag of Body
6. Folded skin surface and recessed scales	Finned surfaces for heat regulation
7. Developed intrategumental secretory apparatus	Total diffusion of mucous into boundary layer of entire body
8. Individual secretory formations	Local regulation of mucous injection on sections of perturbations

Let us consider the named factors in order of arrangement.

The powerful locomotive-propulsive complex which creates high thurst is a necessary prerequisite of high swimming speed of the swordfish. The power N delivered by the impeller of the animal is determined biologically by its power to weight ratio through the total body mass G, relative fraction of muscles c and specific power yield q calculated per unit of muscle mass. And it is expressed hydrodynamically by the thrust of the impeller T, the forward velocity of the center of gravity V and the propulsive coefficient η, which takes into account the power loss in the body-caudal fin propulsion complex. Thus, $N = qcG = (1/\eta)TV$. Here all values are averaged for the period of oscillations of the locomotion-propulsive complex and $q = q(\tau)$ is a function of the total duration of swimming τ and is approximately identical numerically for the muscles of animals and man for which this function has been well studied. Let us show that the power to weight ratio of the body and the hydrodynamic efficiency of the caudal fin of the swordfish are maximum for aquatic animals.

1. The high power to weight ratio of the swordfish follows directly from the comparatively large body mass G with given length L and the relatively high fraction of muscles c. We constructed the graphs $G = f(L)$ for different fishes, but they are not presented in this article. It is sufficient to note that $c = 0.67$ for the swordfish is the highest value for all swimming animals. It is limited by the biologically permissible ratio of the mass of the vitally important organs and tissues of the organism ($c = 0.30$-0.45 for the majority of fish species). The swordfish has a very large especially deep-lying lateral red muscle which is a common feature of fast-swimming fishes, even those isolated in systematic ratio of groups [16].

The high power to weight ratio of the swordfish and of other high-speed hydrobionts is compared by the parameter of the maximum swimming speed V_m (Figure 2). The graph is compiled from experimental data from different literary sources and from our calculations in quasi-steady approximation by the energy method. The length of the water-displacing part of the body $L = 2.0$ meters (the length of the swordfish with sword is 3.0 meters) and the duration of high-speed swimming in bursts $\tau = 3$ seconds were taken as identical for hydrobionts in the calculation.

It is obvious that the power to weight ratio of the swordfish is two or more times higher than that of the high-speed Black Sea dolphin and macho shark and approaches the power to weight ratio of the common thick-bodied tuna. The good agreement

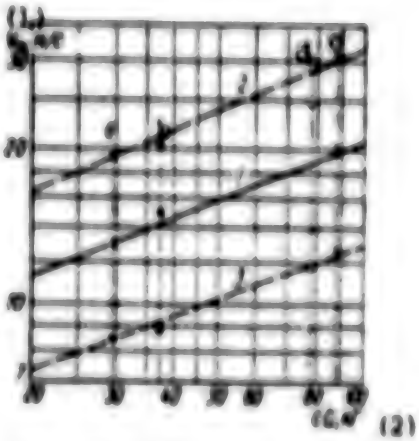

Figure 2. Relationship of Maximum Swimming Speed to Power to Weight Ratio of Muscles of High-Speed Hydrobionts, $V_m(cG)$: 1--observed; 2 and 3--calculated during laminar and turbulent flow modes (in quasi-steady approximation); a--common dolphin; b--macho shark; c--common tuna; d--swordfish

Key:
1. m/s
2. kG

among the curves of observed and calculated maximum swimming speeds in the function of the power to weight ratio of the species considered $V_m = f(cG)$ should also be noted. The hydrodynamic drag of these species corresponds at high Reynolds numbers ($Re = (2\text{-}7)\cdot 10^7$) to some intermediate value for laminar and turbulent modes. Thus, the swordfish, like other high-speed hydrobionts, is also forced to utilize means of reducing hydrodynamic drag at maximum swimming speed.

The observed maximum swimming speed of the swordfish is taken as $V_m = 25$ m/s in Figure 2 according to the authoritative dynamic calculation of Academician A. N. Krilov (cited from [17]). Deviation of this point from the common curve 1 indicates that, unlike other considered hydrobionts, the adopted calculating speed of the swordfish should correspond to swimming duration of $\tau < 3$ seconds. This impulse swimming mode is actually a limiting case compared to other high-speed hydrobionts.

2. The high efficiency of the caudal fin--an efficient flapping impeller of the swordfish--is determined by a number of indicators. To do this, let us write the averaged thrust in the water by density ρ in the form of two functions: initially as that generally accepted for a supporting wing and then similar to the formula for the thrust of a propeller

$$T = c_T S\rho \frac{v^2}{2} = k(l/\lambda)^2 \rho v^2.$$

The area of the supporting surface S of the caudal fin in the swordfish is greatest compared to other Xiphoid fishes and considerably exceeds that of the high-speed common tuna of corresponding length [9]. The value of the dimensionless coefficient of thrust c_T is undoubtedly high if one bears in mind that the aspect ratio of the caudal fin of the swordfish is $\lambda = l^2/S = 7.5$ (i.e., very high for an aquatic animal). The high value of coefficient c_T is also confirmed in special theory of swimming of an elongated body in an ideal fluid [19].

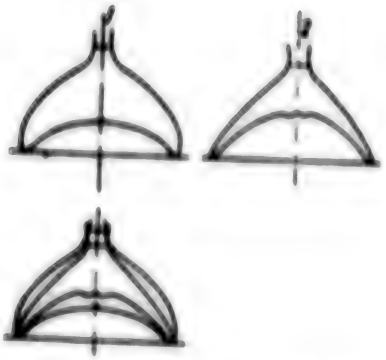

Figure 3. Comparison of Shape of Caudal Fins of Common Dolphin (1) and Swordfish (2) (the dimensions of the fins are reduced to the same span)

On the other hand, the caudal fin of the swordfish has such a large span l that it significantly exceeds the greatest height of the body H, namely $l \approx 2.2H$. However, it does not protrude beyond the ends of the dorsal and abdominal fins (Figure 1); therefore, the caudal fin of the swordfish is still within the range of the vortex layers of other fins, which increases the efficiency of a flapping impeller [19]. At the same time, the relatively long caudal part of the swordfish body and the rigid practically unbending skeleton permit giving large transverse spans A with respect to the center of gravity of the body to the caudal fin, which creates a large streamlined area (lA) of the impeller. At the same time the oscillation frequency n of the fin is also high since the fin itself is rigid and inflexible. The presence of large cartilage longitudinal stabilizers on both sides of the caudal fin (see Figure 1) is typical, which is also a common feature of high-speed fish [9].

Based on that which we previously considered in different aspects of optimization of the shape of the caudal fin impeller in high-speed dolphins [11], let us compare the caudal fins of the common dolphin and swordfish (Figure 3). The flapping impeller of the swordfish is inscribed in that of the dolphin (with identical span). It is known from hydrodynamic theory of wave propulsion in an ideal fluid that the shape of the leading edge and the large depression of the trailing edge are of special significance for its efficiency [19]. The notch of the fin is filled with vortex layers and it works to create thrust, as does an unnotched fin; the hydrodynamic drag of the fin is reduced in a real fluid in this case.

Thus, comparison of the caudal fins of such diverse high-speed hydrobionts shows first that the shape of the fins as impellers varies significantly with an increase of swimming speed of hydrobionts and second the caudal fin of the swordfish, compared to that of the common dolphin, being optimized for maximum high swimming speed for the animal, is characterized by relatively large values of parameters l, A and n and therefore of thrust T with greater stiffness of the system as a whole.

The unique shape of the body and of the protruding parts determines the optimum locomotion and stability of motion of the swordfish and is determined by the following factors.

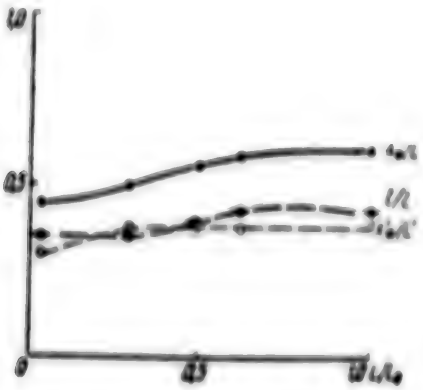

Figure 4. Increase of Relative Distance of Greatest Body Cross-Section as Side of Swordfish Increases $(x_m/L)(L/L_0)$: L_0 = 1.65 meters--total length of adult fish with sword; L--length of young fish of different ages with sword; L'--length of the same fish without sword (the length of the fish was taken to the end of the spinal column); x_m--distance of greatest cross-section from tip of sword; x_m'--distance from end of beak without sword

3. The protruding beak-sword undoubtedly has a different biological and hydrodynamic functional designation in the swordfish.

The biological designation of the sword is to catch food, which follows from factors of ramming large fish by the swordfish, including high-speed common tunas. Photographs of the swordfish jumping into the air at high speed with a fish impaled on the beak have been published frequently. Moreover, cases of the biological significance of the front-protruding parts of the body in other fishes and animals, for example, the sawfish, hammerfish and narwhal, are known.

However, in view of the biological principle of multifunctional nature--superposition of functions, the biological functions of the sword in the swordfish are combined with hydrodynamic functions. This has been confirmed by the calculations and experiments considered above [3, 6, 7], although the results were low in reduction of drag by the sword for the adopted conditions of steady motion of schematized models of the swordfish. There is also another, no less important hydrodynamic designation of the sword which has not even been mentioned before now in the literature: the stabilizing effect of the long sword-like projection on the oscillatory motion of the swordfish with powerful thrusts of the caudal fin. It is quite obvious that the hydrodynamically undesirable large oscillations--yawing of the head part of the body with respect to the center of gravity of the swordfish--should be reduced significantly in the presence of a protruding beak. The foregoing is also confirmed by an increase of the relative length of the sword as size increases and by an increase of swimming speed of the swordfish.

The results of our analysis, according to [8], are presented in Figure 4.

One may note that the different relative length of the protruding beak in different species of Xiphoid fishes depends on the cross-sectional shape and streamlining of it during oscillatory motions. Thus, the longest beak in the swordfish has a

good streamlined lenticular shape in transverse section, the beak of shortest length has poorly streamlined circular cross-sectional shape in the sailfish and the cross-sectional shape of the beak in the marlin is intermediate (lenticular in the supper part and oval in the lower part), but the relative length of the beak is also intermediate.

4. The steep tapered head of the confuser part of the body is optimum for integration with the lone diffuser part of the body of the swordfish (in the presence of a protruding sword). The gill slit is located in the region of the local peak of rarifaction of hydrodynamic pressure on the body [9]. This increases the pressure head at which the water stream is ejected from the mouth cavity through the gills and consequently increases the water flow rate and removal of oxygen from it, which is also necessary for a high-speed fish with high energy metabolism. Moreover, the greatest body cross-section of the swordfish is located at the end of the short tapered head at a relative distance $x_m/L = 0.60$ from the tip of the swrod (Figure 4), which is hydrodynamically feasible. The dimensionless coefficient p of excess hydrodynamic pressure p over static pressure p_{st}, judging by [3, 7], is approximately equal to

$$\bar{p} = \frac{2}{\rho V^2}(p - p_{st}) \cong -0{,}15.$$

It is remarkable that the value of this coefficient at the indicated point differs slightly from that in the absence of a sword ($\Delta\bar{p} = -0.05$).

5. The nonretractable dorsal fin, which is the main and rigid course stabilizer of the swordfish, deserves special attention.

It is known that the dimensions of the fins decrease and they are partially or completely retracted into corresponding "pockets" in the body as the swimming speed of fishes increases [9]. Typical examples are tuna and even Xiphoids themselves of other species--marlins, lancellates and sailfish. However, the large and thick dorsal fin of the swordfish (Figure 4) is not retracted, which is convincing proof of the importance of increased course stabilization for it using this fin at maximum swimming speed. Moreover, the stabilizing significance of the sword during flapping motions of the powerful caudal fin, indicated above, is also reinforced.

It should be emphasized that the apparatus which copy the well-streamlined body shape of the swordfish have long been found in technology. Many modern large gliders, including the best record-setting sailplanes of the OKB [Special design office] of general aviation designer O. K. Antonov, for example, the A-15 metal glider with laminarized wing profile [14], have a similar shape (without a sword). The fuselages of some aircraft also have similar shape of a body rotation, which can be judged by published illustrations [13].

The morphofunctional characteristics of the skin of the swordfish are a means of reducing the hydrodynamic body drag, the need for which from the viewpoint of energy at maximum swimming speed was discussed in paragraph 1 of this article. Systematic data on the skin, scale and mucous covers of many high-speed fishes of different groups and numerous proofs of the hydrodynamic function of the fish mucosa, based on extensive experimental material and theoretical data, were first presented in our collective paper [12]. We note here only some additional features of the coverings of swordfish.

6. The folded skin surface with alternation of longitudinal increases (rolls) and decreases (troughs) and the blunt scales of the swordfish are explained as finning of the body surface for heat regulation and as a means of retaining the mucous. The latter has been confirmed by retention of a stable mucous cover during maximum high swimming speed of the swordfish.

One of the simplest methods of increasing heat transfer from the body surface--development of external ribs on the surface--has long been known [2] and frequently applied in technology. The swordfish is a poikilothermal animal, but one should take into account that the brief bursts at high maximum swimming speed occur similar to an explosion in it, with high release of energy and consequently of heat. The sharp and high temperature increase of the body is a contraindication of the organism and is energetically disadvantageous since it in turn requires increased energy consumption. Moreover, an increase of body temperature by 10-12°C with an increase of the activity of high-speed fish has been frequently noted in the literature. We recall that Academician A. N. Krilov compared the action of the swordfish during attack to that of an artillery shell of a small-caliber high-speed cannon (cited in [17]).

Ribbing the body surface of the swordfish does not increase hydrodynamic roughness, which is quite unacceptable for a high-speed hydrobiont, since the entire body surface of the swordfish is covered with a thick mucous and unevennesses are equalized. Moreover, ribbing of the surface and the partially recessed scales contribute to retention of the thick viscous mucous on the body surface at low swimming speeds when there is no need to utilize the mucous. The mucous on a ribbed surface, especially in longitudinal depressions, is heated somewhat, becomes thinner and less viscous and diffuses to the boundary layer of the streamlining flow at high swimming speed and increase of body temperature of the swordfish.

We note that temperature regulation of the outer coverings by other means is found in many animals, including that of a high-speed fish--the common tuna [18], where it is provided by increased blood circulation in a special branched system of the sanguiferous vessels located near the lateral body surface. The more or less thick layer of subcutaneous fat performs a similar function in homoithermal dolphins [15].

7. The developed intracutaneous secretory apparatus of the swordfish is designed for general diffusion of mucous to the boundary layer. One can note a number of its important features [12]: the secretory cells of only one type (granular), the hydrodynamic function of which has been well established, are found, there are secretory cells on the entire body surface rather than only in the caudal part, there is a branched system of mucous canals in the skin and the pores leading to its surface, including parallel rolls perpendicular to the body, the dextro- and levolateral system of these canals are not connected to each other and permit sequential automatic operation during bending-flapping motions of the body, which is more efficient and economical for total diffusion of mucous. The combination of these unique characteristics of the secretory apparatus of the swordfish undoubtedly indicates its high efficiency.

We note that since tangential stresses on the body surface of the swordfish are reduced appreciably in the presence of a sword [3, 6], the sword seemingly contributes to retention of mucous on the body, which is yet another of its functions.

8. The individual secretory formations serve for additional local regulation of mucous secretion on the body sections of the swordfish where the boundary layer is subjected to the greatest local disturbances. They include recesses in the skin near the gill slits, mucous from which may enter the water discharged through the gills automatically at high speeds until a definite peak of pressure rarifaction is achieved, mucous ampules arranged on both sides of the thick nonretractable dorsal fin and in the wake of the spine behind it in the longitudinal plane [5].

The latter may respond in certain modes of bending-oscillatory motions of the body.

The presence of these additional local secretory formations only in the swordfish confirms even more than it is a limiting case of high-speed hydrobionts. The essence of the matter is that, as convincingly demonstrated in [12], the mucous of high-speed fishes is a very efficient biopolymer coating and may contribute to reduction of hydrodynamic drag of bodies by tens of percent. It is remarkable that the mucous performs a hydrodynamic function at the highest Reynolds numbers of the fastest hydrobionts.

The phenomenon of the swordfish consists not only in the protruding beak and the unusually high maximum swimming speed for the animals, but also in many other features of external structure and outer body coverings.

Sequential consideration of all the isolated factors of high swimming speed of swordfish in different aspects made it possible to determine their relationship and interdependence and to analyze this biohydrodynamic phenomenon as a limiting case of high-speed hydrobionts.

The combination of a powerful locomotion-impeller complex with effective high-speed flapping impeller and morphofunctional characteristics of the body coverings in the biohydrodynamic phenomenon of the swordfish with the unique secretory apparatus, which provides a significant reduction of hydrodynamic drag at high swimming speeds and Reynolds numbers using the mucous, is of greatest interest in the hydrobionic aspect.

BIBLIOGRAPHY

1. Barsukov, V. V., "The Swimming Speed of Fishes," PRIRODA, No 3, 1960.

2. Buznik, V. M., "Intensifikatsiya teploobmena v sudovykh ustanovkakh" [Intensification of Heat Transfer in Ship Power Plants], Leningrad, Sudostroyeniye, 1969.

3. Zolotov, S. S. and Ya. S. Khodorkovskiy, "Characteristics of Frictional Drag of Bodies in the Shape of the Swordfish," BIONIKA, No 7, 1973.

4. Koval', A. P., "Surface Roughness and Some Characteristics of Skin Structure of the Swordfish," BIONIKA, No 6, 1972.

5. Koval', A. P., "Skin 'Ampules' of the Swordfish and Their Possible Functional Significance," BIONIKA, No 11, 1977.

6. Kozlov, L. F., "The Hydrodynamic Function of the Swordfish Beak," BIOFIZIKA, No 3, 1973.

7. Kozlov, L. F. and I. V. Leonenko, "Investigating the Effect of a Sword-Like Tip on the Drag of an Elongated Body of Rotation," BIONIKA, No 7, 1973.

8. Ovchinikov, V. V., "Mech-ryba i parusnikovyye" [The Swordfish and Sailfish], Kaliningrad, Oblizdat, 1970.

9. Pershin, S. V., "Optimization of Body Shapes and the Caudal Impeller in High-Speed Low-Drag Fishes," SB. TRUDOV VYSSHEGO VOYENNO-MORSKOGO INZHENERNOGO UCHILISHCHA, No 61, 1966.

10. Pershin, S. V., "A New Hydrobionic Model of a High-Speed Submerged Body With Cavitation Flow," SB. TRUDOV VYSSHEGO VOYENNO-MORSKOGO INZHENERNOGO UCHILISHCHA, No 63, 1966.

11. Pershin, S. V., "Optimization of the Stern Fin Impeller in Nature on the Example of Cetaceans," BIONIKA, No 3, 1969.

12. Pershin, S. V., L. F. Kozlov, O. B. Chernyshov, A. P. Koval' and V. A. Zayets, "Principles in the Coverings of High-speed Fishes," BIONIKA, No 10, 1976.

13. Petrova, I. M., "Gidrobionika v sudostroyenii" [Hydrobionics in Shipbuilding], (Tsentr. NII tekhn.-ekon. inform.), Leningrad, 1970.

14. "The A-15 Glider in Soaring Flight," KRYL'YA RODINY, No 11, 1972.

15. Tomilin, A. G., "Some Problems of the Ecology of Cetaceans," BYUL. MOSK. O-VA ISPYTATELEY PRIRODY. OTD. BIOL., Vol 49, No 5-6, 1940.

16. Chernyshov, O. B., A. P. Koval' and V. A. Zayets, "Analogy in Development of Some Accessories for Rapid Swimming in Sharks and Bony Fishes," BIONIKA, No 9, 1975.

17. Shuleykin, V. V., "Ocherki po fizike morya" [Essays on Physics of the Sea], Moscow, Izd-vo AN SSSR, 1962.

18. Carey, F. G. and T. M. Teal, "Why is a Tuna Warm?" OCEANUS, Vol 13, No 1, 1966.

19. Lighthill, M. T., "Hydromechanics of Aquatic Animal Propulsion," ANNUAL REVIEW OF FLUID MECHANICS, No 1, 1969.

UDC 599.537+591.173

THE HYDRODYNAMIC CHARACTERISTICS OF THE BLACK SEA DOLPHIN IN DIFFERENT ACCELERATION MODES

Kiev BIONIKA in Russian No 12, 1978 pp 48-55

[Article by V. P. Kayan and V. Ye. Pyatetskiy, Institute of Hydromechanics of the Ukrainian SSR Academy of Sciences]

[Text] From the viewpoint of simulating an impeller, the most promising among aquatic animals is the dolphin, in which the locomotor oscillatory motions are concentrated mainly in the caudal part of the body. Having relatively low energy resources, dolphins can achieve rather high swimming speeds. The well-known Gray's paradox [17] explains this by the rather low hydrodynamic drag of this animal during active swimming.

However, it is not yet possible to determine instrumentally the drag of a swimming dolphin. Therefore, attempts were recently made in different countries to create a theoretical model of the motion of fishes and dolphins [8, 20, 21]. Based on common propositions of thin-body theory and known theorems on conservation of impulse and energy, using the equations of hydrodynamics for a high-aspect wing, Academician of the Ukrainian SSR Academy of Sciences G. V. Logvinovich found formulas for calculating the averaged thrust and hydromechanical efficiency of the impeller of aquatic animals during oscillations which have a large lunate caudal fin (tuna and dolphins) [8]. It is shown that the kinematic characteristics of motion of the caudal fin mainly affect the formation of the animal's thrust.

Experimental data have been published on the kinematics of swimming by the Black Sea dolphin [10] at swimming speeds up to 2.5 m/s, on the basis of which the hydrodynamic characteristics were later calculated from G. V. Logvinovich's formulas [11]. The kinematic characteristics of six Black Sea dolphins in the range of swimming speeds from 1.5 to 6.5 m/s [5] with different acceleration modes were subsequently found. The experimental results were found by high-speed movie filming in a biohydrodynamic channel specially designed for working with dolphins [12]. The body shape and the geometric dimensions of these dolphins are presented in Figure 1 and in the table.

The hydrodynamic characteristics of active swimming of these animals, calculated by the mentioned formulas of G. V. Logvinovich [8], are presented below. In the given case the total thrust of the dolphin impeller, averaged during the oscillatory cycle, was determined by the expression

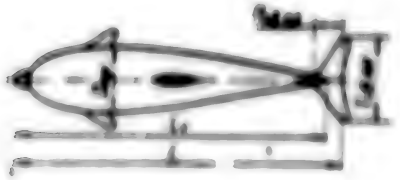

Figure 1. Body Shape of Black Sea Dolphin

$$(F_n) = \frac{\lambda_1'}{1+\frac{1}{\lambda}}\,v^2\left(\frac{A_0}{l}\right)^2\left[\frac{c}{v}\left(\frac{c}{v}-1\right)-\frac{1}{1+\frac{1}{\lambda}}\left(\frac{c}{v}-1\right)^2\right]. \qquad (1)$$

where v is the forward speed of the animal, m/s, c is the speed of propagation of the locomotor wave along the body, m/s, A_0 is the amplitude of the locomotor wave on the trailing edge of the caudal fin, meters, $l = \chi/2\pi$ is the reduced wavelength, meters, χ is the length of the locomotor wave, meters, $\lambda_1' = \rho\pi a^2$ is the reduced mass of separation, kg·s^2/m^2, ρ is water density, 104 kg·s^2/m^4, 2a is the span of the caudal fin, meters, $\lambda = (2a)^2/S_{pl}$ is the aspect ratio of the caudal fin and S_{pl} is the area of the plane of the caudal fin, m^2.

Geometric Dimensions of Experimental Dolphins

(1) Параметр	Номер объекта (2)					
	1	2	3	4	5	6
Полная длина L, м (3)	2,35	2,60	2,60	2,65	2,70	2,62
Длина корпуса $L_к$, м (4)	2,25	2,30	2,24	2,35	2,44	2,32
Корневая хорда хвостового плавника $N_{хв.пл}$, м (5)	0,21	0,22	0,29	0,23	0,22	0,225
Размах хвостового плавника $l_{хв.пл}$, м (6)	0,53	0,52	0,58	0,54	0,59	0,61
Приведенный диаметр миделя $D_{пр}$, м (7)	0,41	0,38	0,415	0,43	0,42	0,433
Масса G, кг (8)	~150	~140	190	185	175	210
Удлинение корпуса, $\lambda_к = \frac{L_к}{D_{пр}}$ (9)	5,5	6,05	5,4	5,4	5,8	5,35
Площадь смоченной поверхности тела Ω, м^2 (10)	2,18	2,26	2,35	2,60	2,65	2,10
Удлинение хвостового плавника (11) $\lambda = l^2_{хв.пл}/S_{хв.пл}$	4,3	3,7	3,5	4,1	4,3	4,1

Key:

1. Parameter
2. Number of object
3. Total length L, meters
4. Body length $L_к$, meters
5. Root chord of caudal fin $N_{khv.pl}$, meters
6. Span of caudal fin $l_{kh.pl}$, meters
7. Reduced mid-section diameter D_{pr}, meters
8. Mass G, kg
9. Aspect ratio of body, $\lambda_k = L_k/D_{pr}$
10. Area of wetted body surface Ω, m^2
11. Aspect ratio of caudal fin $\lambda = l^2_{khv.pl.}/S_{khv.pl.}$

In the special case when the motion of the dolphin is linear and uniform and acceleration of motion of its center of gravity during the period of oscillation is equal to zero, the thrust P_g and drag P_x are equal in absolute value to each other, but are opposite in sign.

The coefficient of total hydrodynamic drag of the dolphin was determined by the formula

$$\zeta = \frac{2P_x}{\rho v^2 S}, \tag{2}$$

where S is the area of the wetted surface of the dolphin, determined by calculation by the geometric dimensions of the body and fins.

The ideal hydromechanical efficiency of the propulsive system of the dolphin, averaged during oscillations and equal to the ratio of its useful work to the total expended work (useful work plus the kinetic energy of the wake), is found by the expression

$$\eta_i = 1 - \frac{1}{1 + \frac{A_0}{l}}\left(1 - \frac{\bar{v}}{v}\right). \tag{3}$$

The kinematic parameters A_0/l and $\bar{v}/v$ required for the calculations at different speeds and accelerations of the dolphin were borrowed from [5]. The aspect ratio of the caudal fin of the investigated dolphins is within the range from 3.5 to 4.3. All calculations were made in tabular form. The results of the calculations of hydrodynamic characteristics of dolphins are presented in graphical form as a function of swimming speed and acceleration.

Figure 2. Dependence of Ideal Hydromechanical Efficiency of Dolphin Impeller on Re Number During Acceleration of Motion, m/s^2: 1--(-0.10 to -0.03); 2--(-0.2 to 0.08); 3--(0.10-0.30); 4--(0.35-0.70); 5--(0.79-1.50); a--uniform; b--equal accelerated motion

The dependence of the ideal hydromechanical efficiency η_i of the dolphin impeller, calculated by formula (3), on Re number is presented in Figure 2. The values of η_i given here correspond to specific swimming modes of dolphins with different accelerations $\bar{v}$ in value and sign, m/s^2, averaged during the period of oscillations of the caudal fin. It follows from the values of η_i that the hydromechanical efficiency of the impeller is somewhat lower in the active swimming mode with forward acceleration (Figure 2, b) when the thrust developed by the dolphin's impeller

exceeds the drag of the surrounding medium, than during uniform swimming of the dolphin (Figure 2, a). A decrease of the spread of values of efficiency and a common tendency toward an increase of it are observed as the speed of motion increases. Compared to [11], higher values of efficiency η_i were found due to the more accurate calculation of the real speed of motion v of the dolphin (variation of the scale of the dolphin's path along the movie frame was not taken into account in [10, 11], which led to a decrease of the value of v and consequently of the ratio v/c).

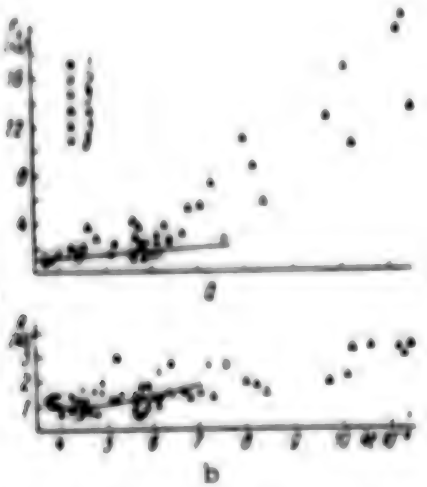

b

Figure 3. Dependence of Thrust of Impeller (a) and of Hydrodynamic Drag (b) on Swimming Speed and Acceleration of Dolphin: 1-5--the same as in Figure 2; 6--acceleration during inertial swimming.

The average thrust of the dolphin impeller (F_x), calculated by formula (1) during the period of oscillations, is presented in Figure 3, a as a function of Reynolds number $Re = vL/\nu$, where ν is the kinematic coefficient of viscosity of water whose value varied in the given case: $(0.93\text{-}1.16)\cdot 10^{-6}$ m^2/s. The solid line which averages points 2 on the graph shows the modes in which the dolphin moves almost uniformly (i.e., F_x and R_x are essentially equal to each other in absolute value). As the swimming speed and acceleration of the dolphin increase, the thrust of its impeller required to overcome hydrodynamic and inertial forces also increases.

For a dolphin to swim with acceleration, the value of the hydrodynamic drag (R_x) averaged during the period of oscillations was found as the difference of the thrust (F_x) and inertial drag (R_i), i.e.,

$$(R_x) = (F_x) - (R_i). \tag{4}$$

According to Newton's second law, a force $m\dot{v}$ must be applied to a body with mass m to move it with acceleration $\dot{v}$. The virtual mass should also be taken into account during motion of a body in a viscous fluid. Since the main mass of the dolphin moves almost without oscillations and moves linearly, and the oscillations are made only by the caudal stem and caudal fin, then in the first approximation, having taken the dolphin's body as an equidimensional ellipsoid of rotation moving along its own longitudinal axis, the expression for the total mass will have the form

$$m = m_g + \lambda_{11}, \tag{5}$$

where $m = G/g$ is the mass of the dolphin, $kg \cdot c^2/m$, G is the weight of the dolphin, kg, $\lambda_{11} = k_{11}\rho V$ is the virtual mass, $kg \cdot c^2/m$, V is the dolphin's displacement, m^3, and k_{11} is the coefficient of virtual mass.

The dolphin's weight was determined by weighing in air and coefficient k_{11} was determined by nomograms of [1]. The values of k_{11} = 0.04-0.05 for experimental dolphins. Finally, the value of R_i was calculated by the formula

$$R_i = m_g(1 + k_{11})(\dot{v}). \tag{6}$$

According to the method presented in [5], the displacements of the dolphin's center of gravity during small time intervals (approximately 0.05 second) were determined and graphs of variation of the dolphin's forward velocity v during the averaging time (1-5 seconds) were constructed. The mean variation of the dolphin's speed ($\dot{v}$) was determined by it for each complete period of oscillations of the caudal fin. The values of hydrodynamic drag determined by formula (4) in the active swimming mode of dolphins are presented in Figure 3, b at different values of accelerations $\dot{v}$ as a function of Re number. The solid line also averages points 2 belonging to modes in which the dolphin moves almost uniformly. The values of drag of a dolphin moving by inertia without bending-oscillatory motions of the body (point 6) are also given here. In this case its hydrodynamic drag was determined by formula (6). Slowing of velocity v was calculated as the mean value during the entire period of averaging. The drag of a dolphin moving by inertia was higher in almost the entire investigated range of swimming speeds than that of a dolphin with active bending-oscillatory motions of the body. The data are indirect confirmation of J. Gray's [17] and T. Wu's [21] hypotheses that the wave motion draws out laminar flow over a body, creating a negative pressure gradient in its caudal part. This hypothesis has also been confirmed by the experimental work of Ye. V. Romarenko [13], who investigated the pressure distribution on an oscillating flexible streamlined body (a rubber wedge).

The coefficients of hydrodynamic drag of a dolphin ζ are presented in Figure 4 as a function of Reynolds number Re, calculated by formula (2). Almost all the values of ζ are located in the transition zone bounded on the bottom by curve 12, which is the values of the coefficient of drag of a technically smooth body of rotation equivalent in shape and size to a dolphin's body during completely laminar flow and bounded on the top by curve 13, which corresponds to the values of the drag coefficient of the same body provided that there is completely turbulent flow mode.

As is known, the drag coefficient of a well-streamlined completely submerged body is proportional to the frictional coefficient of an equivalent plate [3]. The proportionality constant is determined from the set of experimental curves as a function of the ratio of the main measurements of the body L/B and H/B, where L is length, B is width and H is the height of the body [3].

In our case the value of the proportionality constant is k = 1.22 for all the experimental animals. Thus, curves 12 and 13 are the values of the drag coefficients of a technically smooth plate during laminar (curve 10) and turbulent (Curve 11) flow [16], magnified 1.22 times.

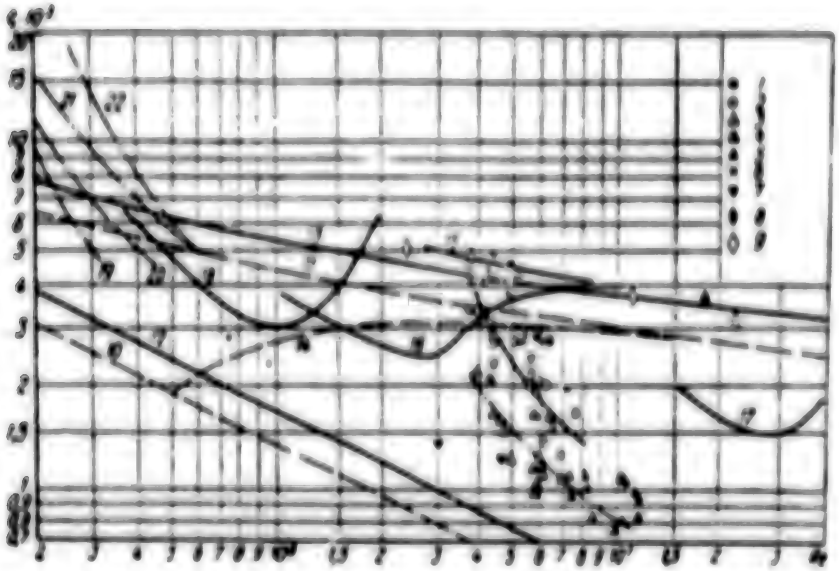

Figure 4. Dependence of the Coefficient of Hydrodynamic Drag of Different Aquatic Animals and Their Models According to Re Number: 1-6--the same as in Figures 2 and 3; 7, 8 and 9--from data of [15], [9] and [19], respectively

The small spread of calculating points can be fully explained by the spread of experimental data by amplitude-frequency characteristics of experimental dolphins. The values of ζ, as in the case for η_i, due to the reasons already outlined above, are somewhat lower than similar values found in [11]. All the values of ζ for Black Sea dolphins are in the zone of mixed flow over their body.

The drag coefficient of a model of the Black Sea dolphin in completely turbulent flow mode (curve 15) and with mixed flow with laminar section up to $\bar{x}_{kr} = 0.687$ (curve 16) [15], also found by computer calculation, are shown in Figure 4 for comparison. The experimental points 7, found by B. N. Semenov, for a Black Sea dolphin with length of $L = 2.05$ meters, moving by inertia in a net enclosure, has a wide spread ($(1\text{-}2)\cdot10^{-3}$ and $(0\text{-}2)\cdot10^{-3}$) and are apparently underestimated, which as the author himself notes [15], is related to the low accuracy of the results and the short averaging time (one second or less). The work of B. V. Kurbatov [7] should also be mentioned here, in which the coefficient of the hydrodynamic drag of some animals moving by inertia in a small biohydrodynamic channel is calculated. A drag coefficient of $\zeta = (15\text{-}25)\cdot10^{-3}$ was found in the range of Reynolds numbers of $Re = (0.5\text{-}1.5)\cdot10^{6}$ for the Azovka dolphin, which is clearly exaggerated (this is probably explained by the strong effect of the walls of the channels since the cross-sectional area was equal to only 0.85 m^2).

Points 9 are the drag coefficients calculated by the wetted surface for a dolphin of $L = 1.86$ meters and $G = 52.7$ kg [19], moving by inertia without bending-oscillatory motions of the body. They correspond to drag of a solid equivalent in shape with almost completely turbulent flow. It should be noted that in the given case the photographs were made in a marine lagoon with an unsealed movie camera from the surface and it is unknown exactly whether the dolphin made any motions with the caudal fin or not during deceleration.

Moreover, attempts were undertaken to determine the drag of a moving dolphin using added drag (a turbulizing ring) [2, 18]. However, the hypothesis that a trained dolphin develops identical thrust both with and without the ring is not supported by critics since it is impossible to compare the thrust of the impeller in two modes without taking into account its kinematic characteristics in both cases.

The dependence of the drag coefficients of "Dolphin" models [9] with body edges made in the form of a body of rotation according to NACA profile of series 66 and calculated by formula (2) on Reynolds number is presented in Figure 4, curve 17. Experimental point 8 corresponds to the drag coefficient of this same model for the case when flow in the bow section of the model is artificially turbulized.

The hydrodynamic drag of the body of a dead Azovka dolphin with length L = 1 meter (curve 18) was determined by towing in a basin [6]. It should be noted that there was a rod in the front part of the dolphin during towing which turbulized the flow somewhat. A rapid increase of the drag coefficient at Re > 10^6 is apparently explained by insufficient submergence of the towed body and accordingly by the effect of the free surface on the measurement results.

The coefficients of hydrodynamic drag of different fish (trout, mullet, bluefish and garfish, respectively), found by calculation, are shown by ζ(Re) by curves 19-22 in Figure 4 [4]. They hydrodynamic characteristics of representatives of eel-like fashion of swimming--garfish--were determined by the formulas proposed in 1970 by G. V. Logvinovich [8].

For representatives of the Scombridae fashion of swimming (trout, mullet and bluefish), the locomotive force which occurs on the fish due to the pulses flowing into the wake of the flow from the trailing edge of the caudal fin [14], is determined by the formula

$$(I) = \frac{\lambda_1'}{2}\left(\frac{A_0}{l}\right)^2 v^2 \left\{\left(\frac{c}{v}-1\right)\left[1-\frac{1}{3}\left(\frac{c}{v}+1\right)\right]-\left(\frac{l}{L}\right)^2\right\}. \qquad (7)$$

Formula (7) for the Scombridae fashion of motion with linear variation of amplitude over the fish's body differs from that presented in [8] for the eel fashion of motion only by the multiplier in the braces. At v/L > 4 when the value of c/v is within the range of 1.05-1.15, the thrust with Scombridae fashion of motion, all things being equal, is 10-15 percent less than that during eel fashion of motion.

One of the factors which contribute to an increase of the hydrodynamic drag of a fish at low speeds is the circumstance that fish do not retract their pectoral and abdominal fins at low swimming speeds, the effective of which on drag was not taken into account in the method of calculation used. As swimming speed increases, the values of the hydrodynamic drag coefficient of fish shift to the zone bounded by curves 12 and 13 and a tendency toward a decrease of hydrodynamic drag coefficient is observed with an increase of the linear dimensions of the test objects and their swimming speed (i.e., with an increase of Reynolds number).

The dolphin's hydrodynamic drag, found to be rather low in our investigations compared to known solids in hydromechanics, can be determined by several specific

features. The streamlined shape of the body (the "Dolphin" model), involving laminar flow, contributes to a decrease of the total drag of the dolphin. The transient nature of the dolphin's forward motion, determined by the nature of action of its caudal ispeller, may also under certain conditions lead to a specific decrease of the drag of models after they are coated with a material having elastic properties.

Analysis of the experimental calculated data presented in Figure 4 shows that the hydrodynamic drag coefficient is rather high at low swimming speeds when the dolphin has an excess of energy resources. The value of ζ decreases significantly with an increase of swimming speed and consequently of Re number and the flow over the dolphin becomes mixed; moreover, a significant part of its body surface is apparently subjected to laminar flow.

Thus, the calculated data found on the basis of experimental investigations on the drag coefficient of the dolphin confirm the hypothesis of low drag of the dolphin compared to ordinary mechanical objects. It is feasible that the results will be checked in the future on mechanical models similar in shape.

BIBLIOGRAPHY

1. Voytkunskiy, Ya. I., R. Ya. Pershits and I. A. Titov, "Spravochnik po teorii korablya" [Handbook on Ship Theory], Leningrad, Sudpromgiz, 1960.

2. Grushanskaya, Zh. Ya. and A. I. Korotkin, "Some Problems of the Hydrodynamics of the Dolphin," "Tezisi IV Vsesoyuz. konf. po bionike" [Report Topics of the Fourth All-Union Conference on Bionics], Vol 6, Moscow, 1973.

3. Droblenkov, V. P., "The Problem of Determining the Drag Coefficient of the Ship Shape," SUDOSTROYENIYE, No 6, 1960.

4. Kayan, V. P. and V. Ye. Pyatetskiy, "Investigating the Swimming Hydrodynamics of Fishes," "Tez. dokl. IV Vsesoyuz. s"yezda po teoret. i prikl. mekhanike" [Report Topics of the Fourth All-Union Congress on Theoretical and Applied Mechanics], Kiev, 1976.

5. Kayan, V. P. and V. Ye. Pyatetskiy, "The Kinematics of Swimming of the Black Sea Dolphin as a Function of Acceleration Mode," BIONIKA, No 11, 1977.

6. Kozlov, L. F, V. Ya. Pyatetskiy and Yu. N. Savchenko, "The Towing Capability and Possible Swimming Speeds of Dolphins," in "Mekhanizmy peredvizheniya i orientatsii zhivotnykh" [The Mechanisms of Locomotion and Orientation of Animals], Kiev, 1968.

7. Kurbatov, B. V., "The Hydrodynamic Drag of Live Nectors," "Tezici IV Vsesoyuz. konf. po bionike," Vol 6, Moscow, 1973.

8. Logvinovich, G. V., "The Hydrodynamics of Swimming of Fishes," BIONIKA, No 7, 1973.

9. Petrova, I. M., "Gidrobionika v sudostroyenii" [Hydrobionics in Shipbuilding], Leningrad, 1970.

10. Pyatetskiy, V. Ye. and V. P. Kayan, "The Kinematics of Swimming of the Black Sea Dolphin," BIONIKA, No 9, 1975.

11. Pyatetskiy, V. Ye. and V. P. Kayan, "The Hydrodynamic Characteristics of Swimming of the Black Sea Dolphin," BIONIKA, No 10, 1976.

12. Pyatetskiy, V. Ye., V. P. Kayan, L. F. Kozlov and N. P. Semenov, "Device for Investigating the Kinematics of Swimming of Dolphins," BIONIKA, No 12, 1978.

13. Romanenko, Ye. V., "The Hydrodynamics of Fishes and Dolphins," MORSKOYE PRIBOROSTROYENIYE, SERIYA AKUSTIKA, No 1, 1972.

14. Savchenko, Yu. N.,and V. T. Savchenko, "Analysis of the Inertial Forces When Calculating the Thrust of a Flexible Swimming Body," BIONIKA, No 7, 1973.

15. Semenov, B. N., "The Existence of the Hydrodynamic Phenomenon of the Black Sea Dolphin," BIONIKA, No 3, 1969.

16. Schlichting, H., "Teoriya pogranichnogo sloya" [Boundary Layer Theory], Moscow, Nauka, 1969.

17. Gray, J., "Studies in Animal Locomotion. The Propulsive Powers of the Dolphin," JOURNAL OF EXPERIMENTAL BIOLOGY, Vol 13, No 1, 1936.

18. Lang, T. G., "Hydrodynamic Analysis of Cetacean Performance," in "Whales, Dolphins and Porpoises," edited by K. S. Norris, Berkeley, Los Angeles, 1966.

19. Lang, T. G. and K. Pryor, "Hydrodynamic Performance of the Porpoise (Stenella attenuata)," SCIENCE, Vol 152, No 3721, 1966.

20. Lighthill, M. J., "Hydromechanics of Aquatic Animal Propulsion," ANNUAL REVIEW OF FLUID MECHANICS, Vol 1, 1969.

21. Wu, T. Y., "Hydromechanics of Swimming Propulsion," JOURNAL OF FLUID MECHANICS, Vol 46, No 3, 1971.

UDC 599.537

DEVICE FOR INVESTIGATING THE KINEMATICS OF SWIMMING OF DOLPHINS

Kiev BIONIKA in Russian No 12, 1978 pp 55-58

[Article by V. Ye. Pyatetskiy, V. P. Kayan, L. P. Kozlov and N. P. Semenov, Institute of Hydromechanics of the Ukrainian SSR Academy of Sciences]

[Text] Study of the physical characteristics of transient flow over fast-swimming marine animals is one of the interesting scientific trends of modern biohydromechanics. Several methods, one of which assumes the use of movie-film data, are now used for quantitative determination and analysis of the hydrodynamic characteristics of swimming by aquatic animals. In this case the experimental animals are placed in on-shore tanks or into net cages located in the open sea and their behavior, speed, trajectory and elements of the kinematics of swimming are recorded using aerial or underwater movie filming. Thus, for example, the swimming motions of dolphins and sperm whales were recorded using underwater movie filming at Marine Land Basin (Florida) with subsequent analysis of the movie frames [6]. In the summer of 1966, the swimming speed and acceleration of two Black Sea dolphins were determined from data of underwater movie filming in a cage [3].

The speed of the Pacific bottlenosed dolphin was measured by a movie camera in the Hawaiian Islands in a small lagoon enclosed with a metal net [4]. Attempts were made to study the kinematic characteristics of swimming of dolphins by surface movie filming in a circular channel with glass walls in the working section of the channel [1]. However, the elements of the kinematics of swimming of dolphins, especially at high speeds, can be determined better on a straight course since the values have a significant error when processing movie films of curvilinear motion of the animal.

The elements of the kinematics of swimming of the dolphin in transient modes were measured by the indicated method in a small tank measuring 15 X 7 meters [5]. The speed and other elements of the kinematics of swimming of the Azov dolphin, which was in the open sea in a net cage measuring 40 X 8 X 5 meters [2] were determined in 1970 using underwater movie filming.

The experimenter must take into account the light absorption and scattering in the water, its transparency, the lighting conditions of the objects under investigation, the hermetic sealing and strength of the apparatus and various attachments used and moreover he must encounter a number of conditioned and unconditioned reflexes of aquatic animals in the presence of feedback from the surrounding environment during underwater movie filming, especially when investigating high-speed

transient processes in an aquatic medium. Thus, the method of determining the speed and other elements of the kinematics of swimming of aquatic animals in tanks, coastal net cages and in the open sea using underwater movie filming also has a number of disadvantages. A special device was developed, manufactured and tested to eliminate them, i.e., to increase the effectiveness of studying the kinematics of swimming of aquatic animals, specifically of dolphins.

The animal under investigation is placed in a straight on-shore channel of rectangular cross-section, in the middle part of which one lateral wall is glazed, and on the other wall and the bottom are placed a rectangular coordinate grid, which permits one to investigate the elements of kinematics of swimming of the animals in the vertical and horizontal planes by methods of surface movie filming (including the use of stereo photography) when the object under investigation is under conditions close to natural. The channel is equipped with special carriages: one moves the bait for the animal at given speeds and the other moves the enclosure cage for catching it in the channel. Moreover, it is equipped with a loading-unloading and transport device with a cage for transfer of the animal to the channel and for moving it inside the channel (figure).

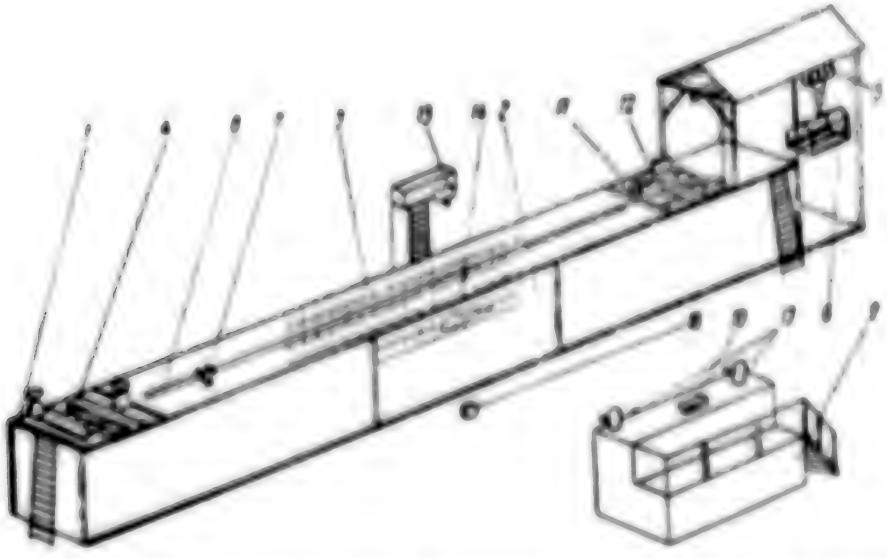

Device for Investigating the Kinematics of Swimming of Dolphins

The channel 1 is a long strong metal structure installed on a rigid foundation, which ensures retention of the linearity of its axial line after being filled with water. The length of the channel is selected as sufficient to provide a "working section" in which the animal under investigation can move with uniform speed. The transverse dimensions of the channel are selected so that its walls and the free surface of the water do not affect the motion of the experimental animal at the required speed.

There is a glazed section 2 with coordinate grid 3 in the mid-part in one of the lateral walls of the channel. The dimensions of the section depend on the dimensions of the animal under investigation; it is desirable that several lengths of the experimental animal be added on the length of the glazed section of the channel.

The filling and drainage system provides rapid replacement of water in the channel, which makes it possible to maintain sufficient transparency of it.

A special enclosure cage 4 is provided to catch the animal in the channel, it is loaded and unloaded by means of a telpher crane 5 and a specially designed transport cage 6. An additional carriage 7 with bait which moves along a monorail 8 extended above the level of the free surface of the water along the channel in its plane of symmetry, is provided to train the animal to swimming speed.

A raised platform 9 with laboratory bench and control console 10 is installed several meters opposite the glazed part of the channel, parallel to it. Electric power is supplied to the bench, due to which the electric drive 11 which services the carriage 7 and also the electric drive 12 designed for the enclosure cage 4 can be switched on. A movie camera 13 for stereoscopic filming of the swimming of the anisal under investigation 14 is installed on this same bench. A movie camera 15 installed on a special tower above the free surface of the water in the channel in the region of its working section serves to record the trajective motion of the animal in the horizontal plane. An electronic timer 16, which is set into motion simultaneously with the movie cameras 13, is located in the visual field of two movie cameras 13 operating synchronously.

The device for investigating the kinematics of swimming of dolphins is used in the following manner.

The animal under investigation, delivered by transport cage 6, is released into the channel and initially trained to swimming speed along the channel using bait. After the indicated goal is reached, the animal begins to swim from one end of the channel to the other at a specific signal of the trainer. The experimenter switches on the movie camera 13 and electronic timer 16 at the moment when the animal passes the "working section" when it is swimming on the background of the coordinate grid 3. The movie cameras 13 are used as a stereo pair, while the third movie camera 15 is switched on to record the motion of the animal in the horizontal plane.

Compared to devices to conduct similar investigations in the open sea, a marine cage or in an ordinary on-shore tank, the given device has the following advantages.

- the angle of viewing the object is increased up to 25 percent with the same filming optics, since the effect of the refractive index upon transition from an air to a water medium is insignificant in the given case and the image size in the visual field is essentially dependent only on the distance between the movie camera and the filming object, while the visual angle of the objective cannot be increased in this manner under underwater conditions (in the open sea, cage or tank) due to light scattering and the inhomogeneity of the water medium with random distribution of the refractive index.

- technique of movie filming is simplified (there is no need to seal the movie camera and other attachments and devices).

- The operating range of the investigations is increased significantly since filming is accomplished in air and light absorption and scattering in the water and the transparency of the water essentially have no effect on the results.

The animal under investigation does not respond to the movie operator since he essentially does not see him and does not hear the noise of the operating camera.

It is more convenient to use stereo filming and also movie recording of the trajectory of motion of the animal in the horizontal plane in the given case compared to underwater movie filming in the open sea.

BIBLIOGRAPHY

1. Pershin, S. V., "Hydrobionic Functions of Transient Harmonic Motion of Fishes and Dolphins as Submerged Bodies of Variable Shape," in "Problemy bioniki" [Problems of Bionics], Moscow, 1973.

2. Pyatetskiy, V. Ye. and V. P. Kayan, "Some Kinematic Characteristics of Swimming of the Azov Dolphin," BIONIKA, No 6, 1972.

3. Semenov, B. N., "The Existence of the Hydrodynamic Phenomenon of the Black Sea Dolphin," BIONIKA, No 3, 1969.

4. Lang, T. G. and R. S. Morris, "Swimming Speed of Pacific Bottlenose Porpoise," SCIENCE, Vol 151, No 371, 1966.

5. Miller, P. P. and H. J. White, "Note on the Swimming Deceleration of a Dolphin," JOURNAL OF FLUID MECHANICS, Vol 38, Part 3, 1969.

6. Slijper, E. J., "Locomoting and Locomotory Organs in Whales and Dolphins," VERTEBRATE LOCOMOTION, SYMPOSIUM OF THE ZOOLOGICAL SOCIETY, London, No 5, 1961.

UDC 597:591.17

INDICATORS OF THE HYDRODYNAMIC DRAG OF SQUID TODARODES PACIFICUS (STEENSTRUP)

Kiev BIONIKA in Russian No 12, 1978 pp 58-62

[Article by B. V. Kurbatov, Institute of Biology of the Southern Seas imeni A. O. Kovalevskiy of the Ukrainian SSR Academy of Sciences]

[Text] Squid occupy a special place among the numerous species of marine animals. The use of a hydrojet impeller for swimming was determined by a number of characteristics in their internal and external body structure. The hydrodynamics of squid is unique. The well-streamlined, spindle shape of the body, suction-blowing of the boundary layer, variation of the body configuration during motion and other characteristics permit squid to achieve rather high swimming speeds [2].

Study of the characteristics of squid which determine the reduction of hydrodynamic drag is of significant interest. Experiments carried out by physical and mathematical modelling are usually related to specific assumptions and simplifications, due to which they are comparatively approximate in nature. More accurate results can be achieved when working with live objects.

The results of experimental determination of the overall hydrodynamic drag encountered by live squid of Todarodes pacificus (Steenstrup) when swimming at different speeds are presented in this article. The data, along with other hydrodynamic characteristics, can be used when determining the characteristics of squid hydrodynamics and when analyzing their efficiency of motion.

The investigations were conducted in August-September of 1973 on an experimental basis. Eight specimens of Pacific squid (see table) were used in the experiments. The squid were caught with squid traps on the day of their experiment. Immediately after being caught, the animals were placed in tanks with sea water, transported to shore and transplanted to net-enclosed ponds (1 X 1 X 0.8 meter) with 1-2 specimens in each. Immediately prior to the beginning of work, the next squid was transferred from the pond to the flow channel in which it swam freely.

The investigations were carried out by a method which we developed [4] using designed equipment consisting of a collapsable flow channel and an automatic system with the recording apparatus (Figure 1). The channel consists of three 2-meter sections connected by bolts and having cross-section of 0.6 X 0.5 meter. Two parallel guides for the platform of the tracking system are installed on 12 supports above the channel (1.5 meter above the water surface). All the structures are manufactured from AMG-5 rolled steel to reduce mass and to protect them against

corrosion. The locomotion and parameters of motion of the animals in the channel were recorded by using the corresponding sensors and movie camera installed on the mobile platform of the tracking system.

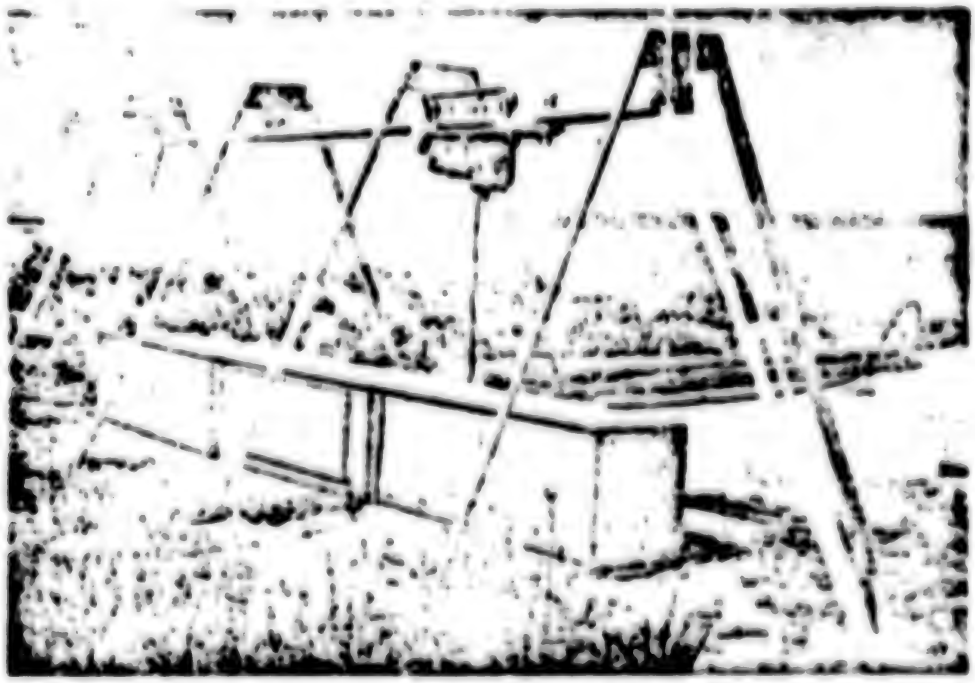

Figure 1. Overall View of Flow Channel

The platform, set in motion by a reversible DC electric motor, moves on rollers along the two guides above the water surface of the channel. Electric energy to power the assemblies of the system and of the recording apparatus is fed to the platform by a freely hanging multistrand cable.

Main Data of Squid Used in Experimental Investigations

[illegible] (1)	[illegible] (2)	[illegible] (3)	[illegible] (4)	[illegible] (5)	[illegible] (6)
1	0.46	0.045	0.050	0.0430	0.374
2	0.41	0.045	0.050	0.0358	0.344
3	0.39	0.045	0.050	0.0339	0.330
4	0.41	0.052	0.056	0.0375	0.315
5	0.43	0.040	0.052	0.0330	0.213
6	0.37	0.050	0.052	0.0325	0.250
7	0.38	0.041	0.044	0.0340	0.213
8	0.35	0.047	0.048	0.0287	0.217

Key:

1. Number of object
2. Total length, meter
3. Greatest height, meter
4. Greatest width, meter
5. Area of wetted surface, m^2
6. Mass, kg

The bottom of the channel is painted in a light tone over its entire length. The reflectivity of its surface and of the body surface of the animal being observed are different even in the presence of active homochromy in the animal. This difference is detected by the scanning photodetectors of the system. The sensing elements of the photodetectors are photoresistors of type FSD-0, connected in a bridge circuit. Short-focus lenses are used as the optical system of the sensors.

The four photodetectors are attached in pairs along the edges of the platform. Each pair scans a section of the water mass over the entire width of the channel and on 0.5 meter along the longitudinal axis. The size of the observation zone under the platform is established by varying the angle of inclination of the sensors to the bottom plane, which significantly accelerates adjustment of the system when working with animals of different size.

When an object of observation is moving along the channel, its image falls into one of the scanning zones and the bridge circuit is unbalanced in this case, which in turn causes the appearance of an error signal. The signal amplitude depends on the contrast of the object on the background of the bottom and the depth of its penetration into the scanning zone, while the polarity depends on the direction of motion.

The unbalancing signal is amplified by two amplifiers (a preliminary and power amplifier) and is fed to the actuating electric motor which moves the platform in the direction of motion of the observation object at a speed proportional to signal amplitude. If the animal is outside the scanning zone, the balance of the bridge circuit of the photosensors is restored. Thus, the platform is constantly over the observation object during operation, moving synchronously with it along the channel. The time constant (0.07 second) and other dynamic characteristics of the system provide stable observation of the animals (with total length of 7 cm or more), moving at a speed up to 6 m/s at acceleration up to 2 m/s^2.

A version of remote control without using photoobservation has been provided in the design of the system. In this case the operator visually observes the animal swimming in the channel, matching the motion of the platform with it by using a portable control console. Information about the speed and direction of motion of the platform (the sensor is a DC tachogenerator) is fed to a N-700 loop oscillograph simultaneously connected to a Konvas-Avtomat movie camera. The simultaneity of connection was provided by a special relay block. Precise comparison of the movie frames with the oscillographs during processing was achieved by frame markers which are superimposed on the oscillograms during filming in the form of vertical lines by an automatic device developed by the author. Each marker on the oscillogram corresponds to a photographed frame.

Active motion of squid is accomplished mainly by a hydrojet impeller, but the animals use undulation of the caudal fin to create locomotive force in cases of slow swimming and when maneuvering at low speeds. The process of hydrojet swimming is accomplished in two steps. The first step is filling the mantle cavity with water and the second is discharge of the water through the funnel. Periodic discharges of a jet of water create a propulsive force, due to which the squid moves. The animal's body moves by inertia with subsequent intake of water after each thrust.

Speed attenuation due to the braking effect of the water is observed in sections of inertial motion. The value of drag can be found by using the known expression

$$F = (m + \lambda)\frac{dv}{dt},$$

where F is the force of total hydrodynamic drag, m is the mass of the squid without water in the mantle cavity, λ is the virtual mass of water and dv/dt is acceleration. Mass m was calculated by the weight of the squid. The value of the virtual mass of water λ was calculated for ellipsoids equivalent to the animals [3]:

$$\lambda = \frac{4}{3}\mu_0 \pi \rho a b c,$$

where μ_0 is the coefficient of the reduced mass of the water, ρ is the density of sea water and a, b and c are the semiaxes of an ellipsoid of rotation equivalent to the animal.

Acceleration dv/dt was determined from experimental data in the following manner. When the movie films were processed by inspection, sections of inertial motion of squid were found at moments of time between discharge of water from the funnel and intake of it (up to 0.1 second). The speed recordings corresponding to these sections on the oscillograms were determined by recalculating the frame markers from the moment the movie camera and oscillograph were switched on. The amplitude values of velocities at the beginning and end of each section of inertial motion were measured on the oscillograms. The real values of velocities corresponding to those measured on the oscillograms were found by the calibrated graph of the velocity sensor.

After this, acceleration: $dv/dt = (h_1 - h_2)k/t$, where h_1 and h_2 are the amplitude values of velocity on the oscillogram, k is the calibrated coefficient of the velocity meter and t is the time of inertial motion, was then calculated for each section of inertial motion.

The coefficients of total hydrodynamic drag (C_x) in all ranges of velocities of inertial motion recorded in the experiments were calculated for each specimen by the formula

$$C_x = \frac{2F}{\rho v^2 S},$$

where F is the drag of water, ρ is the density of sea water, v is the speed of the animal and S is the area of the wetted body surface.

The area S was determined by adding the areas of the elementary plane geometric figures into which the entire external body surface of the animals was arbitrarily divided.

The Reynolds number was calculated by the formula

$$Re = \frac{vl}{\nu},$$

where v is velocity, L is the total body length of the squid and ν is the coefficient of kinematic viscosity of water.

The calculated values of C_x and Re were used to find the function $C_x = f(Re)$ (Figure 2). Since the spread of points for eight squid is insignificant, a single averaged curve is presented in Figure 2. As can be seen, the values of C_x decrease exponentially to 0.008 (at $Re \approx 7 \cdot 10^5$) as Reynolds number increases. Coincidence of the curves for different sized objects indicates an insignificant effect of fluctuation of the total length in the range from 35 to 46 cm on the value of total hydrodynamic drag.

Comparison of the results of measuring coefficients C_x of squid to similar indices of such high-speed fishes as mackerel, bluefish and mullet [1] shows that these values hardly differ at equal values of Re, despite the significant differences in external organization and methods of locomotion of squid and fishes.

Figure 2. Function $C_x = f(Re)$: 1-3--correspond to numbers of objects in table

Establishing the characteristics of motion of squid, due to which hydrodynamic drag during swimming is reduced, is of theoretical interest and may be of considerable significance in hydrobionics.

BIBLIOGRAPHY

1. Alyev, Yu. G. and B. V. Kurbatov, "Hydrodynamic Drag of Live Fishes and Some Other Nekters During Inertial Motion," VOPR. IKHTIOLOGII, Vol 14, No 1, 1974.

2. Zuyev, G. V., "Funktsional'nyye osnovy vneshnego stroyeniya golovonogikh mollyuskov" [Functional Bases of the External Structure of Cephalopod Molluska], Kiev, Naukova Dumka, 1966.

3. Kochin, N. Ye., I. A. Kibel' and N. V. Roze, "Teoreticheskaya gidrodinamika" [Theoretical Hydrodynamics], Moscow, Fizmatgiz, 1963.

4. Kurbatov, B. V., "Method of Experimental Determination of the Total Hydrodynamic Drag of Marine Mammals," "Tez. dokl. V Vsesoyuz. soveshch. po izuch. mor. mlekopitayushchikh" [Report Topics of the Fifth All-Union Conference on Study of Marine Mammals], Makhachkala, 1972.

UDC 532.591.534.222

THE KINEMATICS OF A FLEXURAL-OSCILLATING PLATE

Kiev BIONIKA in Russian No 12, 1978 pp 62-67

[Article by B. M. Dombrov and Ye. D. Sorokodun, Taganrog Radio Engineering Institute]

[Text] When a flexural travelling wave with low vibrational amplitude is propagating along a plate, the components of the plate essentially make linear oscillations in the transverse direction. A flexural wave of finite oscillation amplitude occurs during the motion of many hydrobionts. Therefore, it is interesting to consider the kinematics of the components of a plate along which a flexural wave of finite amplitude is propagating since this may contribute to construction of the physical flow pattern and forces near the plate.

Modelling of a flexural travelling wave by oscillations of the leading edge of the plate is apparently more rational than oscillations of a plate by means of a system of rods attached along the entire length of the plate [4, 2]. But reflected waves occur in this case. Let us take a straight travelling wave propagating along a plate and an inverse travelling wave partially reflected from the trailing edge of the plate. Let us assume that they make themain contribution to formation of the form of oscillation of the plate. The form of oscillation of the plate will then have the form

$$y = a_1 \cos(\omega t - kx) + a_2 \cos(\omega t + kx + \alpha). \tag{1}$$

where x and y are coordinates of the points of the travelling wave. t is time, a_1 and a_2 are the amplitude of the forward and inverse waves, respectively, $f = \omega/2\pi$ is the vibrational frequency, $k = \omega/c$ is the wave number, c is the phase velocity of the travelling wave and α is the phase shift between the two waves travelling opposite each other.

Let us assume that $\alpha = 0$ since by a simple shift of the beginning of time counting and the origin along the Ox axis ($t' = t - (\alpha/2\omega)$ and $x' = x - (\alpha/2k)$), equation (1) can be reduced to the form

$$y = a_1 \cos(\omega t - kx) + a_2 \cos(\omega t + kx). \tag{2}$$

Equation (2) can be rewritten in the form

$$y = (a_1 - a_2)\cos(\omega t - kx) + 2a_2 \cos\omega t \cos kx.$$

i.e., superposition of the travelling and standing waves is established on the plate. As is known, from (2) one can find

$$y = A(t)\cos(kx + \varphi(t)), \tag{3}$$

where

$$A(t) = \sqrt{a_1^2 + a_2^2 + 2a_1a_2\cos 2\omega t},$$

$$\operatorname{tg}\varphi(t) = -\frac{a_1 - a_2}{a_1 + a_2}\operatorname{tg}\omega t.$$

Thus, with the given assumptions the shape of the plate has the form of a sinusoid with variable amplitude (Figure 1). The phase of the wave ($kx + \omega(t)$) is a periodic function of t with period equal to $\pi/\omega = 1/2f$. As a result, the given shape has the form of a "variable travelling wave," which moves similar to a travelling wave but only with irregular velocity and variable amplitude.

A "pure" travelling wave is found at $A(t) = a_1$, $\phi(t) = -\omega t + n\pi$ and $n = 0, 1, 2, \ldots$ $\ldots (a_2 = 0)$ and a "pure" standing wave is found at $A(t) = 2a_2\cos\omega t$ and $\phi(t) = n\pi (a_2 = a_1)$. One can find from (3) the velocity of any point of the plate of the shape under consideration. At $y = y_0$ we find

$$\frac{dx}{dt} = \frac{\omega}{k}\left|-\frac{y_0}{\sqrt{A^2(t) - y_0^2}}\,\frac{2a_1a_2\sin 2\omega t}{A^2(t)} + \frac{a_1^2 - a_2^2}{A^2(t)}\right|. \tag{4}$$

The case when $y = 0$ is the most important. We then find the propagation velocity of the mean point of a "variable" wave. From (4) at $y_0 = 0$ we find

$$V = \frac{\omega}{k}\,\frac{a_1^2 - a_2^2}{a_1^2 + a_2^2 + 2a_1a_2\cos 2\omega t}.$$

It is easy to find

$$\max V = \frac{\omega}{k}\,\frac{a_1 + a_2}{a_1 - a_2} \quad \text{at} \quad \omega t = \frac{\pi}{2} + n\pi,\ a_1 \neq a_2,$$

$$\min V = \frac{\omega}{k}\,\frac{a_1 - a_2}{a_1 + a_2} \quad \text{at} \quad \omega t = n\pi,\ n = 0, 1, 2, \ldots$$

The mean velocity during the period will be equal to the velocity of the standing wave ω/k at $a_2 = 0$:

$$\frac{1}{T}\int_0^T V dt = \frac{\omega}{k} = c, \text{ where } T = \frac{\pi}{\omega}$$

We will not analyze the given shape in more detail. Let us say only that there is no difficulty in deriving simple formulas for calculating all the parameters of the wave under consideration, especially those required when working out methods of experimental investigations.

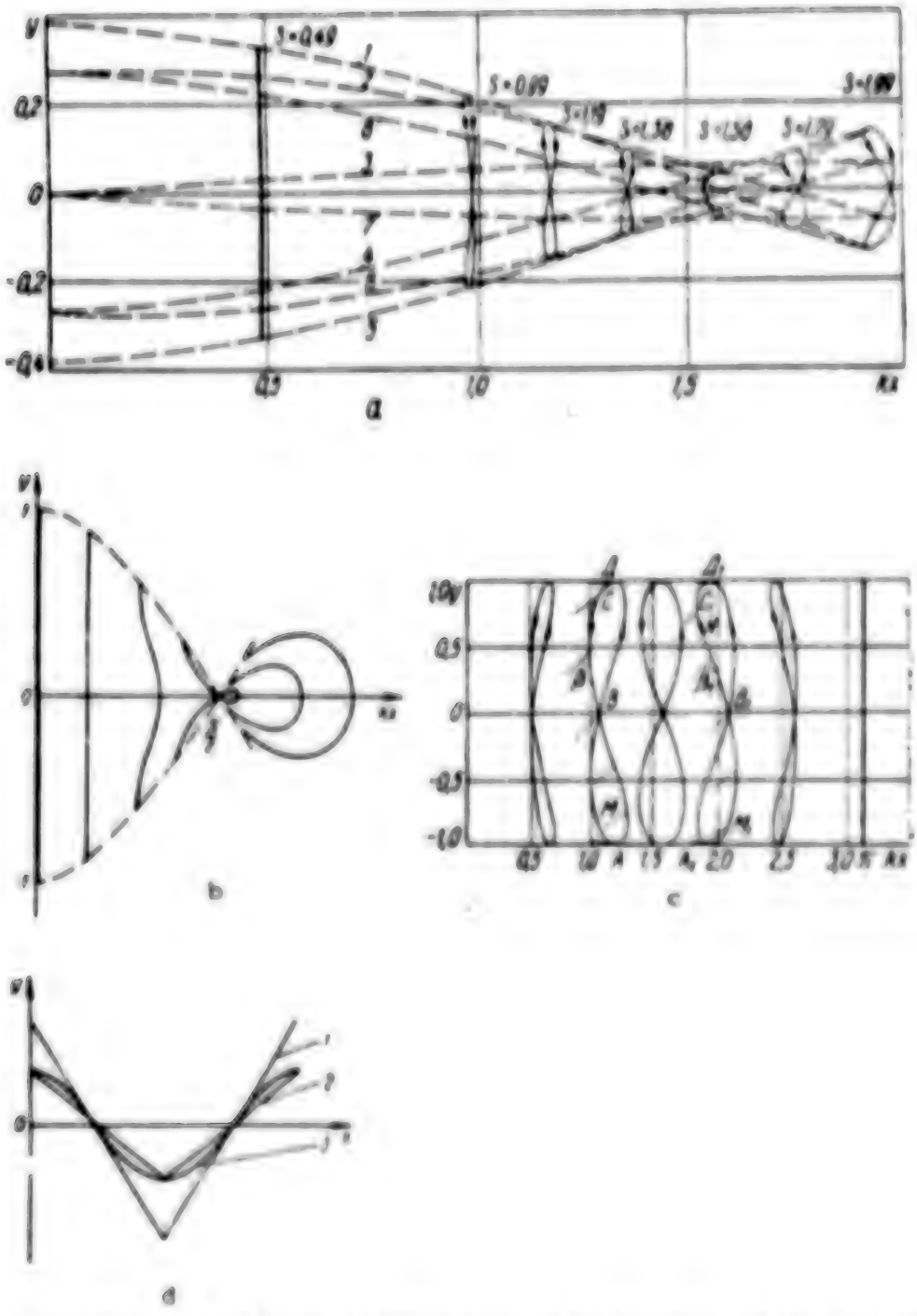

Figure 1. Trajectory and Zone of Variation of Trajectory of End of Plate: a--with length of plate S = const; shape of plate during propagation of two waves travelling opposite to each other along it: 1--ωt = 0; 2--ωt = $\pi/4$; 3--ωt = $\pi/2$; 4--ωt = $(3/4)\pi$; 5--ωt = π; 6--ωt = $(5/4)\pi$; 7--ωt = $(3/2)\pi$; 8--ωt = $(7/4)\pi$; b--incase of a standing wave; c--in case of a "pure" traveling wave; β and β_1 are the angles between the direction of the speed of the end of the plate and the plate; d--broken lines which limit the instantaneous shape of the plate 3.

If a flexural wave of type (3) (i.e., either a standing, travelling or a combination of standing and travelling waves) is propagating along a plate, the trajectories of the points of the plate will be some curves rather than straight lines, as is assumed in the case of small vibrational amplitudes.

One must know the form of the trajectories itself and its characteristics to determine the effect of the trajectories of the points of the plate on the surrounding medium. The length of the plate having shape (3) is equal to

$$\Delta S(x_0, t) = \int_0^{x_0} \sqrt{1 + k^2 A^2(t) \sin^2[kx + \varphi(t)]}\, dx. \tag{5}$$

where x_0 is the abscissa of the end of the plate.

After transformations [1, 3], from (5) we find

$$\begin{aligned} \Delta S(x_0, t) = {} & \sqrt{1 + k^2 A^2(t)}\,[E(\alpha_1, \beta) - E(\alpha_2, \beta)] - \\ & - k^2 A^2(t)\left[\frac{\sin\varphi_1 \cos\varphi_1}{\sqrt{1 + k^2 A^2(t) \sin^2\varphi_1}} - \frac{\sin\varphi_2 \cos\varphi_2}{\sqrt{1 + k^2 A^2(t) \sin^2\varphi_2}}\right]. \end{aligned} \tag{6}$$

where $E(\alpha, \beta)$ is an incomplete elliptical integral of second kind in normal Legendre form:

$$\beta = \frac{kA(t)}{\sqrt{1 + k^2 A^2(t)}}, \quad \sin\alpha_i = \sqrt{\frac{1 + k^2 A^2(t)}{1 + k^2 A^2(t) \sin^2\varphi_i}} \sin\varphi_i, \quad i = 1, 2.$$

$$\varphi_1 = kx_0 + \varphi(t), \quad \varphi_2 = \varphi(t).$$

Equation (6) gives the dependence of x_0 on t (the trajectories of the points of the plate) in implicit form at fixed value of $S(x_0, t) = \text{const}$. Numerical calculation, the results of which are presented in Figure 1, a-c, was carried out to calculate the trajectories. Defining curve 1 (Figure 1, d) having length S as broken, one can find approximately the zone of variation of the trajectory of the end of a plate with length S:

$$\frac{S}{\sqrt{1 + k^2 A^2(t)}} < x_0 < \frac{S}{\sqrt{1 + \frac{1}{\pi^2} k^2 A^2(t)}}$$

For a "purely" travelling wave, the trajectories of the points of the plate can be found by a different method. From (6)

$$\begin{aligned} \frac{dS(t)}{dt} = {} & -\frac{\omega}{k}\left(\sqrt{1 + a_1^2 k^2 \sin^2[\omega t - k f(t)]} - \sqrt{1 + a_1^2 k^2 \sin^2 \omega t}\right) + \\ & + \sqrt{1 + a_1^2 k^2 \sin^2[\omega t - k f(t)]}\, \frac{df(t)}{dt} \end{aligned} \tag{7}$$

To find the trajectories of the points of the plate, let us assume that $\delta(t) = \text{const}$, then from (7) we find

$$\frac{df(t)}{dt} = \frac{\omega}{k}\left(1 - \sqrt{\frac{1 + a^2k^2\sin^2\omega t}{1 + a^2k^2\sin^2(\omega t - kf(t))}}\right).$$

Equation (8) determines the desired function f(t) in implicit form. It is clear that the function f(t) is also dependent on f(0).

It is easy to see that partial solution of equation (7) has the form $f(t) = (\pi/k)n$, $n = 0, 1, 2, \ldots$, i.e., the trajectories of the points on the plate in the special case have the form $x = (\pi/k)n$ and $y = (-1)^n a_1 \cos\omega t$.

One can also arrive at the conclusion of the existence of this partial solution purely logically by considering the figure of a travelling wave.

The trajectories of the end of the plate in the case of propagation of a "purely" travelling wave along the plate $y = a\cos(\omega t - kx)$ are presented in Figure 1, c. The points of the plate under consideration fluctuate, describing trajectories having the shape of figure eights with different slopes. The trajectories have the form of straight lines at points $x = (\pi/k)$. The patterns of the trajectories repeat on segments $[(\pi/k)n, (\pi/k)(n + 1)]$.

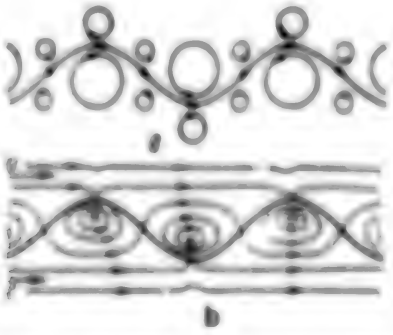

Figure 2. Pattern of Flows Created By Horizontal Movements of Points of Plate (a) and Formed Along an Oscillating Plate (b): U--incident wave; c--velocity of travelling wave

Motion is accomplished counterclockwise in the upper half-plane and it is accomplished clockwise in the lower half-plane. As a result, the tip of the plate always moves in a direction opposite the flow (the flow is directed along the Ox axis) in the extreme positions (when y reaches extreme values) and the velocity of the points of the plate in the extreme positions is considerably greater than in the mean positions. The suggested pattern of flows (based on results found by the trajectories of the points of the plate) near the plate only due to nonlinear postulation of the problem, i.e., taking the trajectories considered above into account, is shown in Figure 2, a. The most interesting are the zones located in the wave troughs; incident flow U will predominate on the wave crests and the flows occurring due to horizontal motions of the points of the plate will be severely distorted and suppressed. The derived pattern is in good agreement with experimental results [5] when the velocity of the incident flow is greater than the wave velocity (Figure 2, b).

It should also be noted that the angle between the direction of the velocity of the point of the plate and the plate is greater on segment MB (Figure 1, c) than a similar angle on segment M_1B_1 and it is opposite on segments CB and C_1B_1.

The angle on segment DCBM under consideration increases and sharply decreases on segment MA. It varies quite differently on segment A_1D_1: it increases on segment D_1C_1N and decreases on segment $NB_1M_1A_1$. It is understandable that the flow pattern in the process of vortex formation in the cases under consideration will be different and therefore the form of the trajectory of the end of the plate (and of the points of the plate) plays a specific role in selection of optimum parameters of the plate (this is especially important in consideration of boundary effects).

Let us note one peculiarity. The end of the plate always moves in the direction of incident flow in the mid-part of the trajectory (in the region of point B) and is seemingly repelled from the surrounding medium and thus creates additional thrust.

The importance of taking the trajectories of the end of the plate into account also follows from analysis of them upon superposition of two waves travelling opposite each other (Figure 1, a). Thus, besides the characteristics presented above, those such as different vibrational amplitude of the end of the plate, different directions of rotation in the derived figures in the form of figure eights and very complex forms of trajectories in the zone of the nodes not realized on the end of the plate during experimental investigations are added.

It is obvious that the motion of the points of the plate is directed toward the flow in the extreme positions prior to node ($kx < (\pi/2)$) and it is directed opposite the flow after node ($kx > (\pi/2)$). The indicated phenomena help one to better analyze the mechanism of vortex formation, the flow pattern near a vibrating plate and to select the plate parameters. All the enumerated principles must be taken into account when constructing a physical model of flow near a vibrating plate along which a flexural wave is propagating.

BIBLIOGRAPHY

1. Gradshteyn, I. S. and I. M. Ryzhik, "Tablitsy integralov, summ, ryadov i proizvedeniy" [Tables of Integrals, Sums, Series and Products], Moscow, Nauka, 1971.

2. Petrova, N. P., "Gidrobionika v sudostroyenii" [Hydrobionics in Shipbuilding], Leningrad, 1970.

3. Yanke, Ye., F. Emde and F. Lesh, "Spetsial'nyye funktsii" [Special Functions], Moscow, Nauka, 1968.

4. Kelley, H. R., A. W. Rentz and J. Siekmann, "Experimental Studies on the Motion of a Flexible Hydrofoil", JOURNAL OF FLUID MECHANICS, Vol 19, Part 1, 1964.

5. Taneda, S. and Y. Tomonari, "An Experimental on the Flow Around a Waving Plate," JOURNAL OF THE PHYSICAL SOCIETY OF JAPAN, Vol 36, No 6, 1974.

UDC 616.126-3-089.28.07:612.13

THE EFFECT OF THE DIFFUSER NATURE OF A CHANNEL AND THE SHAPE OF THE SHUT-OFF ELEMENT ON THE HYDRODYNAMIC DRAG OF ARTIFICIAL HEART VALVES

Kiev BIONIKA in Russian No 12, 1978 pp 67-73

[Article by F. G. Uglov, V. N. Zubtsovskiy, O. N. Bushmarin, P. I. Orlovskiy, Yu. V. Narayev and Yu. A. Perimov, Leningrad Medical Institute and Leningrad Polytechnical Institute]

[Text] There is a danger of an increase of hydrodynamic drag when affected heart valves are replaced with synthetic ones. The value of drag is affected by the characteristics of valve design, which include the ratio of the area of the hydrodynamic opening of the seat to the area of the lateral surface of a truncated cone surrounded by the seat and the shut-off element in its fully open state and also the value of the opening of the seat, the shape of the inlet and outlet, the design of the shut-off element, its inertia, blood flow rate, time of diastolic filling and systolic discharge, heart rate and so on. Along with the enumerated design characteristics of synthetic valves, the value of drag is also dependent on biological factors affecting the configuration of the prostheses. Ingrowing of the seat may lead to constriction of its hydrodynamic opening, while a decrease of the heart chambers, related to improvement of hemodynamics, frequently leads to constriction of the mobility of the shut-off element, constriction of the space and variation of the shape of the lateral channel between the prosthesis and the walls of the ventricle or aorta, frequently called the "tertiary opening." The indicated relationships make it difficult to understand the causes for development of the low cardiac discharge syndrome with all the ensuing unfavorable consequences for the patient. Consequently, the effect of various shapes of channels on the hydrodynamic drag of artificial heart valves should be subjected to careful study.

It is known that the valve in the heart channels is located in the channel with cross-sectional area increasing in the direction of flow, called the diffuser. The angle of diffusion of the left ventricle in the flow paths of patients with acquired heart defects, calculated by means of single-plane cineangiocardiography, according to our data [1], fluctuates in the following range: 55 $\pm$ 15° in patients with mitral stenosis, 72 $\pm$ 9° in patients with mitral stenosis and insufficiency, 96 $\pm$ 19° in patients with mitral insufficiency and 79° in patients with aortal and mitral stenosis, while the angles of diffusion increase as the systolic, diastolic and stroke volume increase.

The purpose of this investigation is to establish the effect of various angles of diffusion of the channels, the distance from the seat to the shut-off element and

calculation of the optimum path of the shut-off element on the drag of the valves. The results of the experiments made it possible to analyze the hydrodynamic properties of some specific domestic artificial microheart valves with shut-off elements in the shape of a ball (MKCh-3-25 and MKCh-3-30), hemisphere (MKCh-3-27) and a lens (MKCh-3-29), which is a necessary condition in selecting the optimum design of a prosthesis prior to surgery.

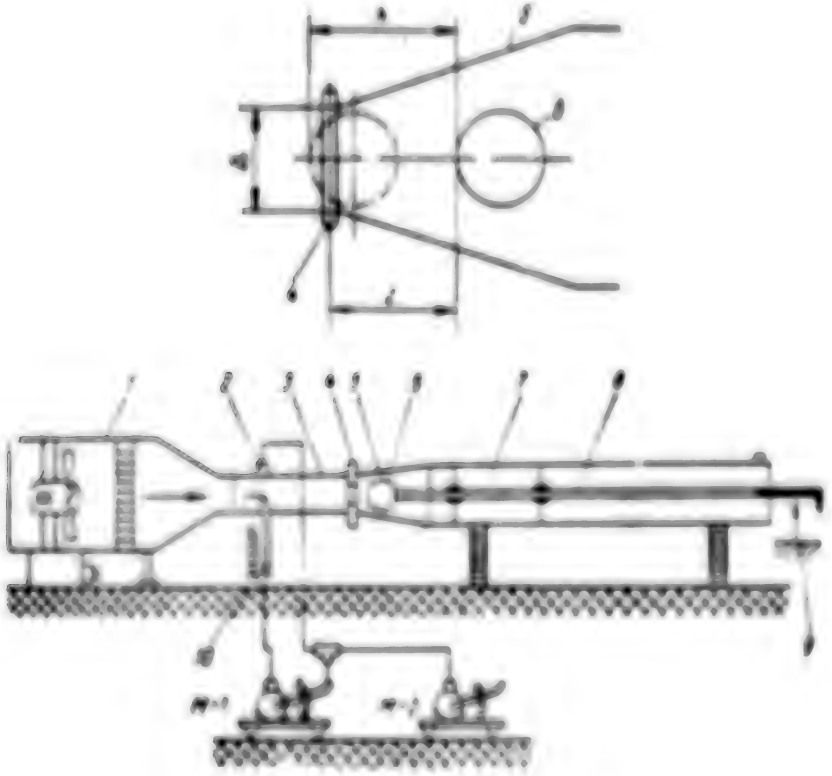

Figure 1. Installation for Investigating the Flow Over Shut-Off Elements of Artificial Heart Valves: 1--blast pipe; 2--first drain opening; 3--cylindrical segment; 4--diaphragm; 5--interchangeable nozzle-diffuser or cylinder; 6--model of shut-off element of artificial heart valve; 7--cylindrical pipe; 8--brass support pipe; 9--attaching device; 10--microtube; M-1 and M-2--alcohol pressure gauges

Simulating the transient flow over artificial heart valves in a biological system is related to considerable difficulties; therefore, a quasi-steady approach was used in this paper. The hydrodynamic criterion of the transient nature of the process is Struhal number (Sh), which is a dimensionless complex of parameters which characterize flow and has the form $Sh = Nd/\bar{u}$, where $N = 1/T$ is the frequency of the process, T is the period of the process and d and $\bar{u}$ is the dimension and velocity. The dimension $d = 0.035$ m is the mean diameter of the left atrioventricular opening. At a pulse rate of 75 beats per minute, $T = 60/75 = 0.8$ second and $N = 1.25\ s^{-1}$. $\bar{u}$ is the mean cross-sectional velocity of blood flow during diastole equal to 0.12 m/s. Thus, the Struhal number for a mitral valve comprises

Sh = (1.25·0.035)/0.12 = 0.365 and it is considerably less for an aortal valve. Consequently, the Struhal number is small and therefore the process of systole may be regarded in the first approximation as consisting of alternating stages of steady flow over the shut-off elements of valves under conditions of cylindrical diffuser channels and those which sequentially replace each other have different expansion angles from minimum to maximum.

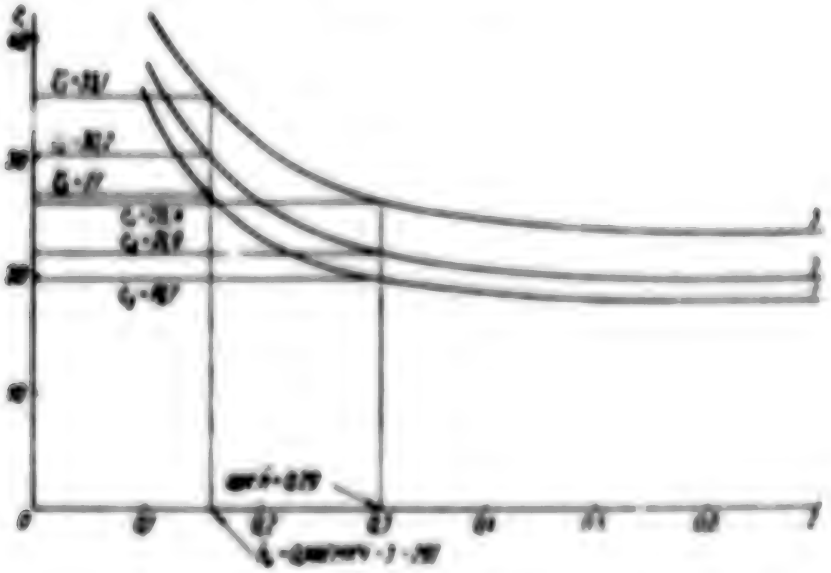

Figure 2. Variation of Drag of Valve Model With Lens-Like Shut-Off Element in Different Channels as a Function of the Distance of the Lens to the Diaphragm at Re = 5,300: 1--diffuser channel, α_2 = 65°; 2--diffuser channel, α_1 = 18°; 3--cylindrical channel

This investigation was carried out in a special wind tunnel (Figure 1) in which the air flow was created by a blower. A cylindrical tube which simulates the left auricle and the left ventricle during systole were connected in series to three different rigid cylindrical channels and diffusers with expansion angles of α_1 = 18° and α_2 = 65° in which the flow over the valve being tested was also investigated. A diaphragm which simulates the seat of the artificial heart valve was located at the point where the cylindrical tube and channels were connected. A model of the shut-off element (a ball, hemisphere or lens) was placed in the working section behind the diaphragm by means of a support--a brass tube. The cylindrical section, which is a continuation of the working part of the installation, had a length of approximately 10 calibers of the channel in front of the diaphragm and was designed to equalize the velocity field disturbed by the diaphragm and the shut-off element under investigation. The installation made it possible to determine the drag of the model by measuring the pressure drop. Two alcohol pressure gauges were used for this.

The M-1 pressure gauge recorded the operating mode, measured the velocity head ($(\rho u^2_{conv}/2) = p_{prim} - p_{stat}$) and was connected to the microtube and to the drain opening in the wall of the cylindrical section in front of the diaphragm. The M-2 pressure gauge measured the pressure loss during flow over the model of the shut-off element. The velocity field in front of the diaphragm was measured by a

velocity tube and the mean flow velocity $\bar{u} = \frac{2}{r_0^2}\int_0^{r_0} u r\,dr$ was calculated, where r_0 is the radius of the cylindrical section located in front of the diaphragm, r is the flow radius and u is the velocity at a point with radius r. The measurements were made at Reynolds numbers close to full-scale: Re_1 = 5,100, Re_2 = 8,100, Re_3 = = 11,300 and Re_4 = 14,000, where $Re = \bar{u}D_1/\nu$ (D_1 is the diameter of the cylindrical channel in front of the diaphragm and ν is the kinematic coefficient of viscosity of air). The installation was made while observing the rules and requirements of hydrodynamic similarity. The ratios of the diameter of the shut-off element and the dimensions of the diaphragm corresponded to those of aerial models of artificial mitral and aortal valves. The range of Re numbers in the tunnel was somewhat higher than the values under natural conditions but this should not significantly affect the results of the experiment.

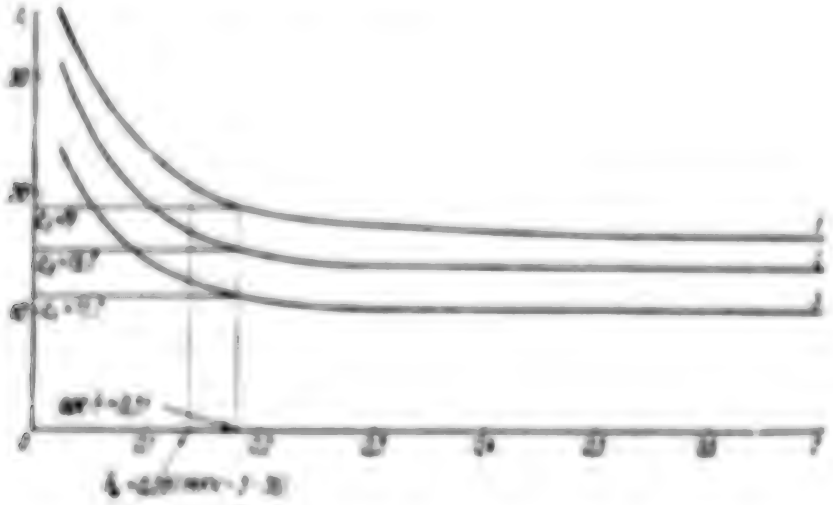

Figure 3. Variation of Drag of Model of Valve With Ball Shut-Off Element in Different Channels as a Function of the Distance of the Ball to the Diaphragm at Re = 5,300: 1--diffuser channel, α_2 = 65°; 2--diffuser channel, α_1 = 18°; 3--cylindrical channel

As a result of the experiment graphs $\zeta(\bar{s})$ were found where $\zeta = \Delta p/\rho(\bar{u}^2/2)$ is a dimensionless coefficient of the drag of the model under investigation, ρ is the density of air, Δp is the pressure drop on the model and $\bar{s} = s/D_1$ is the dimensionless distance from the diaphragm to the shut-off element. The effect of the nature of the channels and also the shape of the shut-off element on the drag of the valves is obvious from the graphs (Figures 2, 3 and 4). The curves of the drag of a lens model $\zeta(\bar{s})$, compared to a hemisphere and ball, proceed significantly higher and vary more sharply as a function of distance $\bar{s}$. The drag of a lens, like any other shut-off element, does not always constantly depend on $\bar{s}$ at a considerable distance from the diaphragm, but is a function of the shape of the body, the ratio of the diameters of the model and channel and also of Reynolds number. The flow in front of the lens sharply changes direction, due to which "impact" of the stream against the wall of the channel occurs, which leads to an increase of the energy loss and also to an increase of drag. As the lens approaches the diaphragm, these losses begin to increase due to an increase of the angle of encounter of the flow with the wall of the channel. When the lens is located very close to

the diaphragm, its drag increases sharply due to reduction of the through section between the diaphragm and the shut-off element, which becomes less than the area of the ring enclosing the lens and the wall of the channel. Upon approach to the diaphragm, the individuality of the shape of the shut-off element loses significance and drag becomes approximately identical for all elements. It follows from the graphs of $\zeta(\bar{h})$ that the most advantageous path of the shut-off element is determined by the value of $\bar{h}$ at which the value of the drag coefficient becomes minimum. This value was also rather large for valves that were unacceptable in design. Therefore, the value of $\bar{h}$ was taken as optimum at which the drag exceeds the minimum by 10 percent. Since the shut-off elements were investigated in three different channels, three values were found for each of them: $\bar{h}_1$, $\bar{h}_2$ and $\bar{h}_3$--in a cylinder and in diffusers. The value of $\bar{h}_{opt}$ was then calculated as the mean value. Using the graphs found on the models, the value of $\bar{h}_{opt}$ can be recalculated for the path of the shut-off element h_{opt} to analyze full-scale valves used in the clinic. Coordinate h is shifted somewhat with respect to coordinate z (Figure 1) since it is read from the front critical point of the shut-off element in the fully closed position, while coordinate z is read from the diaphragm.

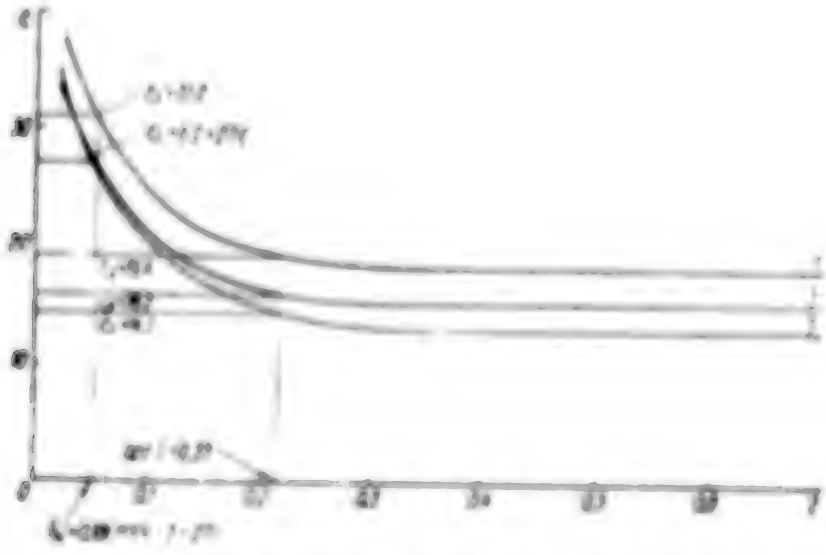

Figure 4. Variation of Drag of Model of Valve With Hemispherical Shut-Off Element in Different Channels as a Function of Distance of the Hemisphere to the Diaphragm at Re = 9,300: 1--diffuser channel, $\alpha_2 = 65°$; 2--diffuser channel, $\alpha_1 = 10°$; 3--cylindrical channel

Based on the calculations, $\bar{h}_{opt}$ is equal to 0.30 for a lens, then $\bar{h}_{opt} = 0.29$, where $\bar{h}_{opt} = h_{opt}/D_1$ (h_{opt} is the path of the lens corresponding to its optimum value). The path of the shut-off element of a full-scale PKCh-1-29 lens-shaped valve $\bar{h}_n$ differs significantly from the calculated value of $\bar{h}_{opt}$ and comprises 0.141, i.e., it is almost one-half as much. It follows from comparison of the curves for a model of a lens-shaped shut-off element in a cylinder and in diffusers (Figure 2) that the lens-shaped element has less drag in the expanded channel than in a cylinder. However, it is still higher than the drag of a hemisphere and tail in the same channel. Improvement of the operation of a lens-shaped valve in an expanding channel indicates that it can be more feasibly used in positions of a heart with

large angle of diffusion of the flow paths. The drag of the given valve is especially high under aortal conditions and with small volumes and small angles of diffusion of the ventricle.

As follows from experiments, the value of Re number slightly affects the shape of the curves which descend only insignificantly with an increase of Re. The most advantageous shut-off element is a ball. Ball valves have the least drag and the flow over them is smoother with less separation zone. Judging from Figure 3, the optimum path of a ball is $\bar{h}_{opt} = 0.31$. If the optimum path of a ball of a full-scale artificial mitral valve is compared to the optimum path according to the graph, one can ascertain that they differ slightly. Thus, $\bar{h}_n = 0.343$ for the MKCh-2-2 valve, $\bar{h}_n = 0.30$ for MKCh-3-2, $\bar{h}_n = 0.282$ for MKCh-3-36 and $\bar{h}_n = 0.257$ for MKCh-3-25. The drag of ball and hemispherical shut-off elements is considerably lower in a cylindrical channel than in a diffuser channel. The given situation has also been confirmed by previous investigations [2]. The increase of the drag of these elements in a diffuser channel, despite the increase of the clearance between the walls of the channel and the shut-off element, is explained by the more intensive and earlier separation of the boundary layer in the channel under diffuser conditions [4]. Although the properties of a ball valve deteriorate somewhat in diffuser channels, this valve is the best of those investigated from the viewpoint of hemodynamics for mitral conditions and is most suitable for aortal conditions.

A hemispherical valve occupies some intermediate position between ball and lens-shaped shut-off elements. The curves of the drag of a hemisphere (Figure 4) can easily be "elevated" with respect to the curves for a ball, but are located below those for a lens. The optimum path of a hemispherical model is $\bar{h}_{opt} = 0.33$, whereas it is equal to $\bar{h}_n = 0.18$ for a full-scale MKCh-3-27 valve. Comparing full-scale valves having a specific path of the shut-off element to the results found from the graphs, it is obvious that the drag of the MKCh-3-27 hemispherical valve in a diffuser of $\alpha_1 = 65°$ with complete opening $\bar{h}_n$ is somewhat higher than the drag of the MKCh-3-20 lens-shaped and MKCh-3-36 ball valves investigated under the same conditions. The drag of a full-scale hemispherical valve is less in the other two channels--a cylinder and a diffuser of $\alpha_1 = 18°$ than that of a lens-shaped valve, but is greater than that of a ball valve. As indicated previously, the drag of a model of a lens-shaped element is higher in different channels than that of a hemisphere. This is explained by the fact that curves of the drag of the models were naturally compared at identical values of $\bar{h}$ in the case of full-scale valves and $\bar{h}_n$ was compared for different values of $\bar{h}$ with complete opening of the shut-off elements, which is related to different value of the path of the shut-off elements of the valves under consideration. It is obvious from the graphs (Figures 2 and 4) that lens-shaped and hemispherical shut-off elements of full-scale valves operate in a very disadvantageous mode in the region of a large value of ζ. The path of the shut-off elements h_n should be increased, i.e., the stops of the body should be lengthened, to improve their hydrodynamic characteristics. However, there is the danger in this case of seizure: the shut-off elements may become a rib along the flow. Moreover, regurgitation, which reduces the operating efficiency of the valve and the heart as a pump as the whole [1-5], also increases significantly. Therefore, an increase of the length of the stops is undesirable.

Thus, it has been established that the diffuser nature of a channel in which the shut-off element is located appreciably affects the nature of flow over the valve.

Therefore, artificial heart valves should be investigated in channels of different shape, corresponding to full-scale conditions, for proper evaluation of their hydrodynamic drag.

The drag of ball and hemispherical valves increases as the angle of diffusion of the channel increases, whereas the drag of a lens-shaped valve decreases.

There is an optimum height of the stops for each design of valves which can be calculated on the basis of the graphs found in the paper. Comparison of the path of ball valves used in clinical practice with experimental results indicates that the path of the shut-off element is close to optimum only in these valves, while it is almost one-half as much in hemispherical and lens-shaped valves.

BIBLIOGRAPHY

1. Dubtsovskiy, V. N., Yu. F. Neklasov, Ye. V. Lovyagin et al, "Measuring the Volumes of the Left Chambers of the Heart Using Single-Plane Cineangiocardiography," KARDIOLOGIYA, No 7, 1971.

2. Dubtsovskiy, V. N., O. N. Bushmarin, A. D. Smirnov and P. I. Orlovskiy, "Investigating the Hydrodynamic Drag of Artificial Heart Valves," GRUDNAYA KHIRURGIYA, No 3, 1972.

3. Kuz'mina, N. B., "Investigating the Functional Properties of Artificial Heart Valves (Experimental Investigation)," Candidate Dissertation, Moscow, 1967.

4. Orlovskiy, P. I., "Hydrodynamic Investigation of Artificial Heart Valves (Experimental Investigation)," Candidate Dissertation, Leningrad, 1975.

5. Perimov, Yu. A., "Developing Designs of and Investigating Artificial Heart Valves," Candidate Dissertation, Moscow, 1974.

UDC 612.82

ADAPTATION OF MECHANISMS OF GOAL-ORIENTED BEHAVIOR OF MAMMALS TO CONDITIONS OF HABITAT IN AN AQUEOUS MEDIUM

Kiev BIONIKA in Russian No 12, 1978 pp 73-78

[Article by V. A. Protasov, Sevastopol']

[Text] Study and simulation of the mechanisms of the goal-oriented behavior of animals is one of the traditional trends of bionics. The practical significance of these investigations is determined primarily by the rapid development of robot technology [1, 11 and so on]. Study of the algorithms of animal behavior is of significance for design of adaptive cybernetic systems as well [10 and others]. It is important from this viewpoint to determine the most abstract operating principles of the nervous system and also to determine the mechanisms of behavior which provide adaptation to specific environmental conditions.

The object of our investigations was cetaceans--Black Sea bottlenosed dolphins (Tursiops truncatus Montagu). Interest in study of the mechanisms of behavior of cetaceans is related both to a high degree of their specialization to feeding conditions in an aqueous medium and to data which have appeared on the specific development of their brain, which retains marked features of primitivism in the structural organization of the neocortex [5 and others]. If one takes into account that cetaceans evolved under favorable, relatively simple conditions distinguished by an abundance of food and a limited number of predators for which cetaceans would serve as food objects, one can assume that these secondarily aquatic animals could retain to a greater degree than terrestrial animals features of the initial brain structure and accordingly some features of higher nervous activity of primary mammals. If this proposition could be confirmed experimentally, one could hope that comparison of the behavior of cetaceans (secondarily aquatic) to the behavior of terrestrial mammals permits one to determine the mechanisms of adaptation of the central nervous system to the specifics of habitat in an aqueous medium and to conditions of terrestrial habitat. It should be taken into account in this case that the behavior of cetaceans even in the range of a single family Delphinidae differs significantly--the most complex and diverse is the behavior of the large representatives themselves. This fact was frequently noted during training [19 and others], but has not been studied in practice until now. Thus, selection of the object of investigations among cetaceans is complex in the plan of the postulated problems and itself requires special investigations. We rather arbitrarily stopped our selection on the more investigated representatives of dolphins--bottlenosed dolphins, distinguished by diverse and complex behavior in captivity--in the given paper. We were guided in this case on the one hand by the desire to find

the most complete characteristics of behavior of at least one representative of cetaceans by comparing our own and literary data and on the other hand we were limited in selection of the object with regard to the worse adaptation of other species of Black Sea dolphins to captivity.

Our investigations were carried out on 14 adult bottlenosed dolphins using from 1 to 7 animals in individual series of experiments. The results of these investigations were already partially published [10-12 and others]. The purpose of this paper is to generalize the available material and to construct a working hypothesis which could serve as the basis after final formulation during discussion for more purposeful collecting of experimental material and formalized description and modelling of it.

It was established as a result of the investigations that simple conditioned motor-food reflexes are formed in dolphins well adapted to captivity as easily and rapidly as in most of the higher terrestrial animals--during 3-10 presentations of the conditioning stimulus, and reinforcement usually requires no more than 20-30 presentations. Simple conditioned defensive reflexes can be developed just as rapidly. On the other hand, inhibition of simple conditioned motor-food reflexes by multiple repetition of a stimulus without food reinforcement is a difficult task for dolphins and occurs more slowly than that of similar higher animals. Thus, inhibition of the simple motor-food reflex occurred in our experiments during three tries in one dolphin and within five in another. Even slower and more difficult inhibition of the reinforced food-catching reflex in an adult female dolphin is described in the paper of L. G. Voronin and L. B. Rozarovitskiy [4]. Inhibition of conditioned reflexes was accompanied in our experiments with dolphins by marked neurotic phenomena which occurred upon presentation of the conditioning stimulus even after the main conditioned-reflex response was suppressed. It should be noted that simple reflexes were not extinguished in dolphins without training for 6-8 months. The persistence of simple conditioned motor-food reflexes was also manifested in a number of cases in the form of a unique "dominance" of these reflexes. Thus, for example, we repeatedly observed how defensive reactions were suppressed in dolphins upon presentation of a conditioning stimulus and how they came into net "traps" or swam through narrow passages in the nets where it was impossible to corral them with the net or to trick them with fish immediately prior to this.

Both cases of rapid formation of a conditioned reflex--within 1-8 experiments--and cases of extremely slow formation--up to 36 experiments according to our data or 76 experiments (149 presentations of a differentiating stimulus) according to data of L. G. Voronin and L. B. Rozarovitskiy [4]--in formation of differentiation in dolphins. Simultaneous presentation of the main and differentiating conditioning stimuli made it considerably difficult in some cases to form differentiations. Bilateral adjustment of the significance of conditioning stimuli occurred in dolphins on the average during the same periods in our experiments as during the initial formation of differentiations. Formation of a second-order conditioned reflex in one of two experimental dolphins occurred within seven experiments and in another it occurred within eight experiments. Conditioned inhibition was formed in the same dolphins within 19 and 9 experiments, respectively. It was shown that a stereotype can be worked out in dolphins with approach only to every third presentation of the conditioning stimulus. In this case the adequate reactions in the experimental dolphin comprised 75-100 percent within 5-6 experiments. Formation of positive and inhibiting conditioned reflexes on chain conditioning stimuli occurred in

dolphins within the same periods as for simple conditioning stimuli. On the whole one can conclude that the conditioned reflexes of the given group, with the exception of individual cases of slow formation of differentiation, form in dolphins within periods which hardly differ from the mean data found in experiments on other higher animals (I and others). The behavior of dolphins during slow formation of differentiation had a number of specific characteristics which will be considered separately.

It was also established that a number of conditioned reflexes in dolphins, unlike other higher animals (I and others), is formed with great difficulty or is not formed at all. These conditioned reflexes may include differentiation of positive conditioning stimuli at the point of reinforcement. Thus, we managed to form a given conditioned reflex in only one case in eight experiments on four dolphins. Neurosis development in the dolphin during formation of the reflex. The developed reflex was unstable and was not restored after extinction when it was replaced by training, despite 600 repeated presentations of the conditioning stimuli in 17 experiments. Formation of "model selection" in dolphins was just as difficult. Model selection could be formed in only one case after prolonged training during five experiments on four dolphins provided that only two pairs of conditioning stimuli were used in the experiment. This group of conditioned reflexes may include isolation of "useful," reinforced elements from a previously formed chain of sequential actions with which chimpanzees and rats coped successfully, but not dolphins, according to data of Yu. D. Starodubtsev [14].

When conditioned reflexes are forming in dolphins, the development of neurosis-like states in the form of generalized spasms and rapid disordered swimming, sometimes changing to relatively persistent disruption of the conditioned reflex activity, is frequently observed [4]. The occurrence of these states not only in cases of slow formation of conditioned reflexes but also during rapid and seemingly easy formation of the conditioned reflex is typical.

The general characteristic of dolphin behavior was first given from aspects of conditioned reflex theory in the work of L. G. Voronin and L. B. Rozarovitskiy [4], in which the marked inertia of the nerve processes and their disruption toward the process of excitation is concluded as are common characteristics of higher nervous activity for dolphins on the basis of studying the dynamics of formation of simple motor-food conditioned reflexes and the dynamics of formation of differentiation in an adult female dolphin. Consideration of the entire aggregate of experimental material permits one to agree on the whole with these conclusions, but it should again be emphasized that the inertia of the nerve processes is not manifested in all cases in an identical degree in dolphins. Relatively rapid formation of even very complex conditioned reflexes such as conditioned inhibition, second-order reflexes, complex stereotypes, bilateral readjustment of the significance of conditioning stimuli and so on can be observed in these animals.

Considering cases of slow formation of conditioned reflexes and especially cases of slow formation of relatively simple differentiations in dolphins, one can isolate a special state, one of the varieties of which L. V. Krushinskiy [6 and others] described as a reaction of "unilateral automatism." In this state the dolphin's behavior is distinguished by monotonicity. The animal rhythmically approaches the location of food reinforcement between signals. If there is the possibility of selection, the dolphin persistently approaches only one of several

possible reinforcement locations without differentiating the conditioning stimuli. One should pay special attention to the fact that under these conditions neurotic phenomena even with a very large number of unreinforced responses following one after the other--up to 57 in our experiments and even up to 400 in the experiments of Yu. D. Starodubtsev [14] are not observed. Time characteristics--the latent period and the "running" time--also remain stable. Neurotic phenomena, if they do occur in these cases, occur only during the stage of reinforcement of the reflex when responses of "automation" disappear. The "adjusting" nature of the "automation" responses and their occurrence in dolphins during the very initial stage of the experiment should also be noted.

"Automation" responses are not mechanisms of behavior inherent only to dolphins. They are manifested to one or another degree in the behavior of other higher animals [7]. However, the degree of their markedness and their main role can be different. Thus, "automation" occurs mainly in lower monkeys [2] and dogs [8] as a response to a difficult task, while it frequently occurs in dolphins as a "adjusting" response [16 and others] at the very beginning of the experiment. This type of "automation" is more typical on the one hand for intact dolphins and on the other hand cannot be explained only by the insufficient degree of adaptation to conditions of captivity since adapted dolphins (actively "begging" food from man and usually catching fish from the hands of the experimenter) were selected for the experiment. As a "adjusting" response, "automation" occurred in some dolphins upon formation of simple differentiations immediately after one or even several rapid formations of a similar reflex in the given animal. As the dolphin is used repeatedly in the experiments, "automation" in the form of a "adjusting" response is manifested ever more rarely, but continues to occur in solution of difficult tasks, as occurred in our experiments and in the experiments of L. V. Kurshinskiy et al [6].

Considering the "automation" response as one of the methods of solving a two-alternative problem, it should be noted that this method may provide the animal with random alternation of signals up to 50 percent of reinforced conditioned reflex responses. In this case the problem of differentiation of two conditioning stimuli will be made to form a simple food-gaining response upon reinforcement of part of the completed responses. Formation of this type of conditioned reflexes causes no difficulties in higher animals [9, 17]. One may assume on the basis of the foregoing that the "automation" response is a mechanism of behavior which provides a probability nature of reinforcement of completed reactions. This mechanism predominates in dolphins taken without preliminary training for experiment and may be suppressed during multiple formation of complex conditioned reflexes as ceasing to be adequate under variable conditions. The tendency toward development of "automation" in dolphins may be explained by the fact that the main type of natural food-gaining responses is collective hunting for the given animals. In this case the "strategy" of probability reinforcement may be a more feasible form of behavior which provides collective actions.

Considering cases of rapid and slow formation of conditioned reflexes, one may also turn attention to the fact that conditioned reflexes with an alternative containing one positive and one negative solution (for example, formation of differentiations with alternate presentation of conditioning stimuli, formation of conditioned inhibition and second-order reflexes and so on) are formed relatively easily in dolphins. Conditioned reflexes which require alternate selection of one alternative

from several possible are formed with difficulty (in our experiments differentiation of positive conditioning stimuli at the location of reinforcement and so on). This characteristic of dolphin behavior may be the result of suppression of search activity in the given animals. The latter has already been noted in observation of dolphin behavior in captivity [19]. It is obvious that formation of conditioned reflexes of first type is possible with much less activity of investigative activity than is required for formation of such complex conditioned reflexes as differentiation of conditioning stimuli at the location of their reinforcement and so on.

The apparently specific, congenital inhibition of orientation-investigative activity in dolphins, the same as the tendency toward "automatism" described above, may be regarded as an ecologically justified phenomenon if one takes into account the factors which distinguish the conditions of existence of secondarily aquatic animals from terrestrial animals. These factors primarily should include increased probability of death in an aqueous medium with "unsuccessful" manifestations of investigative activity and simplified conditions of gaining food.

Conclusions

Judging by literary and our own data, the behavior of dolphins on the whole is distinguished by the following characteristics:

relatively rapid formation of simple food-gaining conditioned reflexes and also by rapid formation of conditioned reflexes with an alternative containing one positive and one negative solution;

the strength of simple food-gaining conditioned reflexes and their specific "dominance;"

inhibition of orientation-investigative activity;

slow formation of conditioned reflexes based on selection of a single alternative from several possible;

increased resistance to a reduction of the probability of food reinforcement;

the tendency toward development of the "automatism" response of an adjusting nature;

the unbalancing of nerve processes in favor of excitation at the stage of specialization of conditioned reflexes.

Considering the indicated mechanisms of behavior in interaction, one may conclude that their specifics determines the increased stability of the formed behavior of dolphins with relatively inconstant variations of external conditions and thus provides increased stability of the general line of behavior formed over a prolonged time.

Analysis of the behavior of dolphins in captivity shows that the primitivism noted by a number of authors in the structural organization of the cerebral cortex of cetaceans is accompanied on the whole by strictly goal-oriented adaptation changes of behavior rather than by primitivism of behavior. In this case dolphins

demonstrate high capability to complicate their behavior in experiments during sequential solution of tasks of increasing complexity.

The data do not presently permit one to directly relate the specifics of dolphin behavior to retention of distinction features of behavior of primary mammals in these animals; additional investigations on the basis of the proposed hypothesis are required for this.

BIBLIOGRAPHY

1. Berg, A. I. and B. V. Biryukov, "The State and Tendency of the Development of Bionics," VOPROSY BIONIKI, Moscow, 1973.

2. Vatsuro, E. G., "The Physiological Mechanism of Differentiation of Positive Conditioning Stimuli By the Location of Reinforcement," TR. FIZIOL. LAB. AN SSSR, Vol 12, 1955.

3. Voronin, L. G., "Analiz i sintez slozhnykh razdrazhiteley u vysshikh zhivotnykh" [Analysis and Synthesis of Complex Stimuli in Higher Animals], Leningrad, Medgiz, 1961.

4. Voronin, L. G. and I. N. Khvatovitskiy, "Some Characteristics of Higher Nervous Activity of the Black Sea Bottlenosed Dolphin," ZHURN. VYSSH. NERV. DEYATEL'NOSTI, Vol 10, No 3, 1960.

5. Konorov, V. P., "The Behavioral Characteristics of Structural Organization of the Brain in Cetaceans," Author's Abstract of Doctoral Dissertation, Moscow, 1974.

6. Krushinskiy, L. V., A. A. Ukhtomskiy, N. L. Krushinskaya and I. L. Dmitriyeva, "Study of the Complex Form of Dolphin Behavior," ZHURN. VYSSH. NERV. DEYATEL'-NOSTI, Vol 12, No 4, 1962.

7. Krushinskiy, L. V., D. A. Flerov, L. N. Molokhina, Ye. I. Ochinskaya and N. P. Popova, "The Extrapolation Reflex and Its Role in the Evolutionary Behavior of Animals," PROBLEMY KIBERNETIKI, No 14, 1966.

8. Kupalov, P. S., N. N. Vayevskaya, V. D. Volkova et al, "Situatsionnyye uslovnyye reflexy u sobak v norme i patologii" [Situational Conditioned Reflexes in Dogs Under Normal Conditions and in Pathology], Leningrad, Meditsina, 1964.

9. Menitskiy, D. N. and V. V. Trubachev, "Informatsiya i problemy vysshey nervnoy deyatel'nosti" [Information and Problems of Higher Nervous Activity], Leningrad, Meditsina, 1974.

10. Protasov, V. A. and D. A. Nurazov, "Maintenance of Dolphins in Captivity and Their Behavior Under Experimental Conditions," TR. VSESOYUZ. NII MOR. RYB. KHOZ-VA I OKEANOLOGII, Vol 80, 1971.

11. Protasov, V. A. and B. F. Sergeyev, "Some Materials Which Characterize the Memory of Dolphins. Memory and Trace Processes," Report Topics of the Third Conference on Problems of Memory and Trace Processes, Pushchino, 1974.

12. Protasov, V. A. and B. F. Sergeyev, "Analysis of the Probability Structure of the External Environment By the Bottlenosed Dolphin," 24th All-Union Conference on Problems of Higher Nervous Activity Devoted to the 125th Anniversary of I. P. Pavlov's Birth. Materials of sectional discussions, Moscow, 1974.

13. Rastrigin, L. A. and A. A. Ermuyzha, "Problems of Bionics and Biocybernetics," in "Bionika i biokibernetika" [Bionics and Biocybernetics], Riga, 1968.

14. Starodubtsev, Yu. D., "Physiological Analysis of Formation of Complex Motor Responses Under 'Free Selection' Conditions in Animals," Candidate Dissertation, Moscow, 1973.

15. Tomilin, A. G., "V mire kitov i del'finov" [In the World of Whales and Dolphins], Moscow, Znaniye, 1974.

16. Uznadze, D. N., "Eksperimental'nyye osnovy psikhologii ustanovki" [Experimental Bases of the Psychology of Set], Tbilisi, Izd-vo AN GSSR, 1961.

17. Khananashvili, M. M., "Mekhanizmy normal'noy i patologicheskoy uslovnorefleksornoy deyatel'nosti" [The Mechanisms of Normal and Pathological Conditioned Reflex Activity], Leningrad, Meditsina, 1972.

18. Yakubovich, V. A., "One Class of Adaptive Systems and the Results of Modelling the Process of Their Self-Teaching on the Computer," in "Mekhanizmy i printsipy tselenapravlennogo povedeniya" [Mechanisms and Principles of Goal-Oriented Behavior], Moscow, 1972.

19. Hediger, H., "Weitere Dressurversuche mit Delphinen und anderen Walen," Z. TIERPSYCHOL., Vol 20, No 3, 1963.

UDC 534.7-612.85

POSSIBILITIES OF DETERMINATION AND ANALYSIS OF THE EMOTIONAL SIGNALS IN THE COMMUNICATIVE SYSTEM OF DOLPHINS

Kiev BIONIKA in Russian No 12, 1978 pp 78-87

[Article by E. N. Khabalkina, G. V. Nikolenko, V. V. Raznadzey, S. A. Kreychi and A. A. Titov, Moscow State University]

[Text] The abundance and diversity of audio signalling in dolphins posed the problem of studying and deciphering it. It is assumed [7, 9] that the function of message transmission is carried by complex whistle-like signals, the main energy of which is concentrated in the frequency range from 2 to 60 Hz. The problem of the level of the communicative system in dolphins still remains debatable in the sense of its "closeness" or "openness." The complex social structure of the school, which requires coordination of the relationship of its members on the one hand and the rich audio activity and complexity of the observed behavior on the other provide the basis to assume that dolphins have an adequately developed system of communications capable of transmission of messages which carry information about specific vitally important changes in the environment by some as yet unknown method of information coding.

The problem of the level and structure of this system can be solved only provided there is separation and differentiation of the elementary units of its signal alphabet.

Careful study of the structure and the acoustic characteristics of these units and the specifics of their use in audio emissions help one to arrive at solution of the problem of methods of coding as well. One of the methods of finding the elementary units of the system is to isolate from the entire set of signals used by the dolphin signals of an emotional nature clearly related to the specific emotional state of the animal in a specific behavioral situation. Papers in which several of these signals related to negative emotions of dolphins--"distress call" [2, 5, 8, 9] are described--indicate that these signals are acoustically rather diverse, but somatically they have a quite specific expression of emotional excitation: dissatisfaction, alarm and fear. Isolation of clearly emotional signals from the entire set of signals and exclusion of them permits one to determine the information content of the other units of the "alphabet" and to facilitate differentiation of them.

Our problem included identification of the emotional signals of dolphins. The criterion of emotionality was multiple repetition of signals of the same type which express a rather specific emotional state of the animal.

The object of the investigation was a single Black Sea bottlenosed dolphin of Tursiops truncatus (a half-grown female) which was maintained for a year in a tank and which was used for a long time in experiments on study of echolocation. It was then transferred to a marine open-air cage for preventive treatment, where it was located for approximately two months. Observations were conducted from the moment the animal was placed in the tank after marine "preventive treatment" and continued for eight days. During this period the audio activity of the dolphin was recorded in nine different situations arising during observation of the animal (Table 1). The material for analysis was phonograms of time-sequential groups of whistle-like signals produced by the dolphin in one or another situation, limited by recording time. The recording was made through an electroacoustical channel whose frequency characteristic provided recording of the signals in the frequency band from 0.5 to 100 kHz. The signals were processed on a dynamic spectral analyzer [2] with preliminary slowing down of the signals by a factor of 4 or 8 as a function of their real length. Approximately 2,000 spectrograms were analyzed.

Table 1. Description of Behavioral Situations By Phonograms (1973)

Number of Phonogram	Date and Time of Recording	Situation
1	1 July, 1320	Initial period of the dolphin's stay in the experimental tank immediately after catching in a marine open-air cage, transport on a litter and placement in the tank
2	1 July, 1700	First submersion of the trainer into the tank and attempts to make contact (play) with the dolphin
3.	1 July, 1800	Feeding the dolphin from catwalks
4	3 July, 1930	Preparing the dolphin for the first experiment to determine the auditory thresholds. Developing conditioned responses to a tonal signal. Regular trajectory of motion and response to tonal signal were encouraged with fish. The dolphin worked poorly.
5	6 July, 1900	Second submersion of the trainer in diving suit into tank. Successful and active contact (play) with the dolphin
6	7 July, 1300	Third submersion of the trainer in diving suit into tank. Successful and active contact (play) with the dolphin.
7	7 July, 1330	Recording of dolphin's signals during unusually strong, suddenly beginning thunderstorm with downpour. The dolphin was extremely excited, was agitated and dived to the bottom frequently and for a long time.
8	7 July, 2000	1. Free swimming of the dolphin in the tank. The animal was in a playful mood. Active play with objects floating in the water and with a rope hanging in the water. Attempts to coax the dolphin to the side of the tank by clapping with the hand on the water were unsuccessful.

[Table continued on following page]

[Table continued from preceding page]

	2030	2.	Unsuccessful attempts to force the dolphin to work in the experiment to determine auditory thresholds. The dolphin continued play (situation 8.1).
9	8 July, 0900	1.	Dolphin was caught in shallow water to place it into transporting tank while other tank was cleaned. The dolphin was excited, but elements of play of situations 2, 5 and 6 were detected.
	0930	2.	The initial period of the dolphin's stay in the transport tank, contact with the trainer and rubbing the skin with a sponge. The dolphin was excited.

All the studied whistle-like signals form three large groups: Tonal harmonic whistles with different laws of variation of frequency-time characteristics of the main tone, narrow band and wide band noise signals with different distribution of acoustic energy within the signal. According to the length of sounding, the communicative signals can be divided into short (5-70 ms), medium (70-500 ms) and long (more than 500 ms). However, since there is no distinctive boundary between them, i.e., the same signal may have a different length of sounding, this division is arbitrary.

Classification of signals by spectral-time features made it possible to group them into 49 types distinguished by the shapes of the generatrices. The frequency-time characteristics of the toneal harmonic signals vary in the frequency range from 3 to 22 kHz for the carrier frequency and from 6 ms to 2 seconds according to the length of sounding [3]. The number of harmonics of the tonal signals fluctuates from 1 to 5 regardless of type. The appearance of higher harmonics frequently does not coincide with the beginning of the main tone and is not dependent on the intensity of the signal. Energy transfer from one harmonic to the other is frequently observed. The whistles may have one or several breaks which are usually shorter than the length of the entire signal by a factor of 10-15. Two-contour signals, in formation of which two independent sources participate, are found in the "texts" (phonograms). The frequency characteristics of the components of a two-contour signal, varying independently of each other, may either intersect or proceed parallel [3, 4].

The acoustic energy of wideband noise signals was concentrated in the frequency band from 1 to 30 kHz. The wideband signals are frequently complicated either by a tonal component or by regions of acoustic energy concentration in the form of formant-structures. Gradual transition from a wideband to a tonal signal by constriction of the frequency band can be followed on the spectrograms. The different types of signals can be combined into sequential chains. All types of whistle-like signals may be accompanied simultaneously by pulsed acoustic emissions of the location click type of different nature.

The wide spread of the parameters of frequency-time characteristics of communicative signals within individual types poses the problem of their possible and relative informative significance. All the whistle-like signals characterized by brevity of

sounding (5-70 ms) are distinguished by the greatest spread of parameters with relative simplicity of the contours and a small set of their types. It is obvious that the dolphin does not manage to accurately control the value of the frequency derivative in time during study of short signals of the same type and controls only its sign with short length of sounding of the signals and accordingly of high rate of variation of their frequency.

As the length of the signals increases, their contours become more and more complicated and two-contour signals and signals with complex spectral structure appear. Among the tonal harmonic signals of long length (from 1 to 2 meters) are found types characterized by high stability and even by absolute coincidence of the parameters of frequency-time characteristics from one signal to another. Sometimes up to 10 or more of these signals may be combined in sequence (strung together) into long linear chains--"trails." All this indicates that the dolphin's capability to fine control of the signal parameters depends on its length. Differences in the parameters of the frequency-time characteristics within individual types are apparently insignificant with respect to information content and do not participate in coding the information in messages. This information content should obviously be assumed in the sign of the derivative frequency in time, the general shape of the signal contour and its spectral structure.

From the viewpoint of isolation of signals an emotional nature, two situations should be noted (Table 1, phonograms 7 and 8), different in nature but accompanied by a large number of whistles of the same type and five types of the more typical signals which meet the criteria of emotionality (Table 2).

Phonogram 7 is a recording of signals of a single dolphin swimming in a closed tank during an unusually severe thunderstorm. The dolphin was strongly excited, swam rapidly, bumped against the tank, stayed on the bottom for a long time and emitted loud whistles of type 1 and 2, Table 2. The situation continued for about two hours and the animal's behavior and the nature of the acoustic signals were identicial during the entire time.

Phonogram 8 was recorded in the evening of the same day as phonogram 7. The nature of the dolphin's behavior in this situation (Table 1) can rather be described by positive emotions. The dolphin was excited, swam rapidly, but actively played with a rope hanging in the water, slapped the water with its tail, jumped out of the water and played with fish. All these actions were accompanied by a large number of loud whistles, primarily of types 1 and 2, as in situation 7. The excitement of the dolphin was so strong that subsequent attempts to force it to work in the experiment were unsuccessful. The recording was made selectively during an active game and during the experiment. As can be seen from Table 2, signals of types 1 and 2 comprise 93.9 percent in phonogram 7 and 81.0 percent in phonogram 8 of the total number of signals. This provides the basis to assume that signals of types 1 and 2 in these situations, expressing extremely emotional excitement of the animal, carry some emotional-semantic load and in one case they are motivated by positive emotions (satisfaction) and in the other by negative emotions (alarm and fear).

A signal of type 1 consists of two parts: from a smoothly increasing frequency characteristic to a maximum during the initial part and sharply decreasing to a minimum with subsequent increase of frequency in the second part (Figure 1, a and b). The frequencies fluctuate in the following range: initial part--7.5-9.5 kHz,

Table 2. Types of Emotional Signals and Their Distribution by Phonograms, percent

(1) № п/п	(2) Тип сигнала	Номер фонограммы (3)								
		1	2	3	4	5	6	7	8	9
1		5	—	—	—	—	—	39,4	65,5	—
2		33,9	7,3	32,9	45,8	81,9	46,5	54,4	15,5	31,4
3		2,0	2,5	1,3	3,4	0,2	27,4	—	—	31,4
4		16,6	37,3	—	3,2	0,2	3,0	—	—	4,6
5		—	0,62	1,32	1,8[illegible]	—	1,84	—	—	2,93
6	(4) Другие типы сигналов	42,5	52,9	65,8	47,6	17,7	23,1	6,1	19	32,6

Key:
1. Number of item
2. Type of signal
3. Number of phonograms
4. Other types of signals

Figure 1. Frequency-Time Characteristics of Signal of Type 1

maximum--15-22 kHz, minimum--6.0-8.0 kHz and final--10-14 kHz. The length of the entire signal varies from 0.7 to 1.2 seconds. The contour can be modified by

breaks in the region of the maximum, lasting from 80 to 100 ms. The information content of these breaks in the region of the maximums (or correspondingly of the minimums) of the frequency characteristics of whistles is doubtful. The most probable mechanism of their formation may be weakening of signal intensity, which arises as a result of natural physiological limitations of the dolphin's phonation apparatus upon achieving the upper or lower boundary of its frequency range. This may serve as an indirect confirmation of the fact that these whistles are primarily emotional.

The parameters of the frequency-time characteristic of the considered signal (Figure 1) vary strongly, although cases of their precise copying (coincidence) are sometimes observed.

It should be noted that signals of types 1 and 2 in situation 7 were regularly accompanied in most cases by a series of pulse signals (clicks) of an echolocation nature and the beginning of generation of the location pulses always accompanied the beginning of the whistle signal, while the end accompanied that part of it in which a maximum frequency characteristic was reached. The distinguishing feature of situation 7 was the absence of usual motivation which stimulates the use of the echolocation apparatus. This element of context was present in situation 8. Generation of echolocation pulses coincided in this situation with the emission of random whistles and was caused by the need to detect targets during the experiment.

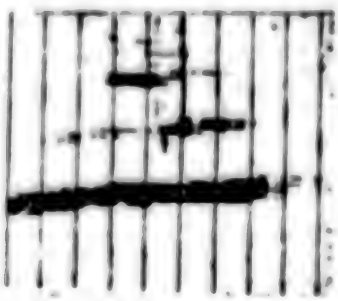

Figure 2. Frequency-Time Characteristics of Signal of Type 2

Thus, the material and namely the absence of usual motivation of a cause-effect relationship between the content of the situation (phonogram 7) and emission of echolocation pulses in it, on the one hand and differences in organization of the whistle-like and pulse signals in sequences ("texts") of phonograms 7 and 8, on the other hand, permit one to assume that the echolocation pulse signals may carry an independent informative load either by averaging through the context of the echolocation situation or jointly with the whistle signals, being in some functional relationship and combining with them in a specific manner. Specifically, one can assume on the material of phonogram 7 that the pulse signals at the beginning of the whistle may perform the function of an "address" or appeal. In the case of echolocation situations, for example, hunting, they may carry information about the species of fish, the number of them and the nature of the behavior, direction and speed of motion.

A signal of type 2 (Figure 2) is essentially an initial increasing part of a signal of type 1 in frequency, but in a lower frequency range. The initial frequency of

the signal varies from 4.5 to 7.6 kHz and the final frequency varies from 6.0 to 9.6 kHz and the length varies from 100 to 500 ms. A modification of the signal is its complication by the noise band, which is uniformly superimposed on this signal in the same time interval (Figure 3). It is typical that in situation 7, when the dolphin is clearly excited and alarmed, a signal of type 2 is observed in 54.2 percent of the cases, whereas these signals number only 15.5 percent in a game situation and pleasure situation (phonogram 8) (Table 2). This type of signal is present in practically all situations in relatively small quantities, with the exception of situation 2 when a signal of type 4 predominates, which is seemingly a mirror reflextion of a signal of type 2 (Figure 4). The frequency-time characteristics of this signal are in the same range as those for a signal of type 2 and it may also be complicated by superposition of a band of uniform noise (Figure 5).

Figure 3. Modification of Signal of Type 2

If the distribution of signals of types 2-5 by situations (Table 2) is considered, one may note that a signal of type 2 is present in all cases when there are elements of newness of the situation, threat or insufficiently clearly marked danger (first being placed in the tank, first feeding by hand, first contact and attempts to play with the trainer in the water, but still with prevalent distrust and vigilance). During adaptation, as the animal becomes accustomed to an unfamiliar situation and prevalent vigilance is replaced by a marked desire to play, a signal of type 3 (the third submersion of the trainer, catching the dolphin in shallow water--the game of "salochki")--situations 6 and 9, 1--appears along with a signal of type 2.

Signals of types 4 and 5 are less determined due to the fewer encounters. However, they reveal a similar trend in distribution on the phonograms, i.e., as the animal becomes adapted to the conditions of the tank the frequency of using signal 4 decreases (from 37.0 to 4.0 percent) and a signal of type 5 (from 0.5 to 3.0 percent) begins to appear along with it (Table 2).

Thus, there is the basis to assume that all the considered types of signals, complication and the dynamics of their use in sequential situations as they develop are related to the process of adaptation of the dolphin to the conditions of the tank and accordingly reflect the different shadings of its emotional state. Complication of the tonal whistle signal by superposition of a noisy component obviously bears a specific semantic load in this context, whose content is hidden in the specific elements of the context itself of multicomponent situations of adaptation. Further analysis of emotional signals showed that the stronger the excitation, the more complex is the frequency characteristic of the signal which expresses this

state. Thus, for example, the desperate protest and resistance of the dolphin to the actions of the trainers during catching in situation 9 (Table 1) was accompanied by typical whistles similar to the signal of type 1, but longer and complicated by the presence of several maximums and minimums in the frequency characteristic (Figure 6). We observed similar whistle signals, but with specific outlining of the contour in different dolphins in similar situations. Examples of these signals, emitted independently by two male dolphins excited by the chase, catching and placing in the transport tank, i.e., a situation similar to 9 (Table 2), are presented in Figures 7 and 8.

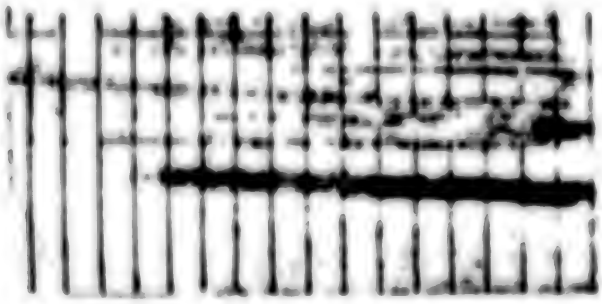

Figure 5. Position of Band of Uniform Noise on Signal of Type 4

The features which permit one to combine these signals into a single type are their long length (on the order of 1-2 seconds) and typical variations of the frequency characteristic in the range from 8-11 kHz at the beginning of the signal to 9-14 kHz at the end of the signal with maximums in the range of 20 $\pm$ 3 kHz and minimums in the range of 7 $\pm$ 2 kHz, i.e., the parameters of these signals are comparable to those of a signal of type 1. The contour of these signals has a different, but specific profile for each dolphin which is characterized by high stability and frequently by absolute coincidence (copying) of the parameters of the frequency-time characteristics from one signal to another. Typical features of these signals in the phonograms ("texts") is their multiple repetition or sequential combining of identical elements up to 10 or more into long chains--"trails." A typical example of this "trail" signal, consisting of a chain of identical, sequentially-joined elements and, as pointed out above, corresponding to extreme emotional excitement of the dolphin, is shown in Figure 8. The fact that the length of the "trail" signal varies slightly compared to the number of components of the elements deserves special attention. In other words, there is no direct functional dependence, except the clearly marked individuality, between these features. Varying the length of the elements comprising the "trail," the dolphin may arbitrarily change their number (from 1 to 10 or more) within the range of sufficiently limited time of sounding a signal of this type. It should be said here that the feature of length of the elements is rather stably retained within the limits of each "trail," i.e., it may vary only from signal to signal.

It was already pointed out above that the number of elements in the "trail" depends on the degree of emotional stress of the dolphin in one or another situation. However, it is not yet possible to clearly answer the question of the features of the context of the situation on which and how their number is dependent. The context of the situation and the structure of the signals accompanying it must be divided into mutually significant elements to do this.

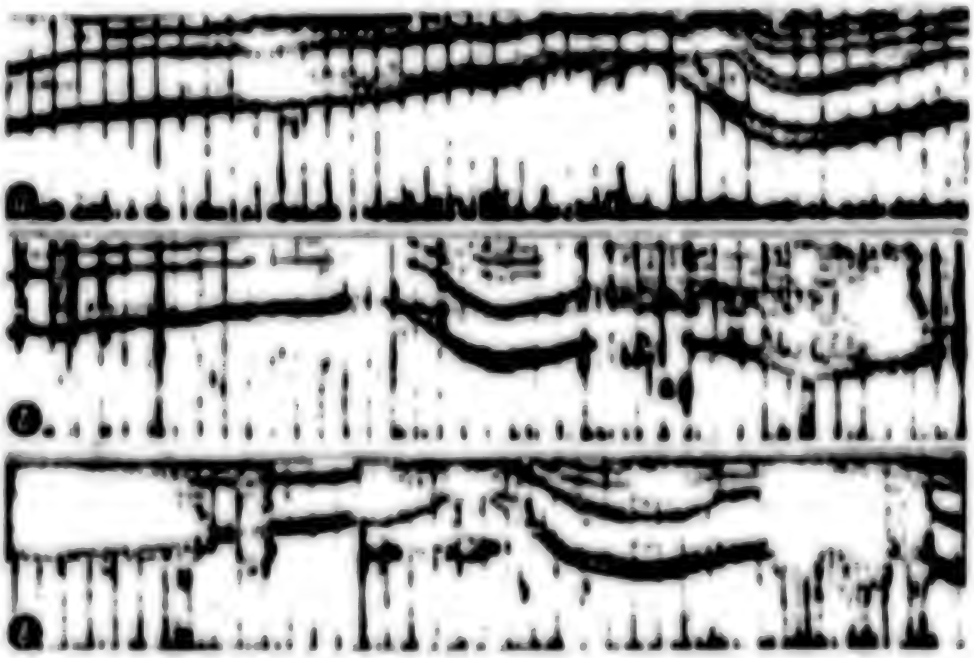

Figure 6. Variants 1(a), 2(b) and 3(c) Frequency-Time Characteristic of Signal in Situation 9

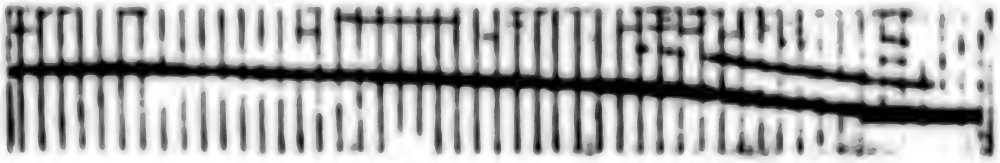

Figure 7. Specific Outline of Signal Contour in Male Dolphin No. 1

Figure 8. Specific Outline of Signal Contour in Male Dolphine No. 2

Thus, the results of the investigation clearly indicate that signals of extreme emotional excitation of dolphins, besides emotional-semantic markedness, are strictly individual and the acoustically rather different signals of different animals may carry an approximately identical semantic load. Thus, for example, signals of types 2, 3, 4 and 5 (Table 2) are observed in three different animals, whereas a signal of type 1 is replaced in one dolphin by a signal shown in Figure 7 and in another by a signal indicated in Figure 8. In some special cases the same signal of the same dolphin may reflect different emotional states in sign (both positive and negative).

Precise reproduction of the same type of signal during multiple repetition or sequential stringing into long "trails" (chains consisting of identical elements) and also their clearly marked specific individual shading permit one to assume their cognitive or orientational function which organizes and coordinates the behavior of the school or of individual specimens. From this viewpoint the hypothesis of an address function of location pulses arranged at the beginning of some emotional-semantic signals of an identification nature (type 1), emitted with no relationship to the echolocation situation, is confirmed.

Conclusions

An attempt was made from a rather large sample of whistle-like signals of dolphins to distinguish the emotional signals related to specific behavioral situations. The criterion of emotionality was considered multiple repetition of signals of the same type. The following conclusions were made as a result of analysis.

Some emotional states of dolphins are accompanied by constant emission of specific types of signals.

Some signals are common for different animals and others are clearly individual.

The signals which accompany the state of extreme emotional excitation, differing significantly in the outline of the contour, have some common features: long length of the signal, approximately identical frequency range and typical alternation of maximums and minimums in the frequency characteristic. Acoustically heterogeneous (individual) signals may describe similar emotional states in different animals.

The length of the signal is a typical feature of the degree of emotional excitation of the animal.

Both negative (fear) and positive (pleasure) emotions may be expressed (accompanied) by the same type of signal in some cases of extreme emotional excitation.

Superposition of noise or pulse clicks on a tonal signal and stringing individual signals into long chains ("trails") with regard to variations in the context of behavioral situations obviously indicates the presence of combinatorial elements used to express (transmit) the degree or shadings of emotional excitation, fulfilling in this case a specific biologically significant semantic load.

BIBLIOGRAPHY

1. Dreyer, J. and E. Evans, "Cetacean Communications," in "Morskaya bioakustika" [Marine Bioacoustics], Leningrad, 1969.

2. Zlatoustova, L. V. and A. B. Nizova, "An Experiment of Acoustical Analysis of Some Dolphin Whistles," in "Morfologiya, fiziologiya i akustika morskikh mlekopitayushchikh" [The Morphology, Physiology and Acoustics of Marine Mammals], Moscow, 1971.

3. Kaznadzey, V. V., S. A. Kreychi and E. N. Khakhalkina, "Whistle-Like Signals of the Bottlenosed Dolphin and Methods of Organizing Them," AKUSTICHESKI ZHURNAL, Vol 22, No 6, 1976.

4. Kaznadzey, V. V., S. A. Kreychi and E. N. Khakhalkina, "Double Formation in Dolphins," Proceedings of the Third All-Union Acoustics Conference, Moscow, 1973.

5. Caldwell, D. K. and M. C. Caldwell, "Individualized Whistle Contours and Bottlenose Dolphins (Tursiops truncatus)," NATURE, Vol 207, No 4995, 1965.

6. Caldwell, D. K. and M. C. Caldwell, "Dolphins Communicate, But They Don't Talk," NAVAL RESEARCH, Vol 25, No 6-7, 1972.

7. Dreher, C. C. and W. E. Evans, "Cetacean Communication," in "Marine Bioacoustics," edited by W. W. Tavolga, New York, 1964.

8. Dreher, C. C., "Cetacean Communication: Small Group Experiments," in "Whales, Dolphins and Porpoises," edited by K. S. Norris, Berkeley-Los Angeles, 1966.

9. Lilly, C. C., "Distress Call of the Bottlenose Dolphin: Stimuli and Evoked Behavioral Responses," SCIENCE, Vol 139, No 3950, 1963.

10. Lilly, C. C., "The Mind of the Dolphin," New York, Pergamon Press, 1967.

UDC 591.42-599.53

MORPHOFUNCTIONAL AND BIONIC ANALYSIS OF THE RECEPTION OF THE DOLPHIN TONGUE

Kiev BIONIKA in Russian No 12, 1978 pp 87-94

[Article by B. G. Khomenko and S. A. Gilevich, Institute of Zoology of the Ukrainian SSR Academy of Sciences]

[Text] Modelling of the sensory systems of those animals which, due to adaptation to specific conditions of existence, have acquired a unique structure of one or another sensory organs, has recently acquired ever more significance.

The organ of taste, the morphological substrate of which is the tongue and the peripheral sections of the olfactory analyzer embedded in it, has been studied least in dolphins whose aquatic habitat was reflected very strongly in the structuer of the nervous system and analyzers.

There has not yet been a detailed description of the morphology of the dolphin tongue and especially of its nervous regulation in the literature. A small number of papers has been devoted to investigating the structure of the tongue of cetaceans (macromorphological--[13, 9, 10, 4, 11] and micromorphological--[6] and there are absolutely no papers on investigation of the macro- and micromorphology of the innervation apparatus of the tongue of cetaceans, although we do find individual data on sources of the nerve supply of the dolphin tongue in [1, 2, 12].

It still remains unclear whether dolphins have taste reception. M. Weber [13], having detected no taste buds on the surface of the tongue, indicates the disappearance of the function of taste sensation in cetaceans (dolphins). A. V. Yablokov [10] described small depressions of 3-5 covered with a single-layer or few layers of prismatic epithelium, alongside which numerous ducts of the mucous-seros glands open, on the surface of the radix linguae of toothed cetaceans. In the author's opinion, these fossae are responsible for the perception of substances dissolved in water. S. Ye. Kleynenberg and colleagues [4] support the same viewpoint with respect to the white grampus. Histological examination of these depressions was carried out by V. Ye. Sokolov and O. V. Volk[illegible]. The authors note the thinness of the epithelium which lines the fossae and the large number of glands at the point where they are found, but do not find morphological structures responsible for the perception of taste sensations. L. I. Sukhovskaya [8, 11], who found formations similar to the conical and mushroom-like papillae of terrestrial mammals and taste cells located in their epithelium, on the bottom of the fossae at the radix linguae, described formations of this type. The capability of dolphins for chemoreception

has been confirmed by experiments of V. Ye. Sokolov and V. B. Kuznetsov [7], but further morphological investigations are required for final determination of this problem.

It follows from the foregoing that study of the structure and especially of the nerve regulation of the dolphin tongue is of interest not only to morphologists, but to other specialists who study these animals, specifically to physiologists and bionicists who simulate sensory systems.

The purpose of this investigation was to provide a systematic description of the macrostructure, micromorphology and mainly the innervation of the tongue in Black Sea dolphins. The material for the investigation were the tongues of Black Sea dolphins--the bottlenose, piebald and porpoise.

Methods of macro-micro preparation after Vorob'yev and staining with hematoxylin-eosin after Van Gieson were used in the investigation. The sections were treated with silver nitrate after Bil'shovskiy-Gross with modifications to determine the intraorgan nerve structures.

It was established as a result of the investigation that the tongue of dolphins is, like that of all other mammals, a muscular organ coated with a mucous membrane in which an apex, body and root can be distinguished. The apex of the tongue of the studied animals is weakly marked. The frenulum is compact and thick and rather deep transverse folds are visible on it. The upper surface or radix linguae is easily bent. No clearly marked grooves--median and transverse--are distinguished on it as an other mammals, but one should note the light transverse outline of the spina linguae and several shallow longitudinal grooves. There is a free surface on the bottom only along the lateral edges and in a very small part of the front section.

The mucous membrane of the organ under study is smooth in the region of the apex and contains no projections or depressions of any kind upon visual and also upon macro- and microscopic examination. There is a large number of small fossae on the body and the radix. Large fossae, the number of which is different and varies from 3 to 7, are located on the boundary between the body and radix linguae at the point where the trough-shaped papillae are located. The radix is coated with projections of the mucous membrane--follicules, an accumulation of which forms the lingual tonsil.

Analysis of histological preparation showed that the tongue of dolphins is coated with a skin-type mucous membrane. The epithelium is multilayered, revealing features of keratosis, which is more sharply marked on the apex. The thickness of the epithelium is not identical in different sections of the tongue, it is least in the region of the apex and it reaches a maximum in the radix.

The natural mucous layer is represented by dense unformulated connective tissue which forms papillae penetrating deeply into the epithelium. We observed a large number of glands whose outlet ducts open in the fossae on the spina linguae. There are especially many glands around the deep fossae located on the boundary between the body and radix linguae. These fossae, unlike other sections of the tongue, are lined with a thin-layer epithelium. We found formations on the bottom and in the

lateral walls of large fossae which are similar in structure to taste buds. Some of them have a shape typical for mushroom-like papillae--a narrower base and wider apex (Figure 1). Papillae are also found which have a conical and elongated ribbon-like shape (Figure 2). These papillae may be regarded as a transition shape from filamentary (which we did not find) to mushroom-like papillae. The papillae which we found are formed by protrusion of the mucous membrane of the tongue itself, coated with a thin-layered epithelium. Secondary papillae are easily distinguishable on the upper surface of these protrusions. Numerous outlet ducts of the glands open up around the base of the papillae.

Figure 1. Mushroom-Like Papilla At Radix Linguae of Azov Dolphin: staining with hematoxylin-eosin (X200)

The said mucous layer in the tongue of the cetaceans studied was not marked; therefore, the mucous membrane is tightly joined to the underlying layer--the muscular aponeurosis.

According to preliminary data of studying sources of nerve supply to the tongue, motor innervation in dolphins is accomplished by branching of the sublingual nerve (the 12th pair of cranial-cerebral nerves). The indicated nerve is formed of different quantities of roots emerging from the brain stem. It must be noted that the number of stems into which the roots are subsequently joined is also not identical [14, 5, 2]. As indicated by our investigations, the sublingual nerve of

Black Sea dolphins emerges from the brain between the olive and the pyrimidal medulla oblongata, leaves the skull cavity through the occipital canal of the occipital bone, after which its roots are joined into the rather thick stem. The stem of the sublingual nerve is directed downward and forward, emerges into the body of the tongue and branches in its own musculature.

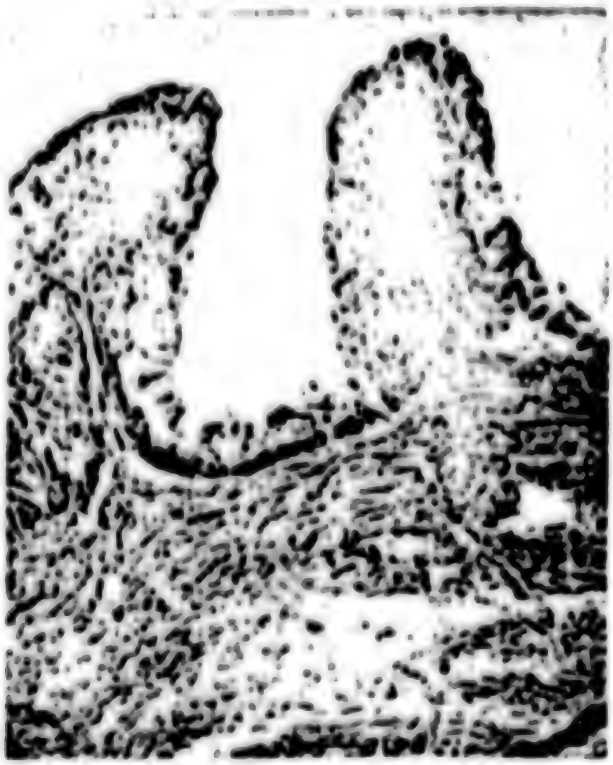

Figure 2. Conical Papillae at Radix Lingua of Azov Dolphin: staining with hematoxylin-eosin (X200)

The main source of sensitive innervation of the dolphin tongue is the lingual branches of the lingual-pharyngeal nerve and the lingual nerve of the mandibular branch of the trigeminal nerve (the fifth pair of the cranial-cerebral nerves) (Figures 3 and 4). The lingual-pharyngeal nerve of Black Sea dolphins emerges from the medulla oblongata in several roots (from 3 to 5), joined into a common steam. The indicated nerve then emerges through the jugular foramen in the skull, is directed caudally and ventrally between the inner carotid artery and the inner jugular vein and is then directed to the pharynx and tongue. The peripheral branches of the lingual-pharyngeal nerve are branched in the intermuscular connective tissue, the mucous membrane of the pharynx and the radix linguae. The remaining sections of the mucous membrane of the tongue are innervated by the lingual nerve from the mandibular nerve, the chorda tympani and the intermedius nerve--branches of the facial nerve, which are very difficult to determine in dolphins.

It was established as a result of neurohistological examinations that the tongue of the studied species of dolphins is abundantly supplied with nerve structures in all their sections. The abundant innervation of the mucous membrane of the tongue should especially be noted. There is a thick nerve plexus, formed both by pulpy

Figure 3. Innervation of Tongue With Branches of Mandibular Nerve: the lower alveolar (1) and lingual (2) nerves of the dolphin are visible: photograph from the book of G. B. Agarkov, B. G. Khomenko and V. G. Khadzhinskiy "Morphology of Dolphins" (Kiev, 1974)

and nonpulpy nerve bundles having different thickness and containing different quantities of nerve fibers, in the mucosa of the studied organ itself. The bundles of fibers, branching and becoming ever thinner, are directed toward the epithelial layer of the mucosa. Degenerating into individual nerve fibers, they form different receptors. We found the most diverse encapsulated nerve endings in the connective-tissue layer. Some of them have an inner and outer capsule. The nerve fiber, having lost its myelin, forms terminal branches in the inner bulb. We relate nerve structures of this type to endings of the bulb of Krause. Especially many of them are found near the epithelial layer of the mucosa in the subpapillary zone. The shape of branching of the axon varies strongly. In some cases this is a bundle of thin filaments which form a bulge on the end (Figure 5) and in other cases the axon, entering the inner bulb, is divided into two or more branches which, being bent, form different loops and coils by which amplification of the perceiving surface of the receptor is achieved (Figure 6).

We found a large number of diverse nerve glomeruli covered with a thin single-layer capsule in the mucous layer of the tongue itself. Along with encapsulated endings, unencapsulated nerve endings of various types are found here. Some of them have the form of diffuse networks and form receptor fields (Figure 7).

Part of the nerve fibers is directed into the connective-tissue papillae. Very frequently they are divided several times here into thinner branches which reach the apex of the papilla and change into the epithelium here. We observed how these thin branches in the epithelium form a number of diverse receptors: these are the thinnest filaments which are lost among the epithelial cells (Figure 8), annuli of different sizes, knobs and loops.

Figure 4. Lingual Nerve and Its Branches Which Innervate the Tongue of the Piebald Dolphin: photograph from book of G. B. Agarkov, B. G. Khomenko,and V. G. Khadzhinskiy "The Morphology of Dolphins" (Kiev, 1974)

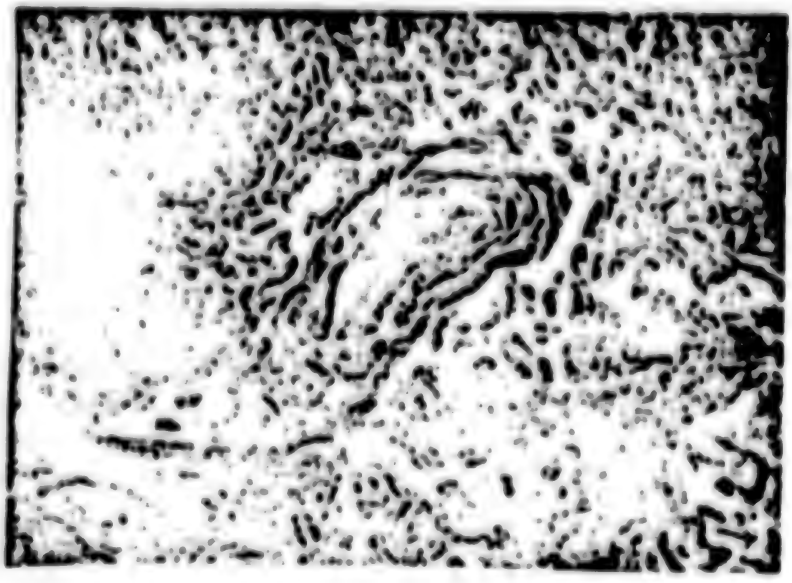

Figure 5. Encapsulated Nerve Ending of Bulb of Krause in Radix Linguae of Piebald Dolphin: impregnation after Bil'shovskiy-Gross (X200)

The terminal nerve devices are arranged rather uniformly in the tongue, but some increase of the number of free and attached nerve endings on the boundary between the boundary and radix linguae and also the significant number of free nerve endings in the epithelium of the fimbria at the apex of the tongue should be noted.

It must be noted in conclusion that the tongue of the investigated dolphins underwent significant changes due to adaptation to the aqueous form of life. The abundant nerve supply and the large concentration of nerve endings indicate highly developed overall sensitivity of this organ. The presence of taste buds permits one to assume the capability of these animals of taste perception, which, however,

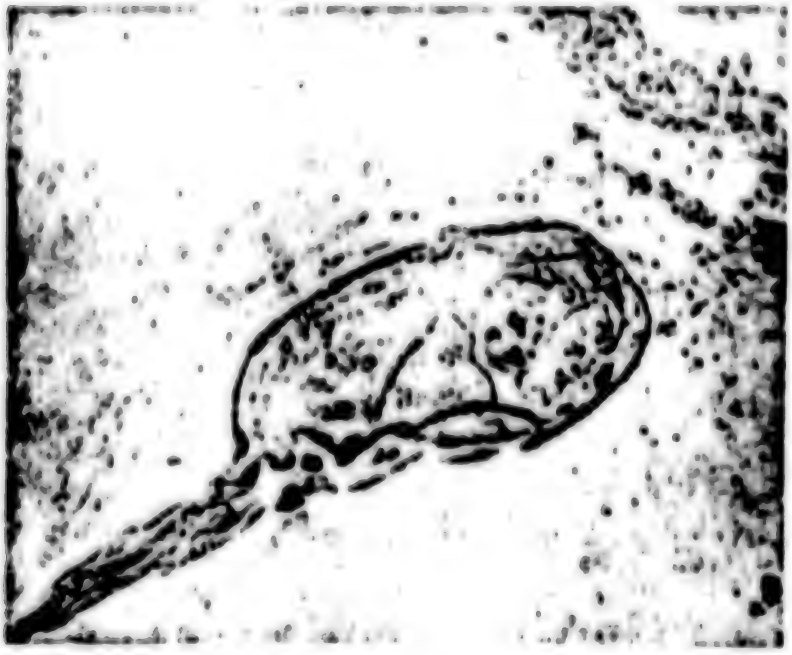

Figure 6. Receptor of Type of Bulb of Krause in Body of Tongue of Bottlenosed Dolphin: impregnation after Bil'shovskiy-Gross (X200)

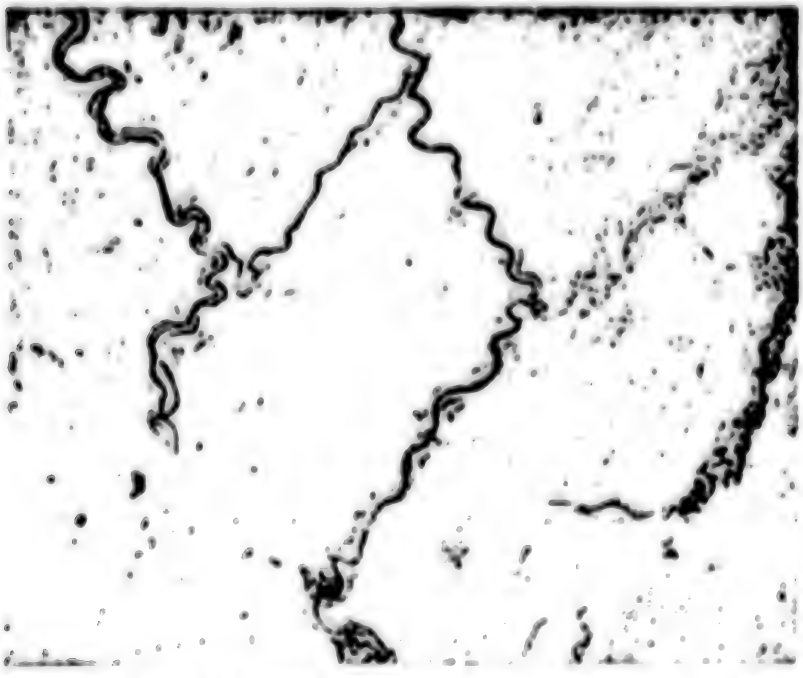

Figure 7. Receptor Field Formed by Free Nerve Endings in Body of Tongue of Bottlenosed Dolphin: impregnation after Bil'shovskiy-Gross (X200)

requires further morphological confirmation; specifically, detailed investigation of the course of the lingual-pharyngeal nerve and also of the chorda tympani, which provide taste sensitivity of terrestrial mammals, is required.

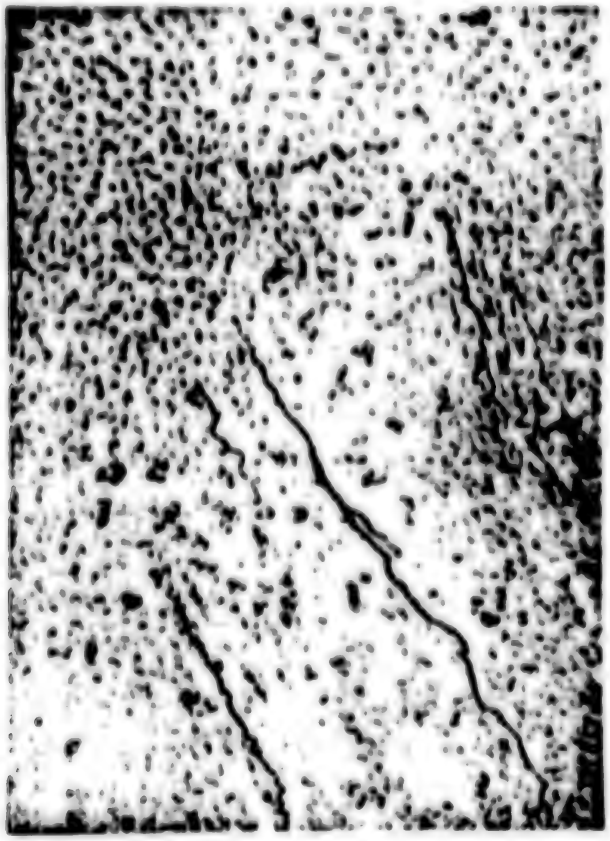

Figure 8. Free Nerve Endings in Epithelium of Radix Linguae of Azov Dolphin: impregnation after Bil'shovskiy-Gross (X200)

BIBLIOGRAPHY

1. Agarkov, G. B., F. G. Valiulina and A. P. Manger, "The Problem of the Topography of the Sublingual and Lingual-Pharyngeal Nerves in Some Cetaceans," Report Topics of the Fifth All-Union Conference on Study of Marine Mammals, Makhachkala, 1972.

2. Agarkov, G. B., B. G. Khomenko and V. B. Slezin, "The Main Morphological Characteristics of the Cerebrum and Cranial-Cerebral Nerves in Dolphins and Other Cetaceans," Report 1, VESTNIK ZOOLOGII, No 3, 1973.

3. Agarkov, G. B., B. G. Khomenko and V. B. Slezin, "The Main Morphological Characteristics of the Cerebrum and of the Cranial-Cerebral Nerves in Dolphins and Other Cetaceans," Report 2, VESTNIK ZOOLOGII, No 1, 1975.

4. Kleynenberg, S. Ye. A. V. Yablokov, V. M. Bel'kovich et al, "Belukha" [The White Grampus], Moscow, Nauka, 1964.

5. Pillery, D and H. Geer, "The Nervous System," in "Kity i del'finy" [Whales and Dolphins], Moscow, 1972.

6. Sokolov, V. Ye. and O. V. Volkova, "The Structure of the Tongue of Dolphins," in "Morfologiya i ekologiya morskikh mlekopitayushchikh" [The Morphology and Ecology of Marine Mammals], Moscow, 1971.

7. Sokolov, V. Ye. and V. B. Kuznetsov, "Chemoreception in the Black Sea Bottle-nosed Dolphin" DOKL. AN SSSR, Vol 201, No 4, 1971.

8. Bel'kovich, V. M. and N. A. Dubrovskiy, "Sensornyye osnovy orientatsii kito-obraznykh" [The Sensory Bases of Cetacean Orientation], Leningrand, Nauka, 1976.

9. Yablokov, A. V., "The Morphology of the Digestive Tract of Toothed Cetaceans," ZOOLOGICHESKIY ZHURNAL, No 4, 1950.

10. Yablokov, A. V., "The 'Sense of Smell' of Marine Mammals," TR. SOVESHCH. PO EKOLOGII I PROMYSLU MOR. MLEKOPITAYUSHCHIKH, No 12, 1961.

11. Yablokov, A. V., V. M. Bel'kovich and V. I. Borisov, "Kity i del'finy" [Whales and Dolphins], Moscow, Nauka, 1972.

12. Khomenko, B. G., "The Problem of the Morphology of the First-Eighth Pairs of Cranial-Cerebral Nerves in Delphinids," ZOOLOGICHESKIY ZHURNAL, Vol 52, No 3, 1973.

13. Weber, M., "Die Saugetiere," Jena, 19[illegible].

14. Jansen, J., "Studies on the Cetacean Brain," HVALRADETS SKR., No 37, 1969.

UDC 599.5

MORPHOFUNCTIONAL ANALYSIS OF THE RECEPTOR APPARATUS OF THE BLOWHOLE, NASAL SACS AND LARYNX OF DELPHINIDS

Kiev BIONIKA in Russian No 12, 1978 pp 94-102

[Article by G. B. Agarkov, A. P. Manger and B. G. Khomenko, Institute of Zoology of the Ukrainian SSR Academy of Sciences]

[Text] Rather extensive experience has been accumulated by natural scientists during study of the anatomy of some organs and specifically of the nasal sacs and larynx of toothed cetaceans [3, 8, 19-26]. In this case the authors, not dwelling on purely descriptive aspects, attempt to carry out functional analysis of the upper respiratory tracts of cetaceans, which is a naturally very difficult task in view of the almost total absence of data on their intraorgan innervation.

In the given paper we investigated sources of innervation of the supercranial meatus nasi and larynx of three species of Black Sea dolphins: the bottlenose, piebald and porpoise (Azov dolphin), which populate the basin of the Black and Azov seas. The histological material was fixed with a 12 percent solution of neutral formalin ranging from 5-7 days to three months. The histological sections were impregnated with silver nitrate after Bil'shovskiy-Gross in Lavrent'yev's modification to determine the nerve structures and their terminal sections.

Study of the afferent innervation of the wall of the blowhole sacs showed that there is a specific dependence between the structure of the different sections and the shape of the receptors imbedded in them. Thus, the majority of receptors in the outer layers of the elastic membrane are free diffuse arborizations of nerve fibers of the same type which supply the connective tissue, vessels, glands and even the epithelium simultaneously with their own terminals. The most differentiated nerve endings are found here in small quantitites. The nerve fibers which provide the beginning of these formations have comparatively small diameter and lose their pulpy membrane long before disintegration of the main cylinder into terminal branches.

Nerve endings which innervate several structures at the same time, most frequently the vessels and surrounding connective tissue, are found in our material. These receptors are known in the literature under the name of "polyvalent" receptors [10, 2]. The structure of most of them is rather simple: an initial nerve fiber is divided into two branches, one of which terminates on the wall of the vessel and the other of which terminates in the surrounding connective tissue.

B. I. Lavrent'yev [10] attributed great significance to the polyvalent receptors, assuming that they are the morphological expression of the short axon-reflexes which regulate the local blood supply by antidromal conduction of the vasodilating impulse.

According to Lavrent'yev, the polyvalent receptors should be regarded as those structures which can accomplish the receptor function by one part and the effector function with the other part.

Ye. K. Plechkov [18] assumes that the polyvalent receptors are the most ancient innervation apparatus in the phylogenetic sense, adapted for maintaining pressor reactions existing in lower animals and the embryos of mammals and which are gradually replaced by depressor reactions and the corresponding reflex mechanisms.

T. A. Grigor'yeva [2] advanced the concept according to which the vascular-tissue receptors regulate metabolic processes on the "capillary-tissue" boundary, in other words they are a morphological substrate of chemoreception. This point of view is maintained by Ya. L. Karaganov [6, 7], A. A. Otelin [14] and others. The fact is that rather frequently one of the components of polyvalent receptors is special cells which, as indicated by experimental work with nerve resection, are derivatives of the glia of Shvannovskaya. This interpretation of the functional designation of the polyvalent receptors is especially intriguing in light of the histochemical investigations of V. V. Portugalov [15], who regards the glial structures of the peripheral nerves as responsible for enzymatic and mediator processes which occur here.

Thus, the vascular-tissue receptors in the dolphin, which has an abundant blood-supply system, are the nerve apparatus by means of which the central nervous system controls the intratissue metabolism.

Another group of nerve endings is found in the median muscular layer of the wall of the meatus nasi. The pulpy fibers penetrate here together with the nonpulpy conductors consisting of general mixed nerve bundles. Both of them propagate through the connective-tissue interlayers which join individual muscle bundles to each other. Part of the pulpy fibers is separated from the nonpulpy components and, continuing their subsequent path, penetrate the intervals between the even smaller groups of muscle fibers and sometimes between individual muscular cells. Here, inside the connective-tissue septa, they lose their pulpiness and degenerate into short nonpulpy branches which soon change to terminal fibrillar lamina. The latter are usually located in special cells and only in rare cases are they located directly in muscular elements. Moreover, the nuclei of the special cells differ sharply by large size, spherical shape and light color of the protoplasm from the elongated and more strongly stained nuclei of muscular cells (Figures 1 and 2). They are apparently similar to the nuclei of cells of Shvannovskaya and apparently play the role of transmitters of stimuli from the muscle to the nerve fiber.

The most numerous in the wall of the blowhole sac are encapsulated receptors, distinguished by the nature of the terminal formations, the structure of the capsules and the number of nerve fibers terminating in the corpuscle. The main mass of these receptors lies on the boundary between the elastic membrane and the epithelium of the blowhole sacs.

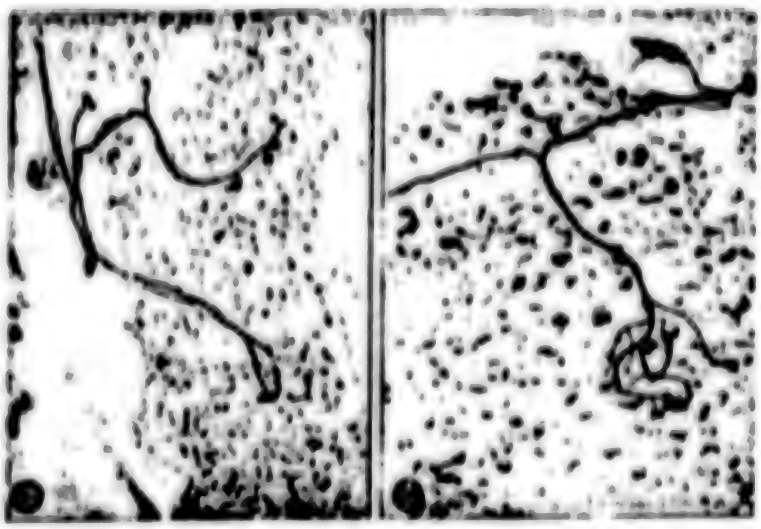

Figure 1. Free Knobby (a) and Bushy (b) Nerve Endings in Meatus Nasi of Common Dolphin: Impregnation after Bil'shovskiy-Gross (X400)

The encapsulated nerve endings of the bulb of Krause type (Figure 3) are located not only in the deep, but also in the surface layers of the epithelial membrane, frequently abutting tightly against the epithelium, and sometimes penetrating far into its mass, being surrounded by a thin interlayer of connective tissue. The walls of the perineural sheath in these encapsulated nerve bodies immediately change to a terminal capsule, while the Shvannovskaya elements form the inner bulb. The size of the encapsulated nerve bodies of the bulb of Krause type fluctuates in the range of 45 X 85 μm and 50 X 125 μm. The individual terminal branches through the intercellular spaces of the walls of the bulbs frequently emerge beyond the latter and terminate in the epithelium, forming similar free clusters.

The characteristics of the arrangement of these bulbs near the free surface of the epithelium of the wall of the blowhole sac are of known interest with regard to the possibility of penetration of pathogenic agents of some infections from the surface of the mucous membrane of the nose to the perineural slits of the peripheral nerve fibers and from here into the central nervous system.

The terminal bulbs are frequently enclosed with capillaries but are sometimes in close contact with the small sanguiferous vessels. Moreover, they are adjacent to the walls of the mucous formations of the blowhole sacs (Figure 3, a and f). These circumvascular formations have been described in many organs and tissues [5], specifically, they were observed in the mucous membrane of the nose by S. A. Pletnev [16] and V. P. Lashkov [11], who evaluate similar structures as receptor apparatus adapted for perception of stimuli related to variation of the tonus of the vascular walls.

Encapsulated glomeruli were found on tangential sections in the connective-tissue papillae penetrating into the epithelial lining of the sac. The number and density of arrangement of the branches are different. The glomeruli have a curved shape and are formed by one, and more rarely by two and three pulpy fibers from 2 to 4 μm in

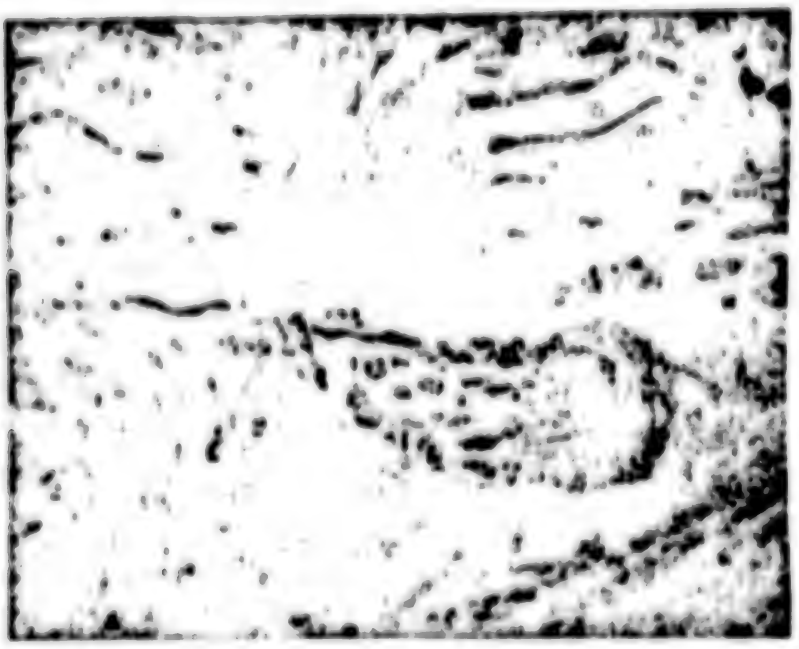

Figure 3. Complex Unencapsulated Nerve Ending With Special Cells in Wall of Meatus Nasi of Bottlenose Dolphin: impregnation after Bil'shovskiy-Gross (X280)

diameter. The dimensions of the corpuscles fluctuate from 48 to 100 μm. A large inner bulb and capsule consisting of 2-3 layers of cells with small nuclei extending along the length is typical for these receptors.

Unique encapsuled enendings (Figure 4) were found in some cases, for which a special method of terminal formation is typical. The nerve fiber, having lost it myelin membrane, penetrates the inner bulb of the corpuscle and passes through to the opposite pole, where it turns and returns to the point of its introduction. Here, without branching, it makes several helical turns, curved toward the opposite pole, around the longitudinal loop. The inner bulb also contains a thin nonpulpy fiber, the method of termination of which has not been established. This encapsulated receptor is apparently supplied with an accessor fiber--Timofeyev's apparatus.

Investigations of the intraorgan innervation of the mucous membrane of the dolphin larynx indicate extensive saturation with nonafferent nerve devices. Most frequently, these are simply built-in receptor apparatus consisting of thin, branching filaments lost among the cells. Besides the branching filaments, the endings may be club-shaped and tendril-shaped and may also have the shape of loops and ringlets (Figure 5). The described endings are most frequently found in the subepithelial layer of the mucous membrane of the larynx and the largest accumulations of them are found in the region of the entrance to the larynx, the respiratory surface of the epiglottis and the arytenoid cartilage which surround the respiratory part of the rima glottidis.

Along with simple nerve endings, complexly structured encapsulated nerve endings are also found in the mucous membrane of the dolphin larynx. Some authors [12] feel that these endings are inherent only to the human larynx and are not found in animals. However, we found typical encapsulated nerve endings in the mucous

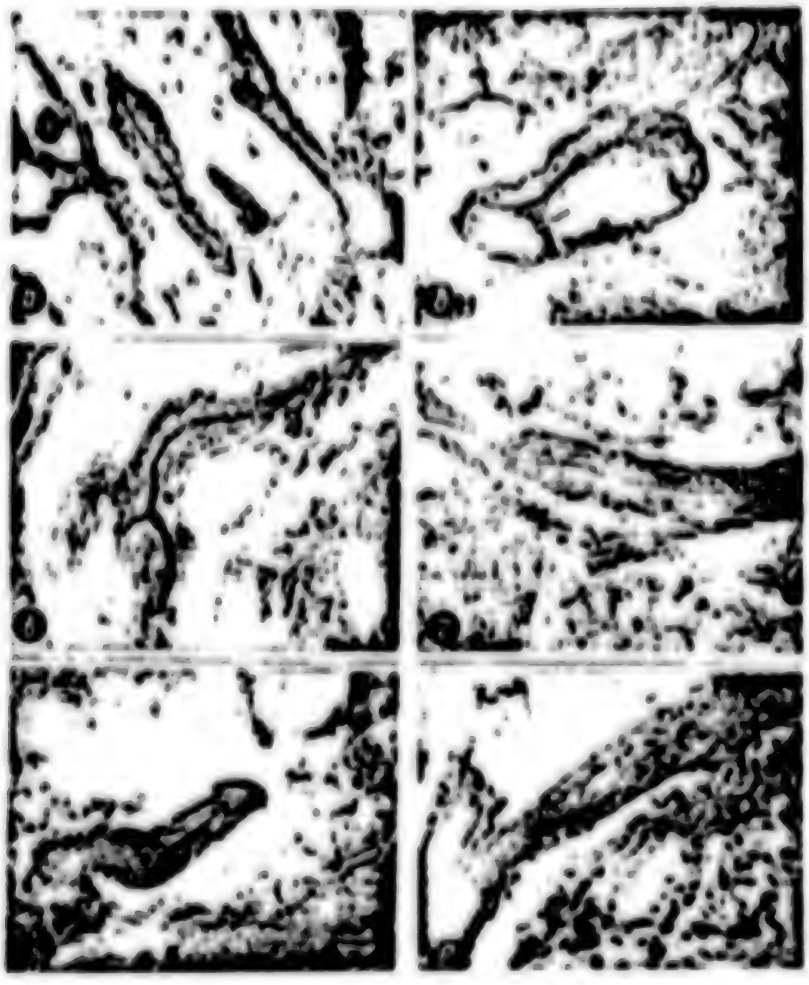

Figure 3. Encapsulated Receptors (a-e) of Bulb of Krause Type: impregnation after Bil'shovskiy-Gross (X200)

membrane of the larynx on preparations of all three of the species of dolphins studied. They are located primarily in the submucous layer and are extended, sometimes somewhat curved formations similar to the bulbs of Krause (Figure 6). The greatest accumulation of them is found in the region of the entrance to the larynx. The mucous membrane of the respiratory surface of the epiglottis is rather abundantly saturated with them and the mucosa of the ventral wall of the larynx is saturated to a lesser degree. The bulbs of Krause could be found only in very rare cases in the mucous membrane covering the inner surfaces of the aretenoid cartilage and also the dorsal and lateral walls of the cricoid cartilage.

The closer the encapsulated nerve endings are located to the epithelium, the more their shape varies. From the curved shape, they acquire an oval and finally a rounded shape. A capsule is easily discernible in these endings. There is sometimes a thick nerve fiber which has uneven contours and occupies approximately 4/5 of the length of the capsule inside it in the vicinity of the small loosely arranged nuclei. The encapsulated nerve fibers seemingly penetrate immediately into the epithelium, the thickness of which becomes approximately one-half at this point.

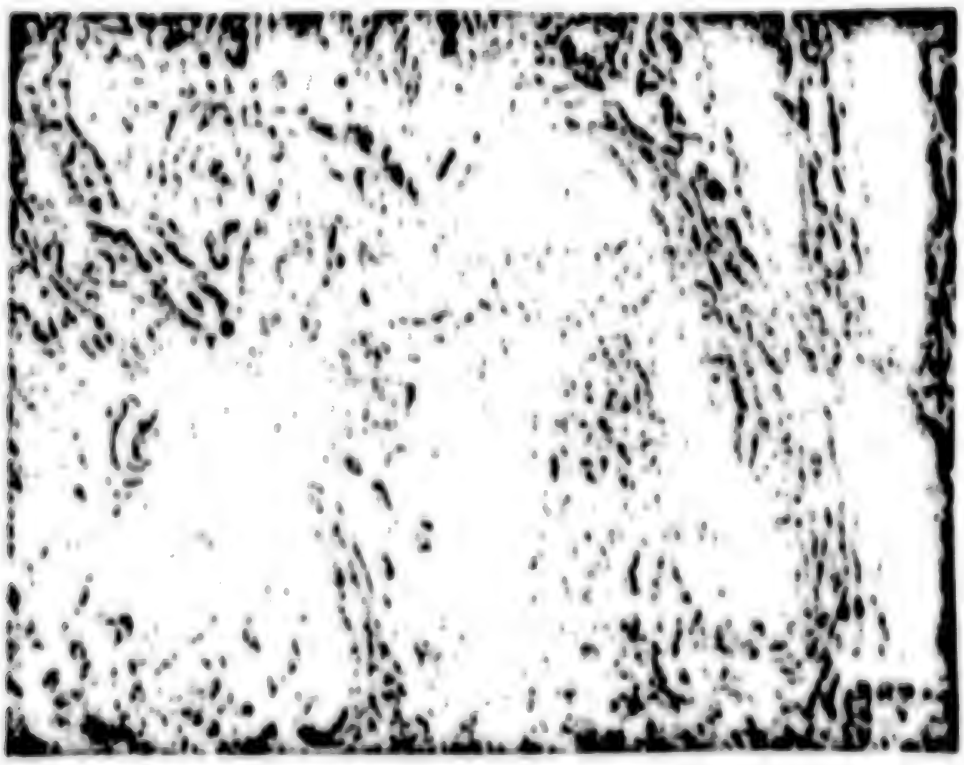

Figure 4. Encapsulated Receptor of Golgi-Mazzoni Type in the Blowhole of the Bottlenosed Dolphin: impregnation after Campos (X200)

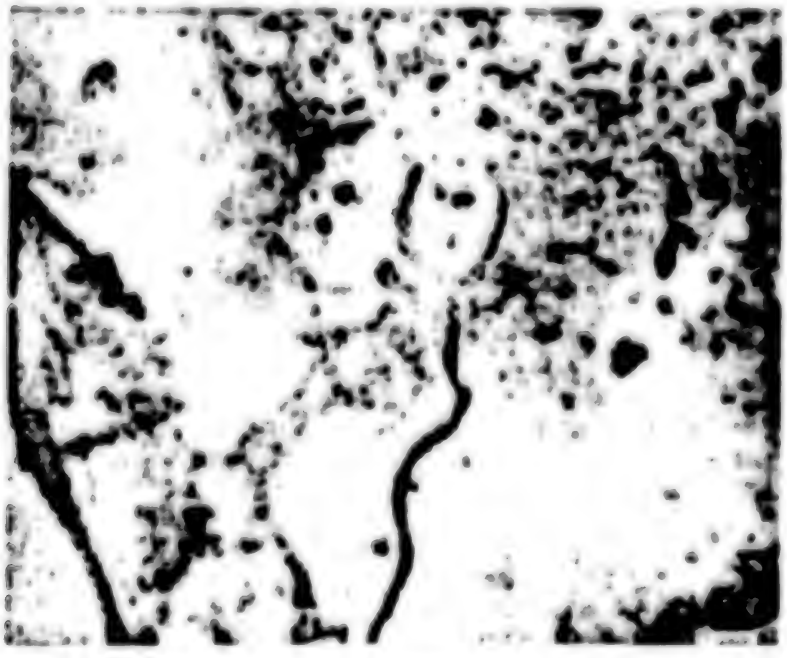

Figure 5. Tendril-Like Fiber Receptor in the Mucous Membrane of the Larynx of the Bottlenosed Dolphin: impregnation after Bil'shovskiy-Gross (X280)

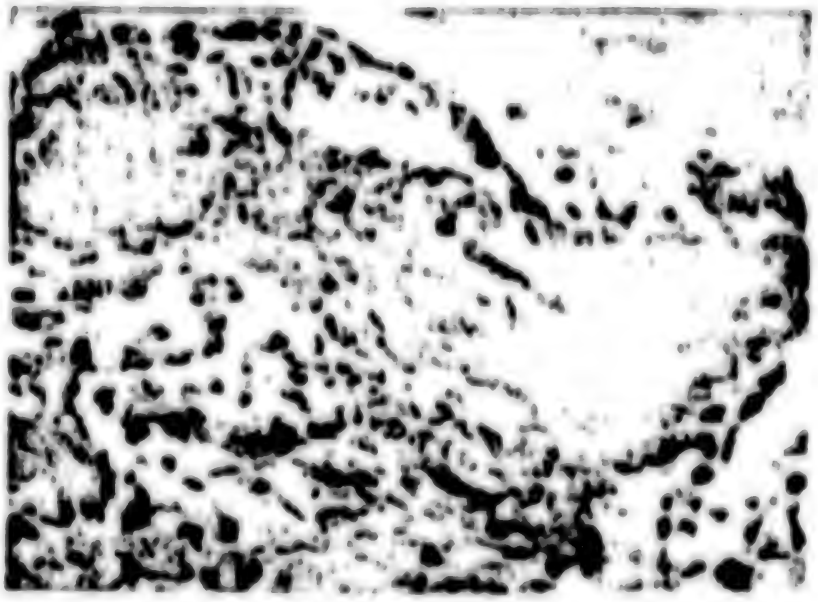

Figure 6. Receptor of Bulb of Krause Type in Mucous Membrane of Larynx of Common Dolphin: Impregnation after Campos (X280)

A decrease in thickness of the epithelium at the point where the nerve endings are located is observed not only in the presence of encapsulated but also above free unencapsulated endings. This fact is apparently of important significance and is related not so much to innervation of the connective tissue and epithelium as to the capability of perceiving stimuli occurring during motion of the air in the lumen of the larynx. Nerve cells arranged singly between the fibers and tightly adjacent to them are found along the path of the nerve stems and bundles travelling independently or comprising loops of the nerve plexi of the mucous membrane of the dolphin larynx, most frequently at the points where they intersect. The nerve fibers sometimes diverge, forming a small space in which one or two cells are located. Some stems are split into two bundles between which are grouped nerve cells which form microganglia (Figure 7). There may be different numbers of cells in the latter. Some contain only several cells and others consist of tens and even hundreds of nerve cells, most frequently concentrated at one point.

The described gangliose cells are polygonal, rather large with intensively colored neuroplasm and large, sometimes eccentrically located nucleus. They are similar in structure to Dogel's cells of second type. The authors found the largest number of them in the form of nodes along the path of the inner branch of the cranial laryngeal nerve and in the mucous membrane of the respiratory surface of the epiglottis and the ventral wall of the larynx. Accumulations of nerve cells in the form of small ganglia, frequently containing only 3-5 nerve cells, are constantly found here. These small nerve nodes are located at the points where the nerve stems branch. Thus, the nerve nodes in the larynx of delphinids are most frequently found at those points where there is a lot of mucous tissue. This fact permits one to assume that there are sensitive neurons which perceive pulses from the glands, connective tissue and sanguiferous vessels, in the neurocellular apparatus of the larynx. The cranial laryngeal artery enters the larynx parallel to the inner branch of the cranial laryngeal nerve. Judging by the fact that the large nerve node is

Figure 7. Microganglia in Wall of Laryngeal Cavity of Azov Dolphin: impregnation after Bil'shovskiy-Gross (X280)

permanently located at the point where the cranial laryngeal artery and its branches enter the larynx and the sanguiferous vessels of different calibers are located in the region where the neurocellular apparatus is located, one may think that the nerve nodes of the larynx also contain vegetative nerve cells which send postganglial fibers to the smooth muscles of the vessels.

Both the inner function of the organ and all internal processes occurring in it are regulated by the stages of the nervous system to the cerebral cortex according to the reflex principle. Local reflex arches enclosed in the nerve nodes located in the organ itself are subordinate to the overlying sections of the central nervous system.

According to data of [17, 4, 11, 1, 9, 3], there are sensitive and vegetative-motor cells in the nerve nodes of the larynx for the smooth musculature. If this is so, then the local reflex arches of this organ are enclosed in the intrawall nerve nodes themselves. In this case the receptors branching inside the ganglia and the axon collaterals signal the central nervous system about its functional states, thus connecting the reflex arches of the next stage into the chain of the regulating effect of the nervous system on the larynx.

BIBLIOGRAPHY

1. Batyreva, N. A., "The Problem of the Morphology of the Nervous Apparatus of the Epiglottis," Author's Abstract of Candidate Dissertation, Kiev, 1949.

2. Grigor'yeva, T. A., "Innervatsiya krovenosnykh sosudov" [Innervation of the Sanguiferous Vessels], Moscow, Medgiz, 1954.

3. Gracheva, M. S., "Morfologiya i funktsional'noye znacheniye nervnogo apparata gortani" [The Morphology and Functional Significance of the Nerve Apparatus of the Larynx], Moscow, Medgiz, 1956.

4. Dogel', A. S., "The Terminal Nerve Apparatus of the Human Soma," ZAPISKI ROSSIISKOY AKADEMI NAUK, Vol 14, 1903.

5. Ivanov, G. I., "Innervatsiya serdechno-sosudistoy sistemy" [Innervation of the Cardiovascular System], Moscow, Medgiz, 1945.

6. Karaganov, Ya. L., "The Nerve Apparatus of the Septum of the Human Mouth," in "Morfologicheskiye zakonomernosti perifericheskoy innervatsii" [The Morphological Principles of the Peripheral Innervation], Kishinev, 1964.

7. Karaganov, Ya. L., "The Afferent Innervation of the Septum of the Human Mouth," in "Voprosy morfologii nervnoy sistemy" [Problems of the Morphology of the Nervous System], Moscow, 1966.

8. Kleynenberg, S. Ye., A. V. Yablokov, V. M. Bel'kovich et al, "Belukha. Opyt morfologicheskogo opisaniya vida" [The White Grampus. Experience of Morphological Description of a Species], Moscow, Nauka, 1964.

9. Kolosov, M. G., "The Receptors of the Ganglia of the Vegetative Nervous System," ARKHIV ANATOMII, GISTOLOGII I EMBRIOLOGII, No 1, 1951.

10. Lavrent'yev, B. I., "The Morphology of the Receptors," Reports Topics of the Jubilee Session of the All-Union Institute of Experimental Medicine, Minsk, 1943.

11. Lashkov, V. G., "Innervation of the Mucous Membrane of the Respiratory Zone of the Nasal Cavity," Report Topics of the 11th All-Union Symposium of Anatomists, Histologist and Embryologists, Kiev, 1958.

12. Lashkov, V. P., "Innervatsiya organov dykhaniya" [Innervation of the Respiratory Organs], Moscow, Medgiz, 1963.

13. Manger, A. P. and B. G. Khomenko, "The Functional Anatomy and Sound-Forming Capabilities of the Upper Respiratory Tracts of Dolphins," BIONIKA, No 9, 1975.

14. Otelin, L. A., "The Dependence of the Structure of Encapsulated Receptors on Their Functions," VOPROSY FIZIOLOGII, No 5, 1965.

15. Portugalov, V. V., "Ocherki gistofiziologii nervnykh okonchaniy" [Essays on the Histophysiology of Nerve Endings], Moscow, Medgiz, 1955.

16. Pletnev, S. A., "The Micromorphology of Innervation of the Respiratory Zone of the Human Nose," Report Topics of the First Belorussian Conference of Anatomists, Histologists, Embryologists and Topographoanatomists, Minsk, 1957.

17. Ploshko, A. K., "O nervnykh okonchaniyakh v gortanii i dykhatel'nom gorle mlekopitayushchikh" [The Nerve Endings in the Larynx and Respiratory Tract of Mammals], Kazan', Kazanskiy universitet, 1896.

18. Plechkova, Ye. K., "Reaktsiya nervnoy sistemy organizma na khronicheskoye povrezhdeniye perifericheskogo nerva" [The Response of the Nervous System of an Organism to Chronic Damage of the Peripheral Nerve], Moscow, Meditsina, 1972.

19. Tomilin, A. G., "The Biology and Physiology of Black Sea Dolphins," ZOOLOGICHESKIY ZHURNAL, Vol 27, No 1, 1948.

20. Khomenko, B. G., "The Histostructure and Innervation of the Sound Apparatus (Meata Nasi) of Dolphins," DOP. AN URSR, SER. B., No 1, 1970.

21. Khomenko, B. G., "The Morphological Bases of the Location Properties of Dolphins," BIONIKA, No 7, 1973.

22. Khomenko, B. G., "Morphofunctional Analysis of the Structure of the Supracranial Respiratory Tract as a Possible Generator of Echolocation Signals," BIONIKA, No 9, 1975.

23. Yablokov, A. V., "The Morphology of the Digestive Tract of Toothed Cetaceans," ZOOLOGICHESKIY ZHURNAL, Vol 37, No 4, 1958.

24. Baer, K., "Die Nase der Cetaceen erlautert durch Untersuchungenen der Nase des Brauntfelsches," BULLETIN OF THE SCIENTIFIC ACADEMY OF ST. PETERSBURG, No 1, 1826.

25. Lawrence, W. and W. E. Schevill, "The Functional Anatomy of the Delphinid Nose," BULL. MUS. COMP. ZOOL, Vol 114, No 4, 1956.

26. Schenkann, E., "The Occurrence and Position of the 'Connecting Sac' in the Nasal Tract Complex of Small Odontocetes," BEAUFORTIA, Vol 19, No 246, 1971.

UDC 597:591.471-591.173

SOME FEATURES OF THE MORPHOLOGY OF THE BRANCHIAL APPARATUS OF FISHES RELATED TO THEIR SWIMMING SPEED

Kiev BIONIKA in Russian No 12, 1978 pp 103-108

[Article by O. B. Chernyshov, A. P. Koval' and A. A. Drobakha, Institute of Zoology of the Ukrainian SSR Academy of Sciences]

[Text] It has been established by investigations of the past few years that adaptation to rapid swimming by all aquatic animals, specifically fish, followed the path of improving the body shape [1], increasing the power to weight ratio [12], changing the method of respiration and also by the emergence of different mechanisms in the skin which contribute to a reduction of hydrodynamic drag [4-9]. It is quite natural to assume that the changes also affected the branchial apparatus of fish during adaptation to rapid swimming since the gills participate in formation of the boundary layer on a significant part of the body, thus playing a significant role in control of the boundary layer of a moving fish [2, 3].

The authors attempt in this article to follow which changes occur in the structure of the branchial apparatus of fish with an increase of their swimming speed and to determine whether there are mechanisms in this organ which specifically regulate the hydrodynamic properties of the ejected water flow. Representatives of two high-speed groups of fishes: 1) tench, roach, perch and pike swimming at Reynolds numbers of $Re \leq 10^5$ and 2) bonito swimming at Reynolds numbers of $Re \leq 10^8$, were selected for this purpose for the investigation.

It was established as a result of investigations that the branchial structure of the examined species of fish are similar in general features and correspond to the literary data. However, some differences in the histological structure of the gills, especially upon comparison of fishes swimming at different speeds, were also found.

As is known [16], the gills of all bony fish consist of five branchial arches, four natural and a fifth reduced. Each arch (Figure 1) has two rows of thin lanceolate epithelial processes--branchial lobes. Each of the two rows of branchial lobes is called half-gills. The gill rakers emerge to the opposite side of the lobes into the mouth cavity from the arches. The entire branchial apparatus is in the branchial cavity, covered on the outside by the gill covers. The bony skeleton of the branchial arch is enclosed in a layer of dense unshaped connective tissue, which, passing through the branchial lobes, forms a crest-like process--

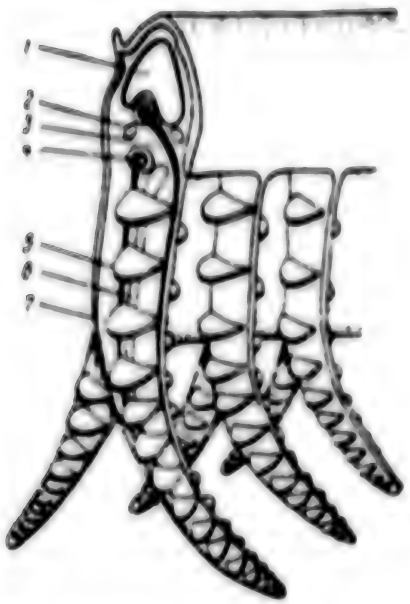

Figure 1. Diagram of General Structure of Gills (After Hughes): 1--branchial arch; 2- nerve; 3--afferent sanguiferous artery; 4--efferent sanguiferous artery; 5--secondary plates; 6--cartiliginous branchial ray; 7--branchial lobe

the interbranchial septum. A layer of integumental multilayer epithelium is located above the connective tissue. The branchial lobe is a thin plate which consists of dense unsaaped fibrous connective tissue. The upper and lower sides of the lobes are covered with thin epithelial folds--secondary plates. The secondary plates are covered with a single-layer epithelium. Sections with two layers of epithelial cells are sometimes found.

The cartiliginous branchial ray comprising the skeletal support of the lobe passes through the center of the lobe or somewhat laterally in the fish of the first high-speed group which we considered. In this case the epithelium which covers the branchial lobe is multilayered and somewhat thinned out on the ends of the lobes. The secretory cells, the distribution of which is irregular on different sections of the gills, are found in the mass of the epithelium along the entire surface of the branchial lobes and the secondary plates with greater or lesser frequency. The shape and dimensions of the secretory cells vary as a function of their location. These cells are arranged in the following manner on a plane histological section: a) they are represented by small cells (6-7 microns), rounded in shape with small spaces between them, on the ends of the branchial lobes, b) the secretory cells are primarily oval in shape up to 13 microns long and the number an average of 100 units per millimeter in the mid-part of the lobe on the inside, the number of secretory cells averages 60 units per millimeter on the inside and they are mainly circular in shape with diameter of 7-9 microns and c) the secretory cells alongside the branchial arch are oval in shape up to 13 microns long and are arranged in compact groups.

The thick multilayer epithelium of the branchial arch forms crypt-like folds on its apical end, in which cells of a somewhat different shape are found. These are very

large cylindrical cells (up to 30 microns long), arranged in a dense group in each of these crypt-like folds. They have a large nucleus located in the central or basal part and a granulated cytoplasm We are in all probability concerned with chloride-secreting cells. Only single, mucous-forming cells typical for the given species are found in the spaces between the crypt-like folds.

The inside of the gill covers also participates directly in formation of the mucous secretion in the branchial apparatus of fishes. There are a significant number of mucous-forming cells in the epidermis lining the inside of the gill covers of tench, roach, perch and pike.

Unlike fishes of the first high-speed group, two branchial rays comprising the skeletal support of the lobe pass through the edges of the lobe in the bonito, a representative of the second high-speed group. The characteristic feature of the structure of the branchial lobes of the bonito is that cartiliginous septa (Figure 2) are located between the two branchial rays at specific intervals. The number and size of the gill-rakers on the branchial arches of the bonito are considerably smaller than those of other considered species of fish. Moreover, the entire surface of the branchial arch is covered with natural conical teeth.

The gills of the bonito are covered with a multilayer epithelium which is distributed in the following manner: a) the epithelium on the ends of the lobes consists of 4-5 layers of epithelial cells, b) it becomes thicker in the mid-part of the lobe in the direction toward the branchial arch and the epithelium of the branchial arch consists of 20-25 layers of epithelial cells and c) the secondary plates are covered with a single-layer epithelium.

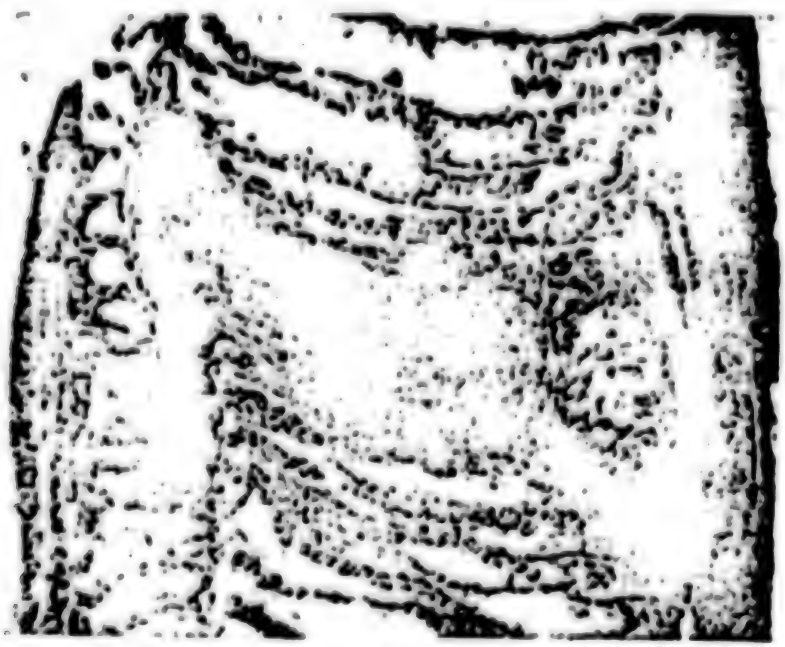

Figure 2. Branchial Rays in Lobe of Bonito and Cartiliginous Septum Between Them (X150)

Secretory cells of oval shape up to 18 microns long are relatively uniformly arranged in the mass of the epithelium along the entire surface of the branchial lobes and the secondary plates between the epithelial cells. The multilayer epithelium of the branchial arch forms crypt-like processes (Figure 3). Unlike fish of the first high-speed group, the epithelium is connected on the lateral surfaces of the branchial arch to the connective tissue in the form of a papillary layer rather than in a solid layer. A considerable number of mucous-forming cells was found on the inside of the gill covers of the bonito. We did not find chloride-secreting cells in the branchial epithelium of the bonito.

The factual material obtained about the structure of the branchial apparatus of fishes, distinguished primarily by the swimming speed and method of breathing (active in fishes of the first high-speed and passive in the bonito) permits one to evaluate and explain to some degree the changes in the gill structure which are related to swimming speed.

Figure 3. Crypt-Like Processes of Epithelium of Branchial Arch of Bonito With Numerous Mucous Cells (X300)

The adaptation of fish to rapid swimming and the related change of the method of respiration lead to significant changes in the structure of the branchial apparatus since the mode of flow through the gills changes. The flow through the gills of fish of the first high-speed group is more or less identical and is not dependent on swimming speed since respiration is subject to a specific cycle. Therefore, the structure of the branchial apparatus is of the same type and comparable in all representatives of the considered species of fish of the first high-speed group, although they do differ in swimming speed [14].

A significant increase of swimming speed of fishes resulted in a change of the method of respiration and this in turn resulted in a change in the gill structure. Thus, for example, two cartiliginous rays which support the lobe and cartiliginous septa between them appear in the branchial lobe of the bonito (Figure 2). These changes were caused, we feel, by the need to develop increased strength and stiffness of the lobe structure under the significant hydrodynamic loads on the gills during direct-flow respiration.

A papillary layer (Figure 4), which provides more rigid connection of the epidermis to the connective tissue, appears on the lateral surfaces of the branchial arches of the bonito to prevent separation of the epidermis from the connective tissue. We observed a similar connection of two layers in the front part of the body where significant hydrodynamic loads occur in fish swimming at significant speeds (the bonito, spotted and yellowfin tuna and sailfish).

There were communications about the hydrodynamic role of the gill-rakers, which, covering the lumen between the branchial arches and the gill cover, laminarize the water flow, fulfilling the role of a hydrodynamic lattice [13]. Analysis of the literary data [11, 16] and our own observations of a number of gill-rakers in different species of fish swimming at different speeds permit one to conclude that the gill-rakers rather perform a feeding and protective function rather than hydrodynamic function. This was confirmed by the fact that a decrease of the number of gill-rakers and their partial reduction is observed as the swimming speed of fishes increases. The gill-rakers in many predatory fish, being reduced, are transformed to tubercles on the branchial arches, which are planted with sharp tooth-spines [10] designed for holding prey. Moreover, fast-swimming fishes (dorado) are found in which the gill-rakers are absent, i.e., there is no hydrodynamic lattice [13].

Figure 4. Papillary Layer of Epithelium on Lateral Surfaces of Branchial Arch of Bonito (X150)

The secretory apparatus of the gills is undoubtedly of the most interest to hydrobionics. The presence of a large number of uniformly arranged mucous-forming cells on the branchial arches, lobes and on the inside of the gill covers, especially in fast-swimming fishes, presumes considerable secretion of mucous into the branchial cavity. It is natural that the mucous is dissolved in the ejected flow, as a result of which hydrodynamic drag is probably reduced both in the region of the gills and beyond them [15].

It was shown earlier that the secretory cells in the front part of the body of the bonito are essentially absent and appear in sections where control of the boundary layer is required. Retention of active secretory fields, the functioning on the inside of the gill covers and directly on the gills of the bonito indicates in all probability their hydrodynamic role. The presence of special crypt-like

structures on the inside of the gill covers and sections of the skin alongside the circumbranchial slit in one of the fastest swimming fishes--the swordfish--again indirectly confirms that the mucous apparatus of the gills and of the branchial cavity performs a hydrodynamic role. It has been even more improved in this case during adaptation to rapid swimming.

The presence of several types of secretory cells in the branchial apparatus of fishes of the first high-speed group, we feel, indicates that the secreted mucous substance carries a polyfunctional load, as on the body surface, and is related to a significant degree to protection of the organism against overgrowth and against clogging by suspended particles. Moreover, control of osmotic pressure, which is taken on by the chloride cells, is also required for freshwater fishes [11].

Thus, it was established as a result of investigations that changes occur in the gill structure in the branchial apparatus of fishes during adaptation to rapid swimming which permit one to conclude that a specific part of the hydrodynamic drag occurring during respiration is reduced due to the mucous-forming system.

BIBLIOGRAPHY

1. Alcyev, Yu. G., "Funktsional'nyye osnovy vneshnego stroyeniya ryby" [The Functional Bases of the External Structure of the Fish], Moscow, Izd-vo AN SSSR, 1963.

2. Alcyev, Yu. G. and O. P. Ovcharov, "Development of the Vortex-Formation Process and the Nature of the Boundary Layer During Motion of Fish," ZOOLOGICHESKIY ZHURNAL, Vol 48, No 6, 1969.

3. Alcyev, Yu. G. and O. P. Ovcharov, "The Role of Vortex Formation in the Locomotion of Fishes and the Effect of the Interface on the Flow Pattern," ZOOLOGICHESKIY ZHURNAL, Vol 50, No 2, 1971.

4. Belyayev, V. V. and A. P. Koval', "The Problem of the Hydrodynamic Function of the Mucous of Some Bony Fishes," BIONIKA, No 6, 1972.

5. Zayets, V. A., "Characteristics of the Skin Structure of Fast-Swimming Sharks," in "Bionika. Materialy IV Vsesoyuz. konf. po bionike" [Bionics. Proceedings of the Fourth All-Union Conference on Bionics], Moscow, 1973.

6. Zayets, V. A., "The Problem of the Variable Roughness of the Skin of Sharks," BIONIKA, No 6, 1972.

7. Koval', A. P., "The Roughness and Some Structural Features of the Skin of the Swordfish," BIONIKA, No 6, 1972.

8. Koval', A. P., "Some Structural Characteristics of the Skin of Bony Fishes Related to Their Swimming Speed," Author's Abstract of Candidate Dissertation, Kiev, 1972.

9. Koval', A. P., "Some Structural Characteristics of the Skin of Tuna and Possible Mechanisms of Reducing Hydrodynamic Drag," in "Bionika. Materialy IV Vsesoyuz. konf. po bionike," Moscow, 1973.

10. Koshina, Ye. S., "The Morphological Characteristics of the Branchial Apparatus With Regard to the Nature of Feeding by Fishes," TRUDY KARELSKOGO FILIALA AN SSSR, No 13, 1958.

11. Krayushkina, L. S., "Chloride-Secreting Cells of Fishes," ARKHIV ANATOMII, GISTOLOGII I EMBRIOLOGII, Vol 67, No 11, 1974.

12. Matyukhin, V. A., "Bioenergetika i fiziologiya plavaniya ryb" [The Bioenergetics and Physiology of Swimming by Fishes], Moscow, Nauka, 1973.

13. Ovcharov, O. P., "The Hydrodynamic Role of the Branchial Apparatus of Fishes During Passive Respiration," ZOOLOGICHESKIY ZHURNAL, Vol 49, No 10, 1970.

14. Radakov, D. B. and V. R. Protasov, "Skorosti dvizheniya i nekotoryye osobennosti zreniya ryb. Spravochnik" [Swimming Speeds and Some Characteristics of Vision of Fishes. Handbook], Moscow, Nauka, 1964.

15. Chernyshov, O. B. and T. A. Kalyuzhnaya, "The Possible Mechanism of the Action of the Mucous Coatings of Fishes," BIONIKA, No 9, 1975.

16. Shmal'gauzen, I. I., "Osnovy sravitel'noy anatomii pozvonochnykh zhivotnykh" [Fundamentals of the Comparative Anatomy of Vertebrate Animals], Moscow, Nauka, 1947.

UDC 597:591.471.43-591.173

THE CRYPT-LIKE MUCOUS-FORMING STRUCTURE OF THE SKIN AND GILL COVERS OF THE SWORDFISH

Kiev BIONIKA in Russian No 12, 1978 pp 108-111

[Article by A. P. Koval', Institute of Zoology of the Ukrainian SSR Academy of Sciences]

[Text] Investigations [1] of the secretory apparatus of the skin of different species of fish swimming at different speeds showed that the structure of the mucous-forming structures varies to a significant degree with an increase of the capabilities of the given object to reach high speeds. These changes are expressed in a decrease of the types of secretory glands of the mucous-forming cells, methods of moving the secretion to the body surface and strict localization of the secretory apparatus in a specific section of the body, depending on the body shape of the fish. The more complex structure of the secretory apparatus related to special body shape [6, 7] is observed in the swordfish and sailfish, swimming in the range of Reynolds numbers of $Re = 10^8$, and expressed in the appearance of specific mucous-forming subcutaneous channels with excretory ducts and chains of "ampules" along the mid-line of the spine [3, 4], i.e., special local systems which participate in secretion of the mucous substance to the boundary layer.

Another local system which produces mucous to the boundary layer is described in this article on the basis of studying the micro- and macrostructures of the skin of the circumbranchial slit and of the gill covers of the swordfish and the morphofunctional significance of this system is discussed.

As was noted, there is a unique structure in the region of the branchial slits on the skin and on the inside of the gill covers of swordfish of different sizes (the study was carried out on nine specimens from 1.2 to 2.9 meters long), which is similar to the crypts of the stomach or intestine in histological sections (Figure 1). However, it should be noted that this is not a solid field of crypts, but various shapes of islets (round, triangular and polygonal) which are distinguished from each other by several protruding connective-tissue ridges (Figures 2 and 3). There are no tooth-like scales which create the initial roughness of the skin, typical for the skin, and there are no channels with excretory ducts (pores) typical for other body sections of the fish in the region where the crypts are located on the skin of the swordfish.

The crypt-like mucous-forming structure in the region of the branchial slits is arranged in a relatively narrow band (2 cm in fish 1.2 meters long and 4 cm in

fish 2.9 meters long) along the edge of the branchial slit, passing somewhat under the closing gill cover. The crypt-like structures are located practically along the entire inside of the gill covers. There are no crypts only on a small section in the center of the gill cover (Figure 3).

The thickness of the surface layer of skin (epithelium) is different in different sections. The thinnest layer (3-4 rows of cells) is observed on the crests of the protruding connective-tissue ridges and a very thick layer (30-40 rows of cells) is located in the center of the islet edged by the ridge. The greatest number of secretory cells, arranged in several rows, is also found at points of a strongly developed epithelial layer.

Figure 1. Crypt-like Processes of Skin of the Swordfish (X300)

The cellular composti on of the crypt-like structures of the skin of the swordfish consists of two types of cells: epithelial and secretory of granular type. The epithelial cells are arranged along the basal membrane in the spaces between the secretory cells. The dimensions of the epithelial cells do not differ from those in other sections of the body and fluctuate from 5 to 6 microns. The secretory cells vary slightly in their size (15-18 microns), but may reach 20 microns in some sections.

As already noted [3-5], there are different structures in the skin of the swordfish which produce mucous (epidermis, channels and ampules). In this case accumulation and excretion of mucous onto the body surface of the fish have their own characteristics. The crypt-like formations of the skin of the circumbranchial slits and of the gill covers can also be added to these structures.

The process of mucous formation in the crypts of the skin of the swordfish can be represented in the following manner: the secretory cell begins to be formed from an ordinary epithelial cell located in the lower layers of the epidermis above the basal layer. Due to the constant growth of the basal layer of epithelial cells, the secretory cell is thrust to the surface of the epidermis, where its membrane is broken due to the mechanical effect of the flow and the contents of a one-time

portion are excreted into the boundary layer. The excreted native secretion swells upon contact with the water and flows along the body surface. The special arrangement of the crypt-like structures (the region of the gill covers and the circumbranchial slits) assumes local production and excretion of the mucous. Formation of the mucous and secretion of it to the body surface of the swordfish from the crypt-like structures is similar in general features to the same process occurring in the epidermis. However, there is more abundant secretion of mucous per unit surface in the first case.

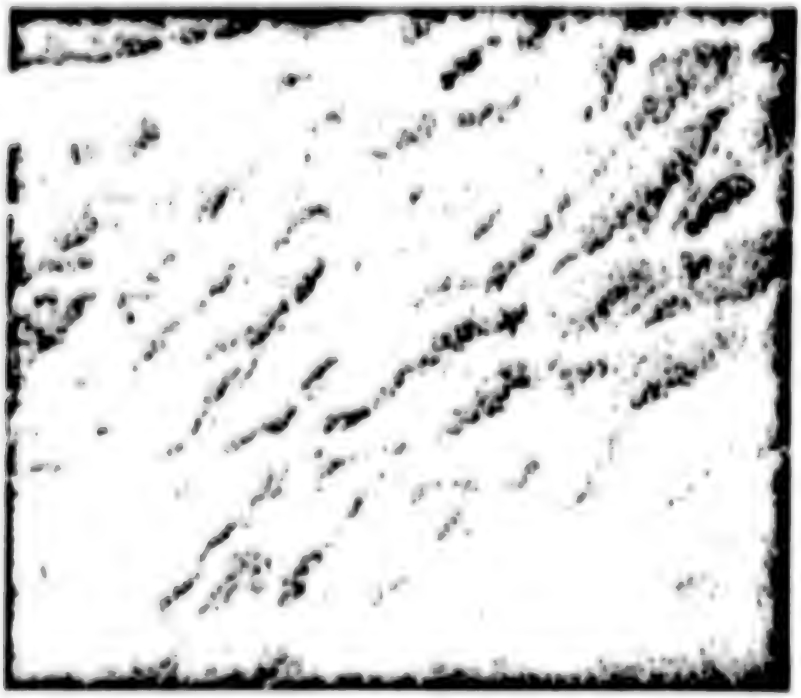

Figure 2. Crypt-Like Structure of Swordfish in Region of Branchial Slit (X20)

Analysis of the swimming characteristics and the structure and arrangement of the crypt-like mucous-forming structure of the skin of the swordfish permits one to assume the functional significance of this formation. Since the swordfish is one of the fastest swimming animals, it is quite natural that specific adaptations developed in it during evolution which assist it to consume its energy resources efficiently. One of these adaptations, we feel, is the crypt-like structure of the skin and the gill covers. The development of this formation may be represented in the following manner. The swordfish, like all fast-swimming fishes (Scombridae), swims with open mouth. The flow of water ejected from the gills during rapid swimming should naturally alter significantly the flow over the body and should affect the hydrodynamics of swimming of the fish. To compensate for the unfavorable effect of respiration on the flow of the boundary layer, the organism developed an adaptation for stabilization of the ejected flow. This adaptation is related primarily to the physicochemical properties of the mucous.

It is shown [2, 8] that the mucous and other high-molecular substances considerably reduce hydrodynamic drag in small additions to the water. This also explains the appearance of special structures which produce mucous in "hydrodynamically unfavorable locations." This section on the body of the swordfish is the branchial slit.

Figure 3. Distribution of Crypts on Inside of Gill Cover

where the mucous generated in the crypt-like structure of the inside of the gill covers and the circumbranchial slits, interacting (being dissolved) with the water flow discharged through the gills, changes its hydrodynamic properties. A similar mechanism of regulation of the water flow discharged through the gills has also been observed in other representatives of bony fishes [9]. However, it is simplified to a significant degree since all the investigated fishes swim at lower speeds and the flow mode is naturally different from that of the swordfish, which swims at Reynolds numbers of $Re \leq 10^8$. The advanced hypothesis of the mechanism of the effect of crypt-like structures of the circumbranchial section of the skin and the inside of the gill covers requires a qualified experimental check.

BIBLIOGRAPHY

1. Belyayev, V. V. and A. P. Koval', "The Hydrodynamic Function of the Mucous of Some Bony Fishes," BIONIKA, No 6, 1972.

2. Kobets, G. F., V. S. Zav'yalova and M. L. Komarova, "The Effect of the Mucous of Fishes on Turbulent Friction," BIONIKA, No 5, 1971.

3. Koval', A. P., "The Roughness and Some Structural Features of the Skin of the Swordfish," BIONIKA, No 6, 1972.

4. Koval', A. P., "The Functional Significance of Some Skin Products of the Sailfish," BIONIKA, No 8, 1974.

5. Koval', A. P. and T. A. Kalyuzhnaya, "Characteristics of Emergence of Mucous to the Body Surface of Fishes," BIONIKA, No 9, 1975.

6. Kozlov, L. F., "The Hydrodynamic Function of the Sword of the Swordfish," BIOFIZIKA, Vol 31, No 3, 1973.

7. Ovchinikov, V. V., "Mech-ryba i parusnikovyye" [The Swordfish and Sailfish], Kaliningrad, 1970.

8. Pyatetskiy, V. Ye. and Yu. N. Savchenko, "The Effect of Mucous on the Hydrodynamic Drag of Fishes," BIONIKA, No 3, 1969.

9. Chernyshov, O. B., A. P. Koval' and A. A. Drobakha, "Some Characteristics of the Morphology of the Branchial Apparatus of Fish Related to Their Swimming Speed," BIONIKA, No 12, 1978.

UDC [591.483:591.472]:599

THE ROLE OF JOINT RECEPTORS IN CONTROL OF LOCOMOTOR ACTS OF EXTREMITIES OF MAMMALS

Kiev BIONIKA in Russian No 12, 1978 pp 111-116

[Article by N. N. Il'yenko, Institute of Zoology of the Ukrainian SSR Academy of Sciences]

[Text] One of the important problems of neurobionics is study of the principles of the structure and functioning of the receptors, extremely necessary for development of sensors which gather various types of useful information. It is presently difficult to name a field of science, technology and medicine which could get along without sensors. One can say without exaggeration that the problem of sensors is one of the most universal. The sensors with which the limb prostheses should be equipped are of special value since "one of the most significant deficiencies of prostheses of the human limbs is the absence of sensitivity in them" [16]. It is known that one cannot achieve smoothness of motion, accomplished proportioned compression and so on due to the absence of feedback on the part of the prosthesis. A unique method of developing these sensors is to study the structure and principles of functioning of natural "sensors"--receptors and modelling of them.

The collective of the Laboratory of Bionics, Department of Evolutionary Morphology, Institute of Zoology of the Ukrainian SSR Academy of Sciences, studying the locomotor apparatus, became convinced that improving the functioning of this apparatus is based on a system of controlling it, one of the fixed components of which is the receptor apparatus of the joints. The importance of the joint receptors to functioning of the locomotor apparatus is indicated indirectly by the following facts. In patients suffering from disruption of conductivity of the sensing channels of the spine [17] or from artificial deafferentation of the extremities [27, 4, 5], motor acts are disrupted and a feeling of motion and of the position of the sections of the extremities in the joints disappears. It is generally impossible to execute highly accurate motions even controlled by vision. But as subsequent experiments showed [24, 8], total anaesthesia of some joints of the extremities leads to similar results.

Based on extensive morphofunctional study of the joints of the extremities of terrestrial mammals [14], the author concludes that the main barrier in the path to perception of the functional dispatches of the locomotor apparatus is the absence of data on the structure and function of the joints, their integrated action and also the insufficiently accurate concepts on the nature of the relationship between the nerve periphery and the organs of locomotion.

However, despite the importance of these problems, little attention was devoted to innervation of the joints until quite recently and data on the morphology and characteristics of functioning of the joint receptors, for example, was insufficient for the demands of biocybernetics. This is related to the fact that the joints themselves were regarded as passive sections of the extremities [9] and such main components of the joints as the capsule, ligament and cartilage were assigned the role of passive accessories [6, 10] while a secondary role was allocated to the nerve structures of the joints during regulation of locomotor acts. Therefore, despite the fact that the hypothesis was advanced even during the past century that the encapsulated receptors of the joints serve to determine the value of the joint angle [29], only the results of electrophysiological investigations conducted on the joints of the extremities [11, 21-23, 25, 26, 30] could serve as a serious basis to look at the nerve structures of the joints from this aspect. It is shown that there are rapidly adapting (encapsulated) and slowly adapted (bush-like) receptors in the joints and that there are also receptors which respond to motion only in a single specific direction (bending or unbending), so that the pulse amplitude in the nerves innervating the joints is increased with an increase of the speed of locomotion and an increase of the angle of the bending-unbending motions in the joints. Since the number of receptors included in the work increases with an increase of the bending-unbending angle in the joint, the hypothesis was advanced that each joint receptor corresponds to a specific part of the arc of motion in the joint. Based on data of electrophysiological investigations and on the fact that the signals coming into the TsNS [Central nervous system] from the joint receptors inform it of precise localization of motion, whereas the centers receive data about the tension of the muscles without precise localization of this displacement from signals of the muscular receptors, the hypothesis was advanced [23], shared even now [17, 7], that the leading role in formation of the program which controls such acts of the extremity as the speed of motion and position of the body in space belongs to the joint receptors rather than to the muscular receptors.

What is the mechanism of the signals of the joint receptors affecting this program?

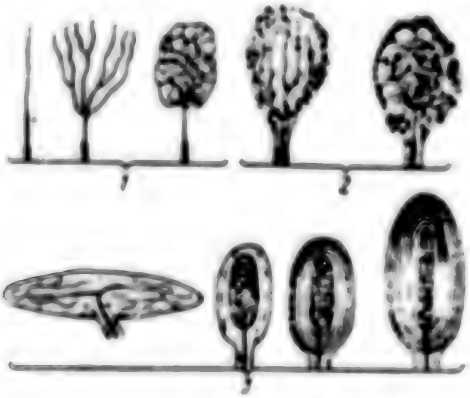

Types of Joint Receptors of Mammals: 1--free; 2--attached; 3--encapsulated

The entire process of locomotion, especially by a quadruped, is realized by the activity of specific groups of antagonistic muscles and by the geometric structure of the joint surfaces of the connected links, which permits mobility in the joints around several axes of rotation. According to new concepts [20], control of the

movements of the human extremities is accomplished by a closed cycle using the following morphological structures: brain-efferent nerves-kinetic patches-receptors-afferent nerves-brain. In this case the path of passage of the signals from the brain to the actuating system has been called the direct communication channel while the path of passage of the signals from the receptors to the brain has been called the feedback channel. Signals travel along the feedback channel from the receptors located directly inside the actuating system (the muscular and tendinous spindles, receptors of the fascies, joints and periarticular tissues). Due to feedback, the centers which direct locomotion receive information about the results of the activity of the muscles and namely the extent to which real motion of the given link of the extremity corresponds to the program generated in the TsNS. After the current changes in the work of the locomotor apparatus are compared, i.e., after the errors between the program and real motion are taken into account, the control system sends out new signals (direct communication), directed toward amplification or attenuation of the work of the muscles, connecting or disconnecting them from work, i.e., specific corrections are introduced into the work of the extremity. Thus, the signals coming into the TsNS from the receptors play an important role in construction of motor acts, providing the centers with adequate and constantly incoming information on the nature of this motion and namely on the rate and localization of displacements between the links of the extremities. In other words, the signals coming from the receptors to the centers carry important information about the result of the action of the centers on the actuating system. It follows from this that the actuating system, due to feedback signals, controls itself to some extent. This agrees with the concepts [1] that "any functional system is continually cyclic in nature and may not exist if it does not receive feedback on the degree of usefulness of the effect produced."

Which joint receptors perform this role and what is their special function in this process?

We and other neuromorphologists [2, 10, 13, 19, 28] determined receptors of three types--free, attached and encapsulated (Figure), in the joints of the extremities of a number of terrestrial mammals. There is the opinion [17] that the participation of the joint receptors in coordination of the work of the extremity would be impossible if it were not specialized to perception of specific types of stimuli. The characteristics of functioning of any receptors are studied by special methods utilized by physiologists. And since only the rate of adaptation is determined by these methods for the joint receptors, we proceeded from the structural characteristics of the receptors, their localization in individual components of the joints and among individual structures of these components, the role of these components in the work of the joint and also from data known in the literature on the function of similar receptors of other tissues when solving the problem of specialization of the joint receptors to specific stimuli.

Based on the fact that the main mass of free joint receptors is localized in the walls of the sanguiferous vessels, joint tissues, in the covering layer of the synovial membrane, the synovial villi and the joint cartilage (other types of receptors are almost never found in these components) and also due to the fact that a specific role is ascribed to these components of the joints--production and utilization of the synovia, one may assume that the free receptors of these very components of the joints signal the centers through the feedback channels of the quantity and physical and chemical properties of the synovia.

During functional analysis of encapsulated receptors, we proceeded on the basis that different shapes of them which we determined in the joints (bulb of Krause, Ruffini's corpuscle, Golgi-Maccioni's body and the pacinian corpuscle) have an essential similarity of structure with the more complex and more fully studied encapsulated receptors--the pacinian corpuscles of the mesentery of the cat. The results of electrophysiological investigations [12] show that the pacinian corpuscles of the mesentery are typical rapidly adapting mechanoreceptors. Electrophysiological investigations of the joints with subsequent histological monitoring of the nerve structures of the joint capsule [30] showed that a quality such as rapid adaptation is also inherent to the encapsulated joint receptors. Encapsulated joint receptors generate signals in response to tension or compression of the joint capsule. Therefore, based on the similarity of structure, localization (deep collagenous-elastic layer of the synovial membrane, fibrose membrane of the capsule and ligament of the joint, the perichondrium and in these tissues--among the collagenous bundles, alongside the sanguiferous vessels and nerve stems) and data of electrophysiological investigations, we assume that the encapsulated joint receptors, like the pacinian corpuscles of the mesentery, are mechanoreceptors.

The functional dispatches of the attached receptors in the organism, compared to dispatches of the free and encapsulated receptors, have been weakly studied. Taking into account that the attached receptors are localized mainly in the same components of the joint as the encapsulated receptors, one may assume that these receptors also respond to mechanical stimuli. But based on the structural features of attached receptors, one should assume that the perception of these stimuli is obviously somewhat different in nature itself that perception by the encapsulated receptors.

The source of mechanical stimuli in the joints of the extremities are the following phenomena: tension and thickening of the joint capsule, displacement of bundles of collagenous fibers, especially during rotational motions in the joints, pressure of the synovial fluid moving in the joint cavity during motion in the joints, compression acting on the joints from the outside (compression and vibration) and passage of a pulse wave and turgor of the fluid of the perineural vagina. As a result, weak mechanical forces acting on the wall of the encapsulated receptors or on the terminal apparatus of the attached receptors located in the tissues of the joints among the collagenous bundles, alongside the walls of the sanguiferous vessels or the perineural vagina of the nerve stem occur. Among the enumerated phenomena, we feel that the main ones should be regarded as tension of the joint capsule andppressure of the synovial fluid, which according to [15, 3], moves in the joint during functioning of the extremity. Since these phenomena occurred constantly in the joints during phylogenesis, part of the joint receptors, performing the role of mechanoreceptors, adapted to their effect.

Thus, the joint receptors deliver information to the centers on compression, the direction and speed of tension of the joint fluid, on the quantitative and qualitative composition of the synovial tissue and so on. This information is compared to the program which controls locomotion and specifically the work of the joint. If errors appear between the program for a given work mode of the joint and information about the processes occurring in the components of the joint at each new moment (for example, insufficient synovia, overbending of the joint or too strong compression of the cartilage), the control system sends signals through the direct communication channels to the muscles, sanguiferous and other systems capable of eliminating this error by bringing all the indicators of the joint to an optimum state.

BIBLIOGRAPHY

1. Anokhin, P. K., "Biologiya i neyrofiziologiya uslovnogo refleksa" [The Biology and Nuerophysiology of the Conditioned Reflex], Moscow, Nedgiz, 1968.

2. Bagryanskiy, I. B., "Comparative Analysis of the Development of Innervation of the Femur-Hip Joint in the Antenatal Ontogenesis of Man and Some Maturonate Animals," Author's Abstract of Candidate Dissertation, Voronezh, 1974.

3. Berezkin, A. G., "The Lability of the Synovial Fluid," in "Mekhanizmy povedeniya i orientatsii zhivotnykh" [The Mechanisms of the Behavior and Orientation of Animals], Moscow, 1969.

4. Bernshteyn, N. A., "O postroyenii dvizheniy" [On the Structure of Motion], Moscow, Medgiz, 1947.

5. Beritov, I. S., "Obshchaya fiziologiya myshechnoy i nervnoy sistemy" [The General Physiology of the Muscular and Nervous System], Vol 1, Moscow, Meditsina, 1966.

6. Volynskiy, F. A., Book Review "Voprosy innervatsii sustavov i kostey" [Problems of Innervation of the Joints and Bones], Kazan', 1951.

7. Granit, R., "Osnovy regulyatsii dvizheniy" [Fundamentals of Regulation of Motion], Moscow, Mir, 1973.

8. Gurfinkel', V. S., Ya. M. Kots and M. L. Shik, "Regulyatsiya pozy cheloveka" [Regulation of Human Posture], Moscow, Nauka, 1965.

9. Diterikhs, M. M., "Vvedeniye v kliniku sabolevaniy sustavov" [Introduction to Clinical Practice of Joint Diseases], Moscow-Leningrad, Medgiz, 1937.

10. Drobyshev, V. I., "Development of Innervation of the Large Joints of the Extremities in Antenatal Ontogenesis of Man," Author's Abstract of Candidate Dissertation, Voronezh, 1960.

11 Zalkind, V. I., "Electrophysiological Investigation of the Functions of the Receptors of the Radiocarpal Jc nts of the Cat," Author's Abstract of Candidate Dissertation, Leningrad, 1972.

12. Il'inskiy, O. B., "Voprosy fiziologii sensornykh sistem (obzory). Mekhanoretseptory" [Problems of the Physiology of Sensory Systems (Reviews). Mechanoreceptors], Leningrad, Nauka, 1967.

13. Il'yenko, M. M., "Tipi nervovikh zakinchen' ta ikh topografiya na nervovomu volokni v suglobakh kintsivok deyakikh ssavtsiv," DOPOV. AN URSR, No 8, 1971.

14. Kas'yanenko, V. G., "Special Physiology of the Organs of Locomotion of Mammals as One of the Timely Problems of Comparative Morphology," ZOOLOGICHESKIY ZHURNAL, Vol 38, No 4, 1953.

15. Kozhevnikov, S. N., S. F. Manziy and I. M. Pryakhin, "Improving the Classification of the Joints of Animals," PRIKLADNAYA MEKHANIKA, No 1, 1965.

16. Lomov, B. F., "Chelovek i tekhnika. Ocherki inzhenernoy psikhologii" [Man and Technology. Essays on Engineering Psychology], Moscow, Sovetskoye Radio, 1966.

17. Oganisyan, A. A., "Elektrofiziologiya provodyashchikh putey spinnogo mozga" [The Electrophysiology of the Conducting Pathways of the Spine], Moscow, Nauka, 1970.

18. Sergeyev, Yu. P., "Morfologicheskiye osnovy reflektornykh kontraktur" [The Morphological Bases of Reflex Contractures], Moscow, Meditsina, 1964.

19. Fedorov, V. P., "Development of the Innervation of the Knee Joint During Antenatal Ontogenesis of Man and Some Maturonate Animals," Author's Abstract of Candidate Dissertation, Voronezh, 1975.

20. Chkhaidze, L. V., "Koordinatsiya proizvol'nykh dvizheniy cheloveka v usloviyakh kosmicheskogo poleta" [Coordination of Voluntary Movements of Man Under Space Fl ght Conditions], Moscow, Nauka, 1968.

21. Andrev, V. G. and E. Dodt, "The Deployment of Sensory Nerve Endings of the Knee Joint of the Cat," ACTA PHYSIOL. SCAND., Vol 28, No 4, 1953.

22. Boyd, J. A. and T. D. Roberts, "Proprioceptive Receptors in the Knee Joint of the Cat," JOURNAL OF PHYSIOLOGY, Vol 122, No 2, 1953.

23. Boyd, J. A., "Nerve Impulses From Proprioceptors in the Knee Joint of the Cat," JOURNAL OF PHYSIOLOGY, Vol 119, No 8, 1953.

24. Brown, J., G. Lee and N. Ring, "The Sensation of Passive Movement of the Metatarso-Phalangeal Joint of the Great Toe in Man," JOURNAL OF PHYSIOLOGY, Vol 126, No 4, 1954.

25. Gardner, E. D., "The Innervation of the Knee Joint," ANAT. REC., Vol 101, No 1, 1948.

26. Godwin-Austern, R. B., "The Identification of Mechanoreceptors in the Costovertebral Joint Excited by Displacement of the Ribs," JOURNAL OF PHYSIOLOGY, Vol 130, No 1, 1967.

27. Mott, F. W. and C. S. Scherrington, "Experiments on the Effect of Sensory Nerves on the Movement and Nutrition of the Limbs. Preliminary Communication," PROC. ROY. SOC., Vol 57, No 3, 1895.

28. Polacek, P., "Receptors of the Joint, Their Structure, Variability and Classification," No 23, Brno, 1966.

29. Rauber, A., "Untersuchungen uber das Vorkommen und die Bedeutung der Vaterschen Korperchen," Munchen, 1967.

30. Scoglund, S., "Anatomical and Physiological Studies of Knee Joint Innervation in the Cat," ACTA PHYSIOL. SCAND., Vol 36, No 1, Suppl. 124, 1956.

6521
CSO: 8344/0332

END

END OF FICHE DATE FILMED

Feb. 10 1981